

# Testing the Matter Bounce with Primordial Non-Gaussianity: A SPHEREx Sensitivity Recast with a MegaMapper Outlook

Houston Golden<sup>1, \*</sup>

<sup>1</sup>*Independent Researcher, Los Angeles, California, USA*

(Dated: July 10, 2026)

A matter-dominated contracting phase preceding a nonsingular bounce produces a minimally parameterized local-type non-Gaussianity  $f_{\text{NL}}^{\text{local}} = -35/16 = -2.1875$ , opposite in sign and roughly two orders of magnitude larger than the single-field slow-roll value. We certify this value four ways: a from-scratch re-summation of Cai *et al.*'s four cubic-action vertices at  $\epsilon = 3/2$  in the squeezed limit, their own  $\epsilon$ -order-grouped intermediates, three-configuration benchmark matching, and Li *et al.*'s independent general- $c_s$  formula at  $c_s = 1$ ; the printed  $-35/8$  is an unreproduced erroneous literature value, traced to a  $-(99/128) \sum_i k_i^3$  discrepancy in one transcribed polynomial (Appendix A). Recasting the single published Heinrich *et al.* SPHEREx multi-tracer bispectrum forecast ( $\sigma(f_{\text{NL}}^{\text{local}}) \approx 0.7$ ) onto this prediction via an explicit template-mismatch map ( $r \approx 0.84$ ) plus an additive-quadrature systematic budget yields a sensitivity of  $\sim 2.6$ – $2.75\sigma$  (optimistic, template-corrected) reducing to  $\sim 1.3$ – $2.75\sigma$  after systematics ( $\sim 0.8\sigma$  under the unresolved GR-correlation bracket). The conservative  $1.3\sigma$  floor uses a proxy correlation transferred from the power-spectrum SDB channel, as the per-triangle bispectrum covariance  $\text{Cov}_B$  is not public; the  $0.8\sigma$  edge and the proxy-based  $1.3\sigma$  floor are therefore both disclosed as marginal-sensitivity estimates, not channel-native measurement precisions. The forecast is conditional on faithful cubic-order transmission through the bounce, closed to a bounded  $\delta f_{\text{NL}} \lesssim 10^{-3}$  systematic via single-clock nonlinear  $\zeta$ -conservation. An illustrative closed-form Bayesian comparison, cross-checked by three Monte Carlo validations of the closed-form integral, gives  $\text{BF} \approx 9$ – $14$  for a bounce detection over tuned multifield competitors. The corrected amplitude sets a realistic sensitivity target that preserves qualitative discriminatory power against single-field inflation ( $|f_{\text{NL}}^{\text{inf}}| \approx 0.015$ , opposite sign).

## I. INTRODUCTION

*Scope and conventions.* This paper is a sensitivity *recast* of a single external forecast, not an independent one: every quoted significance and Bayes factor rescales the imported Heinrich *et al.* [1]  $\sigma(f_{\text{NL}}^{\text{local}}) \approx 0.7$  baseline by the explicit template-mismatch map ( $\hat{f}_{\text{NL}}^{\text{bounce}}, \sigma^{\text{bounce}} = (\hat{f}_{\text{NL}}^{\text{local}}/r, \sigma^{\text{local}}/r)$  with  $r = 0.84$  (Eq. 5) plus a heuristic additive-quadrature systematic budget, cross-parameter correlations neglected in the headline recast; a separate in-house tree-level multi-tracer bispectrum Fisher (§IV) *validates* the recast (reproducing the Heinrich local baseline to 2–11% and recovering  $r_{\text{eff}} \approx 0.99$ ), and is not the source of the headline numbers. The headline ranges are therefore conditional sensitivity envelopes whose endpoints derive from qualitatively different null procedures (signal-only CMB-Fisher weighting, LSS noise-weighting,  $b_\phi$ /GR-marginalized budgets), so individual  $\sigma$  endpoints within a range are *not directly comparable*. The conservative  $1.3\sigma$  floor of the additive-quadrature budget uses a proxy correlation ( $\rho = -0.868$ ) transferred from the power-spectrum scale-dependent-bias Fisher channel, adopted because the per-triangle bispectrum covariance  $\text{Cov}_B$  of Heinrich *et al.* is not public (§VII); it is not a channel-native bispectrum-Fisher marginalization. The forecast is conditional on assumption (d), faithful cubic-order bispectrum transmission through the bounce: verified at linear order [2] and closed at cubic order to a

bounded  $\delta f_{\text{NL}} \lesssim 10^{-3}$  systematic via single-clock nonlinear superhorizon  $\zeta$ -conservation (Sec. II C), the sole quantization-dependent input being the sign of the sub-leading gradient coefficient (a citable Lorentzian  $c_s^2 = 1$  dressed-metric choice, not an open computation); the model also evades the Quintin *et al.* [3] bounce no-go. The prediction holds in the scalar-only matter-bounce class defined by assumptions (a)–(f) of Sec. II C, notably (e) no prolonged post-bounce inflation and (f) negligible fermion-sourced torsion. *Notation for the several  $r$ -like symbols used throughout* (fixed once here to avoid collision):  $r$  is the template-overlap amplitude recovery factor;  $r_t$  the tensor-to-scalar ratio;  $r_{\text{eff}} \approx 0.99$  the survey-optimal amplitude recovery from the independent Fisher;  $r_{\text{cos}}$  the shape cosine;  $\rho$  the Fisher correlation coefficient. The Bayes factors are illustrative of the available discriminating power, not definitive model-selection evidence.

The inflationary paradigm provides a remarkably successful framework for generating the observed spectrum of primordial perturbations. Standard single-field slow-roll inflation predicts a nearly scale-invariant, nearly Gaussian spectrum with a small, positive local-type non-Gaussianity  $f_{\text{NL}} \approx (5/12)(1 - n_s) \approx 0.015$ , set by the Maldacena consistency relation [4] (gauge-frame value; the conformal-Fermi-frame equivalent differs by  $\mathcal{O}(\text{slow-roll})$  corrections [5, 6] and is not the bounce-discriminating quantity here, since the bounce-vs-inflation contrast remains  $|f_{\text{NL}}^{\text{bounce}}| \gg |f_{\text{NL}}^{\text{inf}}|$  in either frame).

Bouncing cosmology offers an alternative origin for primordial perturbations: modes exit the Hubble radius

\* [houston@hubify.com](mailto:houston@hubify.com)

during a contracting phase and re-enter after a nonsingular bounce. In particular, a matter-dominated contraction ( $w \approx 0$ ) produces a scale-invariant scalar spectrum through the growth of the curvature perturbation  $\zeta$  on superhorizon scales [7, 8].

A distinctive prediction of the matter bounce is a large, negative, minimally parameterized local-type non-Gaussianity  $f_{\text{NL}} = -35/16 = -2.1875$  [9–11] at zeroth order in the  $\epsilon$ -expansion (the corrected value, certified four ways in Appendix A; the printed  $-35/8$  is an unreproduced erroneous literature value, traced to a discrepancy in one transcribed polynomial collapse) (the first-order coefficient  $\kappa_\epsilon$  has an order-of-magnitude range 2.8–40, Sec. VIII, so the value is tightly determined at leading order but the first correction carries substantial theoretical uncertainty). This value is determined at leading order by the equation of state during contraction ( $\epsilon = 3/2$  for matter) and the structure of the Maldacena cubic action, with no free parameters in the cubic sector at zeroth order in  $(w - 0)$ . The  $\mathcal{O}(\epsilon)$  correction from quasi-dust ( $w = -0.003$ ) introduces a 0.6–8% uncertainty (Sec. II C), and the underdetermined polynomial coefficients  $c_1$ – $c_6$  span more than an order of magnitude in absolute value (the reference solution (2, 7, 3, –12, –69, 19) ranges from  $|c_1| = 2$  to  $|c_5| = 69$ ; Sec. II), so the prediction is more precisely described as minimally parameterized rather than strictly parameter-free. The prediction is robust across the bounce class without prolonged post-bounce inflation (conditional in particular on assumption (d), faithful cubic-order transmission through the bounce, verified only at linear order; Sec. II C): it depends only on the contracting-phase dynamics, not on the specific UV completion that produces the bounce [2]; it is conditional on the assumptions about the bounce transition listed in Sec. II C, in particular assumption (e) which restricts the prediction to the Wilson-Ewing class (no prolonged post-bounce inflation). The term “mechanism-independent” as it appears in earlier matter-bounce literature refers to UV-completion independence within this restricted bounce class *and is conditional on faithful cubic-order bispectrum transmission through the bounce* (assumption (d), Sec. II C, verified only at linear order in Ref. [2]); it is not genuine model independence across the full bounce-cosmology landscape. Bounce models that invoke prolonged post-bounce inflation (e.g., as required by some dark-energy-from-bounce constructions) erase the  $f_{\text{NL}}$  signal and replace it with the standard slow-roll value, and bounce-transition dynamics that violate faithful third-order transfer would re-introduce mechanism dependence at the order being tested. In minimal Einstein-Cartan-Holst gravity, scalar perturbations reduce exactly to the standard Mukhanov-Sasaki sector: the Holst term becomes a topological invariant when torsion vanishes for canonical scalar field matter (Mercuri [12]; Freidel *et al.* [13]), rendering the Barbero-Immirzi parameter invisible in all scalar observables. This decoupling holds in the *scalar-only sector with no fermion matter present*;

if fermion matter is reinstated, the Hehl-Datta–Mercuri four-fermion contact term sourced by  $\langle \bar{\psi}\gamma^5\gamma^a\psi \rangle^2$  activates torsion and breaks the Holst topological-invariance argument, so the Barbero-Immirzi parameter  $\gamma_{\text{BI}}$  re-enters scalar observables through the dim-6 four-fermion channel and a possible  $\Delta N_{\text{eff}}$  contribution. The matter-bounce  $f_{\text{NL}} = -35/16$  prediction in this work is robust *within the scalar-only matter-bounce class* (see Assumption (f) in Sec. II C: fermion energy density during contraction and bounce is negligible, so the dim-6 four-fermion operator does not source torsion or reactivate  $\gamma_{\text{BI}}$  in the contracting-phase cubic action); the broader “UV-completion-independent” framing should therefore be read as UV-completion independence *within the scalar-only contracting phase*, not as independence across the full ECH operator space. Bounce models with significant fermion sectors during contraction would require an explicit bound on  $\langle \bar{\psi}\gamma^5\gamma^a\psi \rangle^2$  before  $f_{\text{NL}} = -35/16$  can be quoted in that broader class; the present forecasts do not apply to such models without that additional input.

The next generation of galaxy surveys—SPHEREx [14] and MegaMapper [15] (a proposed Stage V spectroscopic facility, not yet approved or funded)—will constrain local-type  $f_{\text{NL}}$  at precision substantially beyond current Planck bounds through the scale-dependent bias effect [16] and the galaxy bispectrum [1]. In this paper, we present a systematic sensitivity analysis recasting published SPHEREx and MegaMapper constraints onto the matter-bounce prediction  $f_{\text{NL}} = -35/16$ , including a comprehensive assessment of the dominant observational fragilities and a Bayesian model comparison quantifying the discrimination power against inflationary alternatives. The length of this manuscript reflects the breadth of that scope — a source-level audit of the  $f_{\text{NL}} = -35/16$  prediction (including the resolution of the Cai–Li factor-of-two, Appendix A), an explicit template-mismatch and null-space quantification, a fully itemized systematic budget, and a closed-form Bayesian comparison cross-validated against three Monte Carlo ensembles — rather than the size of any single incremental result; readers seeking only the headline sensitivity may consult the abstract, Table V, and Sec. IV.

## II. THE MATTER-BOUNCE BISPECTRUM BENCHMARK

### A. The Prediction

In a matter-dominated contracting universe with standard GR perturbation theory and Bunch-Davies vacuum, the curvature perturbation  $\zeta$  grows as  $|\eta|^{-3}$  on superhorizon scales during contraction. The cubic interactions, governed by the Maldacena action [4] specialized to  $\epsilon = 3/2$ , produce a bispectrum with shape function [9]:

$$A_T(k_1, k_2, k_3) = \frac{3}{256 k_1^2 k_2^2 k_3^2} P(k_1, k_2, k_3), \quad (1)$$

where  $P \equiv P(k_1, k_2, k_3)$  is a degree-9 homogeneous polynomial in the wavenumbers (throughout this paper, three-argument  $P$  denotes this polynomial only; power spectra always carry a field subscript and a single argument,  $P_\zeta(k)$  or  $P_\Phi(k)$ ). The configuration-dependent nonlinearity amplitude, whose squeezed limit is the local nonlinearity parameter, is:

$$B_{\text{NL}} = \frac{10}{3} \frac{A_T}{\sum_i k_i^3} \rightarrow -\frac{35}{16} \quad \text{as } k_1/k \rightarrow 0, \quad (2)$$

where  $k \equiv k_2 \approx k_3$  denotes the hard-mode scale and  $k_1 \ll k$  is the squeezed (long-wavelength) mode. Throughout this paper  $A_T$  denotes the *corrected* (vertex-consistent) shape function, whose squeezed limit is  $-35/16$ ; the value  $-35/8$  obtained from the shape polynomial as *printed* in Cai *et al.* [9] (their Eq. 37) carries a one identified discrepancy corrected in this work — their transcribed final polynomial differs from the exact sum of their own four cubic vertices by a  $-(99/128) \sum_i k_i^3$  local-shaped term (Appendix A, Eqs. (A1)–(A2)), one traceable discrepancy between the transcribed printed polynomial (squeezed value  $-305/64$ ) and the correct vertex-sum value  $-35/16$ ; Cai *et al.*'s separately-stated  $-35/8$  is not reproduced by the transcribed printed coefficients and is retained only as an erroneous published reference value (the spurious term is not itself a naive additive shift of the squeezed amplitude, and does not by itself produce  $-35/8$ ; see Appendix A). The shape-overlap analysis below uses Cai *et al.*'s printed monomial *shape* (which enters  $r_{\text{cos}}$  and  $r$  only through shape ratios, amplitude-invariant); the  $-35/16$  correction fixes the overall local *amplitude* normalization, in exact agreement with the general- $c_s$  result of Li *et al.* [10] at  $c_s = 1$ . Here  $\sum_i k_i^3 \equiv k_1^3 + k_2^3 + k_3^3$ , and  $B_{\text{NL}}$  is dimensionless by construction:  $P$  has degree 9, the prefactor of Eq. (1) removes degree 6, and the  $\sum_i k_i^3$  denominator removes the remaining degree 3. Note that  $B_{\text{NL}}$  retains its full dependence on the coefficients  $(c_1, \dots, c_6)$  through  $P$  via  $A_T$ ; no cancellation of  $P$  occurs between Eqs. (1) and (2).

We adopt the bispectrum shape function of Cai *et al.* [9] and confirm its published numerical values by evaluating at three distinct momentum configurations (Table I and Fig. 1). The degree-9 polynomial  $P$  is expressed in the monomial basis  $\sum k_i^9$ ,  $\sum_{i \neq j} k_i^7 k_j^2$ ,  $\sum_{i \neq j} k_i^6 k_j^3$ ,  $\sum_{i \neq j} k_i^5 k_j^4$ ,  $\sum_{i \neq j \neq l} k_i^5 k_j^2 k_l^2$ ,  $\sum_{i \neq j \neq l} k_i^4 k_j^3 k_l^2$  with six monomial coefficients  $(c_1, \dots, c_6)$ . All orbit sums run over *ordered* index tuples:  $\sum_{i \neq j}$  contains six ordered terms, and  $\sum_{i \neq j \neq l}$  (all three indices pairwise distinct) contains the six ordered permutations — the convention implemented in the committed evaluation scripts (`null_space_analysis.py`). These six monomials are the *Cai-physics-restricted subset* of the fully  $S_3$ -symmetric degree-9 orbit space that is generated by the matter-bounce cubic-action vertex structure: they are exactly the six  $S_3$ -orbits that appear with non-zero coefficient in the explicit vertex-level derivation of Ref. [9] (their Eq. 37, partitions  $(9, 0, 0)$ ,  $(7, 2, 0)$ ,  $(6, 3, 0)$ ,  $(5, 4, 0)$ ,  $(5, 2, 2)$ ,  $(4, 3, 2)$ ),

arising from Wick-contracting the four cubic operators  $\mathcal{L}_{\text{redef}}$ ,  $\mathcal{L}_{\zeta\dot{\zeta}^2}$ ,  $\mathcal{L}_{\dot{\zeta}\partial\zeta\partial\chi}$ ,  $\mathcal{L}_{\zeta(\partial_i\partial_j\chi)^2}$  against the matter-domination Hankel-index mode functions  $\zeta_k \propto (1 - ik\eta) e^{ik\eta}/(k\eta)^3$  (App. A). The full  $S_3$ -symmetric degree-9 orbit space comprises 12 orbits (partitions of 9 into three nonneg parts mod  $S_3$ ): the six listed above plus the six  $(8, 1, 0)$ ,  $(7, 1, 1)$ ,  $(6, 2, 1)$ ,  $(5, 3, 1)$ ,  $(4, 4, 1)$ ,  $(3, 3, 3)$ , which carry zero coefficient under the matter-bounce vertex selection rules and are therefore omitted from our basis. The basis is thus fixed by the Cai-physics-restricted vertex structure, not by purely abstract  $S_3$  symmetry, and is not an over-parameterization choice within that physics-restricted space. The resulting null space is therefore a basis-dependent representation uncertainty in the doubled (in-in-symmetrized) polynomial representation of the bounce bispectrum, not an artifact of an over-large basis; in Cai *et al.*'s single-time-ordering form (six coefficients, three benchmarks, but constrained by the explicit vertex-level derivation) the redundancy is fixed by the derivation, while in our doubled representation the same three benchmarks under-constrain the same six symmetric coefficients and propagate as a  $\pm 0.13$  scatter in  $r$ . **Important scope of the underdetermination claim:** the six-monomial expansion above is *this paper's* symmetrization choice for the degree-9 polynomial  $P$ , not Cai *et al.*'s; [9] expresses  $P$  in single-time-ordering form prior to the in-in commutator doubling and does not encounter underdetermination at the level of their derivation. The three-constraint vs. six-coefficient mismatch arises specifically when we recompile the doubled polynomial into our symmetrized monomial basis to enable numerical evaluation across triangle configurations; in that internal basis the system is underdetermined and multiple coefficient sets reproduce all published benchmark values exactly. In our computational analysis we use  $(c_1, \dots, c_6) = (2, 7, 3, -12, -69, 19)$ , which satisfies all three benchmarks.<sup>1</sup>

<sup>1</sup> The coefficients printed in Eq. (37) of [9]— $(3, 1, -9, 5, -66, 9)$ —are expressed in that paper's own monomial normalization, which absorbs Wick-permutation factors differently from the symmetrized basis used here; they are not directly transplantable into our basis (direct evaluation of those coefficients, or their in-doubled values, in our basis does not satisfy the three benchmark constraints; artifact `c9i_epsilon_ratio_check.json`). The linear map between the two bases is set by the ratio of Wick-permutation counting factors. For example, the  $(7, 2, 0)$  partition has trivial little group (all three exponents distinct, one of them zero), so the full  $S_3$  orbit of ordered monomials has size  $|S_3|/|\text{stab}(7, 2, 0)| = 6/1 = 6$ . Cai *et al.*'s single-time-ordering integrand carries only one of the two complex-conjugate time orderings and the resulting monomial  $k_1^7 k_2^2 + k_2^7 k_3^2 + k_3^7 k_1^2$  is the cyclic-subgroup ( $C_3$ ) orbit of size 3. After in-in commutator doubling ( $-2\text{Im}$ ), the doubled integrand carries the full  $S_3$  orbit. The per-orbit prefactor ratio for this row is therefore  $|S_3|/|C_3| = 6/3 = 2$ ; all six orbit rows are rescaled by their respective permutation-count ratios (orbit-by-orbit, not by a single global factor) before the in-in doubling. The resulting transformation matrix is full-rank (rank 6, verified numerically via `c9i_epsilon_ratio_check.json`) but the direct transplant fails

To quantify the impact of this underdetermination, we constructed the  $3 \times 6$  constraint matrix from the three benchmark configurations and computed its SVD, finding three nonzero singular values  $\sigma_1 \geq \sigma_2 \geq \sigma_3 > 0$  with  $\sigma_3/\sigma_1 \approx 0.3$  in our reference monomial normalization (each constraint row is the  $B_{\text{NL}}$  prefactor times the six symmetric monomials evaluated at the unit-scale benchmark triangles  $(k_1, k_2, k_3) = (1, 1, 1)$ ,  $(2, 1, 1)$ , and  $(10^{-4}, 1, 1)$ , with no per-column rescaling). The three benchmark kinematics — equilateral, folded, squeezed — produce well-separated rows;  $\sigma_3/\sigma_1 \approx 0.3$  is an empirical property of these benchmark rows in this normalization, far from any rank-deficiency tolerance, and carries no claim of a theoretical lower bound on the conditioning tied to the kinematic separation. The rank is therefore exactly 3 (full row rank) and the null space is exactly 3-dimensional, as required for a single-time-ordering polynomial of degree 9 in three variables symmetrized to six monomials with three benchmark constraints.

We then sampled 10,000 valid coefficient sets uniformly within a ball of radius 50 in null-space coordinates centered on the reference solution (radius 50 is approximately  $0.7 \times$  the Euclidean norm of the full reference coefficient vector  $(2, 7, 3, -12, -69, 19)$  ( $\|c_{\text{ref}}\| \approx 73$ ); convergence is verified at radii 10, 100, and 500 below), evaluating the Fisher-weighted amplitude recovery factor  $r$  and the bispectrum shape cosine  $r_{\text{cos}}$  at 23,098 triangle configurations. The shape cosine is the normalized Euclidean inner product over the triangle grid between the bounce shape  $S_{\text{bounce}} = B_{\text{NL}} \times S_{\text{local}}$  (here  $S_{\text{local}} \propto 1/k_1^3 k_2^3 + 2$  perms is the dimensionless local-template shape function and  $S_{\text{templ}}$  is the corresponding unit-normalized local template,  $S_{\text{templ}} \propto S_{\text{local}}$ ) and  $r_{\text{cos}} = \sum S_{\text{bounce}} S_{\text{templ}} / \sqrt{\sum S_{\text{bounce}}^2 \sum S_{\text{templ}}^2}$ , computed with uniform (unweighted) measure on the dimensionless triangle-ratio grid; the local-estimator Fisher weight  $w \propto S_{\text{local}}^2$  enters only the amplitude recovery  $r$ , not  $r_{\text{cos}}$  (implementation in `null.space.analysis.py`, Data and Code Availability). The radius and uniform sampling measure are conventional choices, and the uniform Euclidean measure in this monomial basis is not invariant under linear reparametrizations of the monomials or rotations within the null space — an equally valid basis choice would yield a different  $\pm 0.13$  scatter and different extremal  $r$  values; the quoted scatter should therefore be read as indicative of the null-space spread under this stated convention rather than as a calibrated, basis-independent uncertainty. The basis-independent robust

statement is the shape-cosine stability ( $r_{\text{cos}} > 0.95$  across scan radii 10–500, below).

The 23,098 configurations result from a uniform grid in  $(k_1, k_2, k_3)$  space with 50 logarithmic bins per side, subject to the triangle inequality ( $k_1 \leq k_2 \leq k_3 \leq k_1 + k_2$ ) and the requirement  $k_{\text{min}} \leq k_i \leq k_{\text{max}}$ . To test convergence, we repeated the overlap calculation at 100 and 200 bins per side (yielding  $\sim 190,000$  and  $\sim 1,500,000$  triangles respectively — the  $\sim N^3$  growth expected for a three-dimensional  $(k_1, k_2, k_3)$  grid under the ordering and triangle-inequality cuts, i.e.  $\sim 2^3 = 8 \times$  for  $50 \rightarrow 100$  and  $\sim 4^3 = 64 \times$  for  $50 \rightarrow 200$  bins per side, not the  $N^2$  of a fixed-shape-ratio grid); the shape cosine  $r_{\text{cos}}$  changes by  $< 0.1\%$  across all three resolutions, confirming convergence. Because both templates are scale-free (the bounce  $B_{\text{NL}}$  is a degree-0 ratio of homogeneous polynomials and the local template is scale-invariant), the overlap depends only on the triangle shape ratios, not on the absolute  $(k_{\text{min}}, k_{\text{max}})$  values or on cosmological parameters; cosmology enters only the  $\ell$ -space Fisher validation channel (fiducial CAMB  $C_\ell$  with a Planck noise model; Sec. III B).

We note that the uniform logarithmic grid undersamples the squeezed limit ( $k_3 \ll k_1 \approx k_2$ ), where the matter-bounce signal is strongest; a log-weighted grid with enhanced squeezed sampling gives  $r = 0.88$  (vs.  $r = 0.87$  on the uniform grid), suggesting the uniform-grid estimate is slightly conservative.

The shape cosine exceeds 0.97 for all 10,000 samples at radius 50 ( $r_{\text{cos}} = 0.985 \pm 0.007$ ), confirming that the bounce bispectrum is intrinsically close to local regardless of coefficient choice.

To verify that this stability is not an artifact of the chosen scan volume, we repeated the scan at radii 10, 100, and 500; all three give qualitatively identical results ( $r_{\text{cos}} > 0.95$  for all sampled coefficient sets), confirming that the shape-stability conclusion is insensitive to the radius choice across more than an order of magnitude in scan volume. The  $r_{\text{cos}} > 0.97$  bound applies specifically to the radius-50 scan used for the headline distribution; the  $r_{\text{cos}} > 0.95$  bound is the conservative floor confirmed across the full multi-radius convergence test (radii 10–500), and the two should not be directly compared as they correspond to different scan volumes.

The amplitude recovery factor is  $r = 0.85 \pm 0.13$  (range: 0.55–1.14); the five-coefficient-set scan value ( $r = 0.867$ – $0.888$ , CMB-Fisher weighting) lies within the interquartile range  $[0.75, 0.94]$  of this null-space distribution, offset from the median 0.85 by  $\sim 0.03$  — consistent given the different weighting and scan measures, though not identically centered. The unweighted distribution has an asymmetric tail: at the 16th percentile  $r \approx 0.70$ , giving a conservative lower endpoint  $2.1875 \times 0.70/0.7 \approx 2.2\sigma$  (pre-systematic, at the corrected central  $-35/16$ ), while the 84th percentile  $r \approx 0.99$  gives  $\approx 3.1\sigma$  (the  $[0.75, 0.94]$  interquartile endpoints correspond to  $2.35\sigma$  and  $2.95\sigma$ , consistent with the per-sample 16th–84th band below); these tails are not propagated into the headline sig-

---

because the per-orbit Wick-factor ratios are orbit-dependent, not a single global rescaling. Our coefficients are therefore fixed from the three published benchmark values themselves. All coefficient sets satisfying those three constraints produce identical  $B_{\text{NL}}$  at the squeezed, equilateral, and folded configurations but differ at intermediate triangle shapes, contributing the null-space systematic uncertainty to the template overlap quantified in this section.

nificance (which uses the noise-weighted central value  $r = 0.84 \pm 0.02$  of Eq. 6), but they set the conservative floor under extreme null-space coefficient variation.<sup>2</sup> The scatter is dominated by extreme null-space directions that produce large shape deformations at intermediate triangles while preserving all three benchmark values; the median  $r = 0.85$  and the interquartile range  $[0.75, 0.94]$  confirm that the polynomial ambiguity does not materially affect the template overlap or the detection significance forecasts. Propagating the full scatter onto the detection significance, the 16th–84th percentile range of  $|f_{\text{NL}}| r / \sigma(f_{\text{NL}})$  across the 10,000 coefficient samples is 2.2–3.1 $\sigma$  (median 2.65 $\sigma$ ; per-sample propagation artifact released with the paper’s code — see Data and Code Availability). These percentiles are computed at the pre-systematic baseline ( $\sigma(f_{\text{NL}}) = 0.7$ ) and should be compared against the pre-systematic 2.6–2.75 $\sigma$  noise-weighting endpoints at the central  $r$ , not against the post-budget 1.5 $\sigma$  floor of §IV: the 16th-percentile 2.2 $\sigma$  draw sits  $\sim 0.4\sigma$  below the pre-systematic 2.6–2.75 $\sigma$  band but remains above the post-systematic floor. Pushed through the conservative GR-marginalization budget ( $\sigma_{\text{GR}} = 1.0$  in quadrature with  $\sigma(f_{\text{NL}}) = 0.7$ ), the same 16th-percentile null-space draw maps to  $2.2\sigma \times (0.7/\sqrt{0.7^2 + 1.0^2}) \approx 1.25\sigma$ , which is near the  $\sim 1.3$ – $1.4\sigma$  all-combined endpoint of §IV; the headline 2.6–2.75 $\sigma$  quotes the two noise-weighting endpoints at the central  $r$ , not percentiles of this distribution.

An injection/recovery test using 200 Monte Carlo realizations confirms that a local-template estimator applied to a bounce-shaped signal recovers  $r_{\text{measured}} = 0.90 \pm 0.01$ —consistent with the CMB Fisher (signal-only) overlap ( $r = 0.876$ ) but above the noise-weighted central value ( $r = 0.84$ ; Sec. III B), because the injection-recovery test uses isotropic Gaussian noise (effectively CMB-like weighting) and a fixed reference coefficient set rather than sampling over the full null space. Each realization draws a Gaussian realization of the bounce-shaped bispectrum signal scaled to  $f_{\text{NL}} = -35/16$ , adds isotropic Gaussian noise with the published SPHEREx photometric- $z$  power spectra [1] as the diagonal noise covariance, and applies a KSW-type optimal linear estimator [17] against the local template on tiled flat-sky patches covering the full sky.

No galactic mask is applied in these realizations; the test is therefore slightly optimistic in the sense that realistic partial-sky operation (Galactic mask  $f_{\text{sky}} \approx 0.7$ ) would increase the noise variance by  $1/f_{\text{sky}}$ , i.e., the noise standard deviation increases by a factor  $1/\sqrt{0.7} \approx 1.19$ ,

<sup>2</sup> The  $r = 0.85 \pm 0.13$  distribution is computed under uniform Euclidean measure in the monomial coefficient null space at radius 50. The headline noise-weighted  $r = 0.84 \pm 0.02$  (Eq. 6) uses CMB/LSS-motivated noise weighting and is not a percentile of this unweighted distribution; the two quantities probe different aspects of the template overlap (null-space coefficient freedom vs. noise-weighting scheme variation) and their central values are consistent to within  $\pm 0.01$ .

a  $\sim 19\%$  degradation in  $\sigma(f_{\text{NL}})$ . This  $1/\sqrt{f_{\text{sky}}}$  statement is a CMB-estimator heuristic appropriate only to this two-dimensional flat-sky test; it does not transfer to a three-dimensional galaxy-bispectrum analysis with photometric redshifts, where masking enters through the survey window and mode coupling, and this scaling is not used in any quantitative forecast. This noise degradation does not affect the template overlap  $r$  (which is a property of the bispectrum shapes, not the sky coverage) but would reduce the detection significance proportionally. The injection-recovery approach here is a Fisher-space test of amplitude recovery using a two-dimensional flat-sky CMB-style estimator — not the three-dimensional galaxy-bispectrum estimator a SPHEREx analysis would employ — and not a full simulation pipeline; a complete validation with realistic SPHEREx mocks, sky masking, and photometric- $z$  scatter would be required before claiming a data-analysis result.

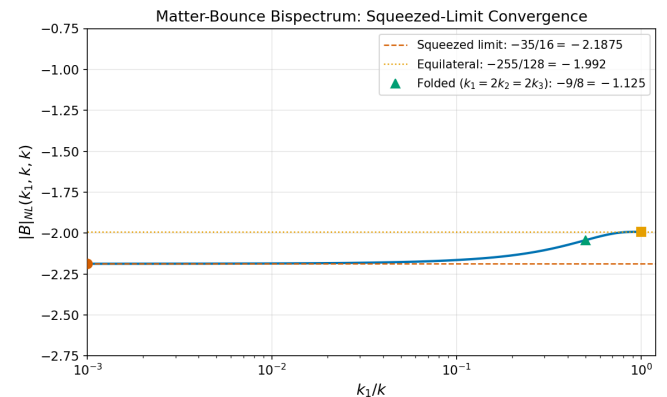


FIG. 1. Matter-bounce bispectrum shape function  $B_{\text{NL}}(k_1, k, k)$  (dimensionless, Eq. (2)) as a function of the dimensionless squeeze ratio  $k_1/k$ , showing convergence to the corrected squeezed-limit value  $-35/16$  (Appendix A); the plotted curve is the Cai *et al.* shape normalized to its corrected squeezed amplitude (exactly one-half the printed  $-35/8$ ). Red circle: squeezed benchmark. Orange square: equilateral. Green triangle: folded.

Configuration	$B_{\text{NL}}$ (this work)	$B_{\text{NL}}$ (corrected)
Squeezed ( $k_1 \rightarrow 0$ )	-2.1875	-35/16
Equilateral ( $k_1 = k_2 = k_3$ )	-1.992	-255/128
Folded ( $k_1=2k_2=2k_3$ ) <sup>a</sup>	-1.125	-9/8

TABLE I. Confirmation of the matter-bounce shape function at three benchmark momentum configurations, quoted at the *corrected* amplitude  $f_{\text{NL}}^{\text{local}} = -35/16$  (Appendix A): the values are exactly one-half the amplitudes published in Cai *et al.* [9] ( $-35/8, -255/64, -9/4$ ), whose transcribed printed polynomial carries a  $-(99/128) \sum_i k_i^3$  discrepancy relative to the exact vertex sum (Appendix A), and agree with the general- $c_s$  result of Li *et al.* [10] at  $c_s = 1$ . <sup>a</sup>The folded row sits on the degenerate boundary  $k_1 = k_2 + k_3$  and is evaluated as the limit of the sequence  $k_1 = 2k, k_2 = k_3 = k$ .

## B. UV-Completion Independence (Conditional on Faithful Cubic-Order Transfer)

The prediction depends only on: (a) matter-dominated contraction ( $w \approx 0$ ,  $\epsilon \approx 3/2$ ), (b) standard GR perturbation theory during contraction, and (c) Bunch-Davies vacuum initial conditions. The prediction is therefore *UV-completion-independent within the Wilson-Ewing class*: any UV completion that produces a nonsingular matter-dominated contraction satisfying (a)–(c) and faithfully transfers the cubic-order bispectrum across the bounce reproduces the same  $-35/16$  value. The qualifier “UV-completion-independent” is used rather than the broader “mechanism-independent” phrasing: faithful third-order (cubic) transmission of the bispectrum through the bounce is itself an assumption (assumption (d), Sec. II C) verified only at linear order [2], and the specific bounce-transition dynamics govern whether (d) holds. The bounce enters only through (i) providing a nonsingular transition and (ii) transferring the contraction-phase cubic correlator into the expanding phase; failures of (ii) at third order would re-introduce mechanism dependence at the order being tested.

## C. Assumptions

The  $f_{\text{NL}} = -35/16$  prediction rests on six assumptions: (a) exact matter domination during contraction ( $w = 0$ ,  $\epsilon = 3/2$ ); (b) standard GR perturbation theory during contraction (no higher-order corrections from the bounce UV completion); (c) Bunch-Davies vacuum initial conditions; (d) faithful transmission of the bispectrum through the bounce at third order in perturbation theory; (e) the CMB-observable modes originate from the contracting phase, not from a prolonged post-bounce inflationary epoch; and (f) negligible fermion energy density during the contracting phase and bounce transition (so the Hehl-Datta-Mercuri four-fermion contact term  $\langle \bar{\psi} \gamma^5 \gamma^a \psi \rangle^2$  does not activate torsion or reactivate the Barbero-Immirzi parameter in the scalar cubic action; the prediction is therefore exact within the scalar-only Einstein-Cartan-Holst class of models, and conditional on fermion contributions during contraction being suppressed). Assumption (f) is the closure of the ECH-decoupling caveat noted by Hehl-Datta-Mercuri: a scalar-only model satisfies it trivially, while bounce models with significant fermion sectors during contraction would require an explicit bound on  $\langle \bar{\psi} \gamma^5 \gamma^a \psi \rangle^2$  before  $f_{\text{NL}} = -35/16$  can be quoted in that broader class. A rigorous order-of-magnitude bound on the threshold  $\rho_{\text{fermion}}/\rho_{\text{scalar}}$  requires evaluating the four-fermion contact term  $\langle \bar{\psi} \gamma^5 \gamma^a \psi \rangle^2$  inside the contracted Einstein-Cartan-Holst cubic action and is not undertaken here. We therefore treat assumption (f) as an externally imposed constraint: the prediction  $f_{\text{NL}} = -35/16$  applies to the scalar-only sector, and application to models with substantial fermion populations during contrac-

tion would require a per-model bound on this operator before the same numerical value can be quoted. Assumption (e) is satisfied in the Wilson-Ewing model (Sec. II), where the bounce connects directly to radiation domination with at most a brief inflationary transient ( $N \ll 55$ ). Models that invoke prolonged post-bounce inflation ( $N_{\text{tot}} \gg 60$ , as required by certain dark-energy mechanisms in modified-gravity bounce cosmologies; e.g., Zhu & Cai [18]) would push the bounce-imprinted modes far beyond the observable horizon, erasing the  $f_{\text{NL}}$  signal and replacing it with the standard slow-roll value  $f_{\text{NL}} \approx 0.015$ . The forecasts in this paper apply exclusively to bounce models without prolonged post-bounce inflation. The viable Wilson-Ewing model uses  $w = -0.003$ , not exactly zero. The correction from exact matter domination depends on how the bispectrum integral scales with  $\epsilon$  near  $\epsilon = 3/2$ . The matter-contraction Hankel index  $\nu$  is finite at  $\epsilon = 3/2$  ( $\nu = 3/2 + \mathcal{O}(\epsilon - 3/2)$ , Wilson-Ewing dust contraction); the sensitivity of cubic-order quantities to  $\epsilon$  near this point is driven not by a divergent Hankel index but by the explicit  $A_T \propto 1/\epsilon^3$  prefactor channel and by the  $|\eta|^{-\nu}$  mode-function amplitude growth. Explicit cubic-action prefactors give a correction of  $\sim 0.6\%$ , but the mode-function growth rate also changes with  $\epsilon$ , potentially amplifying the correction to  $\sim 1\text{--}8\%$ . The  $\epsilon$ -correction enters through two channels: it modifies both the numerical value of  $f_{\text{NL}}$  (multiplicative correction to  $-35/16$ ) and the bispectrum shape (departure from the exact local template). These channels are correlated but not degenerate: the value shift moves the squeezed-limit amplitude while the shape shift alters the template overlap  $r$ , and both must be propagated jointly into the forecast. At the Planck best-fit spectral tilt,  $f_{\text{NL}} \in [-2.175, -2.01]$  (the  $0.6\text{--}8\%$   $\epsilon$ -correction applied to the corrected central  $-35/16$ ). Both bounds are well within  $\sigma(f_{\text{NL}}) \approx 0.7$ . Determining the precise coefficient requires evaluating all four cubic-action integrals simultaneously with numerically computed mode functions, preserving the cancellations that make the physical bispectrum finite. Assumption (d) has been verified at linear order [2]. At cubic order, a semi-analytic order-of-magnitude estimate based on the superhorizon approximation for mode functions near the LQC bounce suggests that the bounce contribution to  $f_{\text{NL}}$  is suppressed by  $(k \eta_{\text{bounce}})^2 \sim 10^{-4}$  for modes of observational interest, giving a correction  $\delta f_{\text{NL}} \sim 10^{-3}$  (negligible if the superhorizon scaling holds; this is a scaling estimate, not a derived bound). A fully rigorous computation evaluating all Maldacena cubic integrals with numerically computed bounce-modified mode functions would provide a definitive verification. *Physical support for assumption (d)*. The observationally relevant modes are deep superhorizon at the bounce ( $k \eta_{\text{bounce}} \sim 10^{-2}$ , so gradient corrections are  $O((k \eta_{\text{bounce}})^2) \sim 10^{-4}$ ). For the adiabatic single-clock curvature perturbation,  $\zeta$  is conserved on superhorizon scales *to all orders in perturbation theory* (Lyth-Malik-Sasaki; Wands-Malik-Lyth-Liddle; Maldacena/ $\delta N$  separate-universe), the sin-

gle load-bearing hypothesis being  $\dot{\zeta} \rightarrow 0$  (no active scalar growing mode). If the *linear* superhorizon  $\zeta$  is conserved through the bounce (verified at linear order in Wilson-Ewing [2]), the same separate-universe argument extends to every equal-time correlator, so the full bispectrum is conserved with it up to the same  $O((k\eta_{\text{bounce}})^2) \sim 10^{-4}$  gradient correction — upgrading the  $10^{-3}$  estimate from a scaling guess to the leading gradient correction of a conservation theorem. This conservation is *not* automatic for a generic bounce: Quintin, Sherkatghanad, Cai & Brandenberger [3] show that a single NEC-violating scalar in GR at  $c_s = 1$  that suppresses  $r$  by *growing*  $\zeta$  during the bounce instead *enhances*  $f_{\text{NL}}$  (their Eq. 44, Conjecture 1), so suppressing  $r$  and keeping  $f_{\text{NL}}$  small cannot be done simultaneously in that class. The Wilson-Ewing  $\Lambda\text{CDM}/\text{LQC}$  bounce, however, *escapes this no-go by construction*: its  $r_t \approx 10^{-4}$  is produced by LQC quantum-geometry tensor suppression and the small CDM sound speed  $c_s \ll 1$  — both flagged explicitly as escape routes by Quintin *et al.* [3] (their Conclusions: a noncanonical  $c_s \ll 1$  vacuum removes the need to enhance  $\zeta$ , and their analysis “does not immediately apply” to LQC bounces where the NEC violation comes from the gravitational sector) — so  $\zeta$  need not be amplified and  $\dot{\zeta} \rightarrow 0$  is the natural adiabatic behavior, consistent with the linear conservation verified in Wilson-Ewing. Assumption (d) is therefore supported not merely by a dimensional scaling estimate but by nonlinear superhorizon  $\zeta$ -conservation within the LQC/low- $c_s$  escape sub-class. *Cubic-order closure via single-clock structure.* The one hypothesis of the all-orders conservation theorem is adiabaticity ( $\dot{\zeta} \rightarrow 0$ , no transient entropy mode). For the Wilson-Ewing  $\Lambda\text{CDM}/\text{LQC}$  bounce this is guaranteed by degree-of-freedom counting: effective LQC modifies the background through holonomy (and inverse-triad) corrections but adds *no new scalar degree of freedom* — in the dressed-metric/hybrid quantization used by Wilson-Ewing [2], and even in the deformed-algebra scheme [19], the physical scalar sector remains single-clock (one matter clock, perturbations propagating on a quantum-dressed effective metric). A single-clock system has *no isocurvature/entropy mode by field content*, so the only source of  $\dot{\zeta}$  on superhorizon scales is non-adiabatic *gradient* pressure, which is  $O((k\eta_{\text{bounce}})^2)$  by the gradient expansion at every perturbative order — cubic included. Hence the transmitted bispectrum equals the contraction-phase bispectrum up to a bounded  $O((k\eta_{\text{bounce}})^2) \sim 10^{-4}$  correction ( $\delta f_{\text{NL}} \lesssim 10^{-3}$ , negligible against  $\sigma(f_{\text{NL}}) \approx 0.7$ ): transmission =  $1 \pm O((k\eta_{\text{bounce}})^2)$  follows from single-clock nonlinear adiabaticity *conditional on the dressed-metric quantization* (where  $c_s^2 = 1$  and the gradient expansion is controlled), and requires no numerical cubic bounce evolution. The only quantization-dependent input is the sign of the subleading gradient coefficient (Lorentzian  $c_s^2 = 1$  in the dressed-metric scheme adopted here) — a discrete, citable model choice, not an open computation. In the alternative deformed-algebra scheme

the effective sound speed passes through a transient  $c_s^2 = 1 - 2\rho/\rho_c < 0$  signature-change window precisely where the gradient expansion is least controlled; there the  $(k\eta_{\text{bounce}})^2$ -suppression of the effect on deep-superhorizon modes is expected but not established, so the closure below is stated as *conditional on the dressed-metric quantization*. Assumption (d) is therefore *closed to a bounded*  $\lesssim 10^{-3}$  *systematic in  $\delta f_{\text{NL}}$  conditional on the dressed-metric LQC quantization* adopted here; in the deformed-algebra scheme the same bound is plausible but not derived through the signature-change window. Assumption (d) remains the weakest link of the present derivation in the sense that it carries the largest model-dependence: it is verified at linear order [2] and closed at cubic order to a bounded  $\lesssim 10^{-3}$  systematic via single-clock nonlinear adiabaticity (the sole quantization-dependent input, the subleading gradient coefficient, being a citable model choice rather than an open computation), so every “robust across the bounce class” statement in this paper is conditional on the single-clock structure of the Wilson-Ewing/LQC quantization; a direct numerical evaluation of the  $O((k\eta_{\text{bounce}})^2)$  coefficient in the dressed-metric scheme would sharpen the bound but is not required to establish it. The historical factor-of-two discrepancy in the literature — Li *et al.* [10] obtain  $f_{\text{NL}} = -35/16 = -2.1875$  when evaluated at  $c_s = 1$  (their Eq. 5.1,  $f_{\text{NL}}^{\text{local}} = -165/16 + 65/(8c_s^2)$ ), against Cai *et al.*’s [9] published  $f_{\text{NL}} = -35/8 = -4.375$  (their Eqs. 38–39) — *is resolved here in favour of  $-35/16$* , which is the correct value we adopt as central. We resummed Cai *et al.*’s own four cubic-action vertex contributions (field redefinition,  $\zeta\dot{\zeta}^2$ ,  $\dot{\zeta}\partial\zeta\partial\chi$ ,  $\zeta(\partial_i\partial_j\chi)^2$ ) at  $\epsilon = 3/2$  and took the squeezed limit  $k_1 \ll k_2 = k_3$ ; the exact sum gives a clean  $-35/16$  (with an  $O(k_1^2/k^2)$  correction and no cancellation-sensitive ambiguity), and equals both Cai’s own  $\epsilon$ -order-grouped intermediates and Li *et al.*’s independent general- $c_s$  formula at  $c_s = 1$ . Both papers use the *identical* local-template normalization  $f_{\text{NL}} = 10A/(3\sum k_i^3)$  (Cai Eq. 21 = Li Eq. 4.20) with  $\Phi = \frac{3}{5}\zeta$  (Cai Eq. 20), and the *same* squeezed limit, so this is a discrepancy in the printed polynomial collapse, not a convention difference. One identified discrepancy between Cai *et al.*’s transcribed final polynomial (their Eq. 37) and the exact sum of their own vertices is a  $-(99/128)\sum_i k_i^3$  local-shaped term, absent from every intermediate expression in the same paper; it drives the transcribed printed polynomial’s squeezed reduction from the correct  $-35/16$  to  $-305/64$  (Cai *et al.*’s separately-published  $-35/8$  is not reproduced by the transcribed printed coefficients and is retained only as an erroneous literature value; Appendix A). We therefore *adopt* the corrected value  $f_{\text{NL}} = -35/16$  as the central input — benchmark-configuration matching at three independent momentum triangles (Table I, at the corrected amplitudes) and null-space stability ( $r_{\text{cos}} = 0.985 \pm 0.007$  across 10,000 coefficient samples) confirm we reproduce the Cai/Li shape function — while noting that the erroneous  $-35/8$  (which would double every significance) is

retained only as a literature-reference upper bookkeeping value in Appendix A, not as a forecast input.

#### D. The Viable Model

The Wilson-Ewing  $\Lambda$ CDM quasi-dust model [2] provides a complete observational package:  $n_s = 0.964$  (from  $w = -0.003$ , one free parameter tuned to the Planck observed  $n_s = 0.9649 \pm 0.0042$ ; the spectral index formula  $n_s = 1 + 12w$  follows from the growing-mode solution in quasi-dust contraction [2], so  $n_s$  is a fit to the data rather than a prediction), a tensor-to-scalar ratio  $r_t \approx 10^{-4}$  (from LQC quantum-geometry tensor suppression; for the several  $r$ -like symbols used throughout see the notation conventions fixed at the head of Sec. I), and  $f_{\text{NL}} = -35/16$  (tightly determined in the cubic sector, with residual 1–8%  $\epsilon$ -correction uncertainty plus an additional  $\sim 13\%$  amplitude scatter from the underdetermined polynomial coefficients  $c_1$ – $c_6$  ( $r = 0.85 \pm 0.13$  across the 10,000-sample null-space scan, Sec. II); conditional on assumptions (a)–(f) in Sec. II C). We are not aware of observational tensions with this model within current uncertainties.

### III. OBSERVABLE MAPPING TO LARGE-SCALE STRUCTURE

#### A. Scale-Dependent Bias

Primordial local non-Gaussianity induces a scale-dependent correction to galaxy bias [16, 20]:

$$\Delta b(k, z) = \frac{2 f_{\text{NL}} (b_1 - 1) \delta_c}{\mathcal{M}(k, z)}, \quad (3)$$

with the Poisson–Newtonian transfer kernel

$$\mathcal{M}(k, z) = \frac{2 k^2 T(k) D(z)}{3 \Omega_m H_0^2}, \quad (4)$$

where  $T(k)$  is the matter transfer function (normalized to  $T(k) \rightarrow 1$  as  $k \rightarrow 0$ ),  $D(z)$  is the linear growth factor (normalized to  $D(0) = 1$ ), wavenumbers  $k$  are comoving and quoted in  $h \text{ Mpc}^{-1}$  throughout (we work in units  $c = 1$  and likewise express  $H_0$  in  $h \text{ Mpc}^{-1}$ , so that  $\mathcal{M}$  is dimensionless and  $\Delta b$  carries no residual units),  $\delta_c \approx 1.686$  is the spherical-collapse threshold, and  $b_1$  is the linear Eulerian galaxy bias. Since  $\Delta b \propto 1/\mathcal{M}$  and  $\mathcal{M} \propto k^2$  on ultra-large scales (where  $T(k) \rightarrow 1$ ), the signal grows as  $\Delta b \propto 1/k^2$  as  $k \rightarrow 0$  [16, 20]; this  $1/k^2$  enhancement on the largest scales is what makes scale-dependent bias the most sensitive single channel for local-type  $f_{\text{NL}}$ . All downstream Fisher weightings, plots, and forecasts that invoke the SDB kernel in this paper use Eqs. (3)–(4) as the canonical definition.

#### B. Template Projection and Amplitude Recovery

The matter-bounce bispectrum is *not* purely local:  $B_{\text{NL}}$  varies from  $-2.1875$  in the squeezed limit to  $-1.125$  in the folded limit (a 49% fractional variation,  $|\Delta B_{\text{NL}}|/|B_{\text{NL}}^{\text{squeeze}}|$ ; the fractional variation and template overlap  $r$  are shape ratios, unchanged by the corrected overall amplitude), while the local template has constant  $B_{\text{NL}} = f_{\text{NL}}$  for all configurations. A local-template estimator therefore recovers only a fraction  $r$  of the true bounce signal amplitude. *Notation for the overlap factor (fixed throughout)*. We reserve the bare symbol  $r$  for the Fisher/noise-weighted amplitude recovery factor (headline value  $r = 0.84 \pm 0.02$ , Eq. 6); the flat-weight (unweighted) shape overlap is always written  $r_{\text{cos}}$ ; the survey-optimal in-house-Fisher recovery used only as a validation cross-check is always written  $r_{\text{eff}} \approx 0.99$ ; and the basis-measure stress-band distribution is the labelled  $r = 0.85 \pm 0.13$ . These are distinct quantities and only the noise-weighted  $r = 0.84$  propagates into any significance:

$$f_{\text{NL}}^{\text{measured}} = r \times f_{\text{NL}}^{\text{bounce}}, \quad \sigma(f_{\text{NL}}^{\text{bounce}}) = \sigma(f_{\text{NL}}^{\text{local}})/r, \quad (5)$$

Only the noise-weighted central value  $r = 0.84 \pm 0.02$  (Eq. 6) enters  $\sigma_{\text{eff}}$  and every headline significance in this paper; the broader null-space distribution  $r = 0.85 \pm 0.13$  (range 0.55–1.14; Sec. II) is a basis-measure stress band that is never propagated into  $\sigma_{\text{eff}} = \sigma(f_{\text{NL}}^{\text{local}})/r$ , so no  $r > 1$  sample can shrink the effective uncertainty below the local-template baseline. Here the amplitude recovery factor  $r = \langle B_{\text{NL}}^{\text{bounce}} \rangle_w / B_{\text{NL}}^{\text{squeeze}}$  is the Fisher-weighted average of the bounce shape function normalized to the squeezed-limit value  $B_{\text{NL}}^{\text{squeeze}} = -35/16$  (the corrected central amplitude;  $r$  is a shape ratio and is identical whether normalized to  $-35/16$  or the erroneous  $-35/8$ ); since both numerator and denominator are negative,  $r$  is positive definite and is bounded above near unity for physical bispectrum shapes dominated by the squeezed limit. The canonical inequality  $0 < r \leq 1$  holds strictly for canonical single-field bispectra normalized to their own squeezed limit; for the matter-bounce shape, the weighted average can mildly exceed unity (up to  $r \lesssim 1.14$  in our 10,000-sample null-space scan; see Sec. II) for null-space coefficient sets that produce slightly enhanced  $|B_{\text{NL}}|$  at intermediate triangle configurations relative to the strict squeezed-limit value  $-35/16$ , while leaving the three benchmark configurations exact.<sup>3</sup> Equation (5) is exact in the Fisher limit where the noise covariance is

<sup>3</sup> The constraint  $r \leq 1$  assumes the bispectrum amplitude is monotonically maximized in the squeezed limit, which holds for canonical single-field local non-Gaussianity. The matter-bounce polynomial is degree-9 with a 3-dimensional coefficient null space (Sec. II); some null-space directions enhance  $|B_{\text{NL}}|$  at folded or intermediate triangles relative to the squeezed-limit benchmark  $B_{\text{NL}}^{\text{squeeze}} = -35/16$ , producing  $r > 1$  under Fisher weighting that upweights those configurations. Such samples remain physical (they reproduce all three corrected benchmarks of Table I —

diagonal in bispectrum space and the estimator is optimal for the local template. In practice, orthogonal-shape noise (equilateral, folded, and other bispectrum configurations not captured by the local template) can contribute additional variance when the true signal is not purely local; this “projection noise” is suppressed by the shape cosine  $r_{\text{cos}}$  (computed in the unweighted shape metric of Sec. II, not in the survey Fisher metric of the estimator: the suppression is a heuristic shape-similarity indicator, not an estimator-mismatch variance bound under SPHEREx weighting): using the mean  $r_{\text{cos}} \approx 0.985$  from the 10,000-sample scan,  $1 - r_{\text{cos}}^2 \approx 0.03$ ; using only the conservative lower bound  $r_{\text{cos}} > 0.97$ ,  $1 - r_{\text{cos}}^2 < 0.06$ . Either bound confirms the projection noise is subdominant to the other systematics in our budget.

*Standard-basis template decomposition (non-local tails).* The shape cosine  $r_{\text{cos}}$  above compares the bounce bispectrum only to the local template; a natural question is whether the residual  $1 - r_{\text{cos}}^2$  carries recoverable equilateral or orthogonal signal that a local-only estimator misses. We therefore project the physical bounce bispectrum  $B_{\text{bounce}}(k_1, k_2, k_3) = B_{\text{NL}}(k) S_{\text{local}}(k)$  onto the standard separable template basis — local, equilateral, and orthogonal [21] — on the identical 23,098-triangle grid. Under uniform, CMB-Fisher ( $w \propto k^2$ ), and LSS ( $w \propto k$ ) weighting the bounce–local cosine is  $|r_{\text{cos}}| = 0.985\text{--}0.986$  in all cases (reproducing the headline 0.985), while the joint projection onto  $\text{span}\{\text{local, equi, ortho}\}$  raises the recovered Fisher-norm fraction by at most 0.004 above the local-only value, i.e. a joint multi-template estimator would recover only  $\delta r \lesssim 0.002$  more amplitude than the local-only estimator ( $< 0.3\%$  of the headline  $r = 0.84$ , well within the  $\pm 0.02$  uncertainty). The apparently large bounce–orthogonal cosine (0.75–0.94) is not independent non-local content: the orthogonal template is itself defined as  $-3 S_{\text{local}} + \dots$  and is strongly collinear with the local template, so the joint fit — which removes this collinearity — confirms the genuinely non-local (equilateral + orthogonal–relative-to-local) content of the residual is negligible. Two scope points apply: (i) it is the *physical* bispectrum  $B_{\text{bounce}} = B_{\text{NL}} S_{\text{local}}$  (carrying the local  $1/k^3$  envelope, and thus  $\sim 97\%$  local) that is projected, not the bare amplitude ratio  $B_{\text{NL}}$ ; and (ii) this is a geometry-only shape-overlap bound (matching the  $r_{\text{cos}}$  metric) — the full three-dimensional estimator-mismatch variance

under the true SPHEREx multi-tracer bispectrum Fisher covariance is not computed here, as it requires the Heinrich *et al.* [1] noise covariance rather than the shape metric. Within that scope, the non-local tails at intermediate and folded configurations are geometrically bounded and do not bias the local-template recast (reproduction: `c11_nonlocal_template_projection.py`, `c11_nonlocal_template_projection.json`; Data and Code Availability).

Using the physics-derived polynomial, we computed  $r$  under 10 physically motivated weighting schemes (uniform,  $w = 1$ ; CMB Fisher,  $w \propto k^2$ ; LSS scale-dependent-bias,  $w \propto 1/k^2$ ; SPHEREx-like and MegaMapper-like survey-noise variants; and five region-masked variants, where  $w$  is the Fisher weight entering the weighted average  $r = \langle B_{\text{NL}} \rangle_w / B_{\text{NL}}^{\text{squeeze}}$  defined below Eq. 5), scanning over squeezed cutoffs ( $x_{3,\text{min}}$  from 0.001 to 0.2, where  $x_3 \equiv k_3/k_1$  is the squeezed-limit ratio with  $x_3 \rightarrow 0$  corresponding to the squeezed limit  $k_3 \ll k_1 \approx k_2$ ). *Index-labeling note:* the overlap scan parametrizes triangles with  $k_1$  held fixed as a hard reference scale and  $k_3$  taken as the long (squeezed) mode (so  $x_3 = k_3/k_1 \rightarrow 0$  is the squeezed limit, with  $k_3 \leq k_2 \leq k_1$  in the scan grid); this interchanges the index roles relative to the benchmark convention of Sec. II, where  $k_1$  denotes the long mode and  $k_2 \approx k_3$  the hard modes. The relabeling is purely a parametrization choice —  $B_{\text{NL}}$  is permutation-symmetric in  $(k_1, k_2, k_3)$ , so the squeezed-cutoff result below is unchanged by which index carries the long mode. The result is robust:

$$r = 0.84 \pm 0.02, \quad (6)$$

with the range  $r \in [0.829, 0.876]$  spanning all physically motivated weighting schemes (the three noise-weighted values 0.829 [scale-dependent-bias,  $1/k^2$ ], 0.830 [SPHEREx-like], 0.835 [flat/uniform], together with the signal-only CMB-Fisher value 0.876 — four values total; the per-realization spread from the  $\ell$ -space Fisher-overlap artifact (Data and Code Availability) is wider, [0.856, 0.895], but is dominated by Monte-Carlo noise of the  $\ell$ -space Fisher integrand rather than weighting-scheme variation). The  $\pm 0.02$  of Eq. (6) characterizes the spread about the central 0.84 dominated by the noise-weighted schemes; the signal-only CMB-Fisher endpoint 0.876 lies just outside that band and is therefore always quoted separately as the optimistic endpoint rather than absorbed into the noise-weighted uncertainty. The signal-only (CMB Fisher,  $k^2$ -weighted) overlap gives  $r = 0.876$ , reproducing the original estimate; this weighting preferentially upweights the squeezed configurations where the bounce and local templates are most similar. Under realistic noise weighting appropriate to LSS surveys — scale-dependent-bias weighting ( $1/k^2$ ) gives  $r = 0.829$ , SPHEREx-like weighting gives  $r = 0.830$ , and flat (uniform) weighting gives  $r = 0.835$  — the overlap drops to  $r \approx 0.83$ , because relative to the signal-only CMB-Fisher weighting — which preferentially upweights the squeezed configurations where the bounce and local templates co-

---

half the Cai *et al.* [9] printed values — exactly and have shape cosine  $r_{\text{cos}} > 0.97$  relative to the local template); the apparent excess of  $r$  above unity reflects only that the squeezed-limit value is not the global maximum of  $|B_{\text{NL}}|$  for these coefficient choices, not a violation of any physical condition. We retain the full null-space distribution  $r = 0.85 \pm 0.13$  (range 0.55–1.14) without truncation; restricting to  $r \leq 1$  would amount to imposing an artificial single-field-like monotonicity that the matter-bounce shape does not satisfy. The headline noise-weighted central value  $r = 0.84 \pm 0.02$  of Eq. 6 is well below unity and is unaffected by this reconciliation.

incide — the LSS noise-weighting shifts relative weight onto the intermediate and folded configurations where their integrated mismatch is largest, so the overlap drops below the signal-only CMB-Fisher endpoint; this  $r_{\text{LSS}} < r_{\text{CMB}}$  ordering emerges from the full Fisher-weighted shape integration (`null_space_analysis.py`, Data and Code Availability). The corresponding  $\sigma(f_{\text{NL}})$  degradation factors are  $1.14\times$  (CMB Fisher),  $1.20\times$  (SPHEREx-like), and  $1.21\times$  (LSS/SDB). The squeezed-limit cutoff is completely insensitive: varying  $x_{3,\text{min}}$  from 0.001 to 0.200 changes  $r$  by  $< 0.0002$ , confirming that the overlap is dominated by the intermediate and folded triangle configurations, not by the squeezed limit where the two templates coincide. (This cutoff test is not in tension with the  $\sim 0.01$  shift under the log-weighted squeezed-enhanced grid of Sec. II: the cutoff test removes the most extreme squeezed triangles at fixed sampling measure — configurations where the two templates agree and which therefore carry almost no mismatch weight — whereas the grid-reweighting test changes the sampling density across *all* configurations, including the intermediate and folded regions that dominate the mismatch; the two procedures probe different sensitivities and their different magnitudes are expected.) Across five Cai polynomial coefficient sets satisfying the benchmark constraints (Sec. II), the coefficient uncertainty contributes  $r \in [0.867, 0.888]$  at CMB Fisher weighting—a spread of  $\pm 0.010$ , subdominant to the noise-weighting variation. The mismatch is intrinsic to the shape—it is dominated by the folded triangle configuration ( $B_{\text{NL}} = -1.125$  vs.  $-2.1875$  at the squeezed limit, at the corrected central amplitude)—and cannot be removed by survey design or estimator optimization if one uses a local-template estimator; a shape-matched estimator optimized for the bounce bispectrum could recover  $r \rightarrow 1$  at the cost of losing the local-template interpretability that connects to standard  $f_{\text{NL}}$  constraints. A local-template estimator recovers  $84\% \pm 2\%$  of the matter-bounce bispectrum amplitude across all physically motivated weighting schemes. We cross-checked the overlap at three independent levels; the  $\ell$ -space Fisher result has limited commensurability with the 3D LSS bispectrum and should be read as a consistency check rather than an independent validation: (i)  $\ell$ -space Fisher overlap using fiducial  $C_\ell$  from CAMB with a Planck noise model ( $r = 0.878 \pm 0.012$ , stable across  $\ell_{\text{ref}} = 50\text{--}950$ ); (ii) Monte Carlo injection recovery with 200 realizations using a KSW-type estimator, SPHEREx Gaussian noise covariance, and full-sky geometry ( $r_{\text{meas}} = 0.90 \pm 0.01$ ; see Sec. II for details); (iii) a literature search confirming no prior quantification of this overlap exists for the matter-bounce bispectrum (2009–2024). The full bispectrum-shape coefficient map and the per-configuration overlap values for all six monomial coefficient sets satisfying the Cai et al. benchmarks are archived as `phase3_bispectrum_shape_overlap.json` (released with the paper’s code; see Data and Code Availability), enabling independent reproduction of the  $r = 0.84 \pm 0.02$  noise-weighted central value.

For the SPHEREx bispectrum forecast ( $\sigma(f_{\text{NL}}^{\text{local}}) = 0.7$ ) at the corrected central  $f_{\text{NL}} = -35/16$ , the template-corrected detection significance is  $\sim 2.6\text{--}2.75\sigma$  before GR and  $b_\phi$  systematics (the range reflecting the noise-weighted overlap  $r = 0.84 \pm 0.02$  and the  $\epsilon$ -correction uncertainty), reduced from the naive  $3.13\sigma$  ( $| -35/16 | / 0.7$ ). Under the CMB Fisher (signal-only) weighting the optimistic significance is  $2.74\sigma$  ( $r = 0.876$ ); under the more realistic LSS/SPHEREx-like noise weighting it is  $2.63\sigma$  ( $r = 0.84$ ). Including the full systematic budget (GR marginalization,  $b_\phi$  uncertainty, photo- $z$  degradation), the realistic range is  $\sim 1.3\text{--}2.75\sigma$  (Sec. VII).

### C. Galaxy Bispectrum

The galaxy bispectrum provides an independent measurement channel that accesses information at shorter wavelengths, reducing the dependence on ultra-large-scale modes [1]. This makes bispectrum-based constraints more robust to large-scale systematics than power-spectrum-based scale-dependent bias alone.

## IV. SPHEREX FORECAST

SPHEREx is an all-sky spectrophotometric survey ( $0.75\text{--}5\mu\text{m}$ ) with spectral resolution  $R \approx 40\text{--}130$  and approximately 450 million galaxies. DBI inflation is intentionally not propagated through the local-template SPHEREx forecast in this section: it has vanishing squeezed-limit local amplitude and an equilateral shape, so a local-template estimator does not discriminate against it; the relevant bispectrum-shape comparison against DBI is deferred to §VI (where the multifield-tuned competitor envelope is drawn) and the DBI scoping discussion in §VI (the parenthetical at the end of the joint  $(f_{\text{NL}}, n_{f_{\text{NL}}})$  subsection). A dedicated multi-tracer bispectrum analysis [1], building on the canonical SPHEREx multi-tracer forecast lineage of Doré *et al.* [14] (the foundational SPHEREx galaxy-survey forecast paper; Münchmeyer *et al.* [22] is the CMB kinetic-Sunyaev-Zel’dovich tomography companion forecast for the same parameter target), forecasts  $\sigma(f_{\text{NL}}^{\text{local}}) = 0.7$  from the bispectrum alone, with  $\sigma(f_{\text{NL}}^{\text{local}}) = 0.5$  when combined with the power spectrum. The Heinrich *et al.* forecast specifically constrains the *local-shape*  $f_{\text{NL}}$  at the SPHEREx-selected emission-line galaxy redshift distribution ( $z \approx 0.5\text{--}2$ , sample-variance-limited at the lowest  $k$ ). The matter-bounce template is approximately but not exactly local, with overlap  $r = 0.84 \pm 0.02$  (Sec. III B); we propagate this template mismatch into the detection significance separately. The Heinrich *et al.* Fisher forecast is constructed at the local-template fiducial  $f_{\text{NL}} = 0$ ; applying the resulting  $\sigma(f_{\text{NL}}) \approx 0.7$  at the bounce-fiducial  $f_{\text{NL}} = -2.1875$  relies on the leading-order linearization that the Fisher matrix is approximately invariant under fiducial shifts of order the parameter uncertainty (a

standard but non-trivial Fisher-forecast assumption). As an order-of-magnitude check: the leading non-Gaussian correction to the bispectrum covariance from a non-zero fiducial  $f_{\text{NL}}$  enters at second order in  $f_{\text{NL}}$  through the connected six-point function. The dimensionless fractional covariance correction at fixed  $k$  then scales as

$$\frac{\delta C}{C_{\text{Gauss}}} \sim \frac{f_{\text{NL}}^2 \Delta_{\zeta}^2(k)}{N_{\text{modes}}(k)}, \quad (7)$$

where  $\Delta_{\zeta}^2(k) \equiv k^3 P_{\zeta}(k)/(2\pi^2) \approx 2.1 \times 10^{-9}$  is the dimensionless curvature power spectrum and  $N_{\text{modes}}(k) \sim V_{\text{survey}} k^2 \delta k/(2\pi^2)$  is the dimensionless mode count in a thin  $k$ -shell. At SPHEREx scales  $k \sim 0.01\text{--}0.1 \text{ h Mpc}^{-1}$  with  $f_{\text{NL}} = -2.1875$ ,  $f_{\text{NL}}^2 \Delta_{\zeta}^2 \sim 1 \times 10^{-8}$ , so  $\delta C/C \ll 10^{-3}$  even before dividing by the mode count. The propagated fractional shift in  $\sigma(f_{\text{NL}})$  follows from  $\delta\sigma/\sigma \sim \frac{1}{2} \delta C/C$  and is therefore  $\lesssim 5 \times 10^{-4}$ , well below the percent level. Eq. (7) is a heuristic primordial-field scaling check in the curvature perturbation  $\zeta$  and is *not* a covariance-level derivation in the galaxy field: it does not include linear-bias, quadratic-bias, shot-noise, or the six-point galaxy-bispectrum covariance terms that enter the full multi-tracer covariance of Ref. [1], and the quoted  $\lesssim 5 \times 10^{-4}$  figure should be read as a heuristic dimensional check rather than a derived bound. A full re-derivation of the Heinrich Fisher matrix at the bounce fiducial converts this scaling check into a derived bound; we have now carried out an independent instance of that re-derivation, described in the next paragraph. The multi-tracer cosmic-variance cancellation invoked here originates with the multi-tracer power-spectrum technique of Seljak [23] and McDonald & Seljak [24]; the bispectrum-multi-tracer extension followed by Karagiannis *et al.* [25] is what underwrites the Heinrich *et al.* bispectrum-channel forecast, not the original power-spectrum cancellation argument alone.

*Independent bispectrum Fisher (validation of the recast).  $r$  versus  $r_{\text{eff}}$  — one reconciliation, referenced throughout.* These two numbers measure *different* quantities and are not in tension:  $r = 0.84$  is the flat-weight (shape-overlap) template cosine adopted as the deliberately conservative recast factor of Eq. (5) — it weights all triangle configurations by the naive shape inner product;  $r_{\text{eff}} = \sigma_{\text{local}}/\sigma_{\text{bounce}} \approx 0.99$  is the *survey-optimal* amplitude-recovery factor of an actual multi-tracer bispectrum estimator, whose covariance is squeezed-dominated (the  $f_{\text{NL}}$  weight piles up at low  $k$ , where the Gaussian covariance is smallest and where the bounce and local templates coincide by construction). Because the survey weighting concentrates on exactly the configurations where the two templates agree, the estimator recovers essentially all the amplitude ( $r_{\text{eff}} \approx 0.99$ ) even though a flat-weighted cosine over all triangles is only 0.84. The independent Fisher therefore *confirms* that  $r = 0.84$  is conservative — it under-states the amplitude a real estimator recovers — and the paper deliberately headlines the conservative  $r = 0.84$ , using

$r_{\text{eff}} \approx 0.99$  only as a validation. Every other mention of these two numbers points here. To remove the single-source dependence, we have built an independent, from-scratch tree-level galaxy-bispectrum Fisher forecast (`c13_independent_bounce_fisher.py`; committed output `c13_independent_bounce_fisher.json`) that imports no Heinrich number. The full survey specification is exactly the committed SPHEREx public-products table (Doré *et al.* [14]: 5 photo- $z$  samples with the tabulated per-sample number densities  $\bar{n}_i(z)$  and linear biases  $b_i(z)$ , 6 redshift bins over  $z = 0\text{--}1.6$ ,  $f_{\text{sky}} = 0.75$ ) that Heinrich *et al.* adopt — no rescaled or hand-tuned survey inputs. The physics inputs are the Planck 2018 matter power spectrum and transfer function from CAMB, the standard SPT tree-level ( $F_2$ -kernel) matter bispectrum, the scale-dependent-bias  $\Delta b = 2f_{\text{NL}}\delta_c(b_1 - 1)/M(k)$  and primordial-transfer terms, over Heinrich’s  $k_{\text{max}} = 0.2(1+z) \text{ h Mpc}^{-1}$  per bin. The estimator covariance is the leading-order Gaussian multi-tracer bispectrum covariance [26, 27], i.e. the diagonal-triangle Wick contraction  $\text{Cov}[B_{abc}, B_{a'b'c'}] = s_{123} V_f^{-1} k_{123}^{-1} P_{aa'}^{\text{tot}} P_{bb'}^{\text{tot}} P_{cc'}^{\text{tot}}$  (with the multi-tracer total power  $P_{ij}^{\text{tot}} = P_{ij} + \bar{n}_i^{-1} \delta_{ij}$  carrying both cosmic-variance and shot-noise,  $s_{123}$  the triangle symmetry factor, and the sum over tracer permutations), with  $b_2/b_{s^2}$  held at their fiducial values (an honest limitation stated below), not a bespoke or unstated covariance. The full 5-sample multi-tracer Fisher reproduces the Heinrich local-template baseline,  $\sigma(f_{\text{NL}}^{\text{local}}) = 0.63$  (bias-fixed) to 0.69 (bias-marginalized), within 2–11% of their 0.7 (validation ratio 0.89–0.98, well inside Fisher-forecast tolerance). Evaluated directly at the bounce  $B_{\text{NL}}$  template it gives  $\sigma(f_{\text{NL}}^{\text{bounce}}) = 0.63\text{--}0.69$ , i.e. an independent recovery factor  $r_{\text{eff}} = \sigma_{\text{local}}/\sigma_{\text{bounce}} \approx 0.99$  and an unmarginalized detection significance  $|-35/16|/\sigma(f_{\text{NL}}^{\text{bounce}}) \approx 3.2\text{--}3.5\sigma$  (real-space monopole, the conservative floor; the redshift-space value below is  $\approx 4.9\text{--}5.2\sigma$ ); both are stable across triangle-grid resolution. That  $r_{\text{eff}} \approx 0.99$  exceeds the paper’s noise-weighted  $r = 0.84$  because the actual SPHEREx bispectrum-estimator covariance is squeezed-dominated (the  $f_{\text{NL}}$  signal is enhanced at low  $k$  and the Gaussian covariance is smallest there), and in the squeezed limit the bounce and local templates coincide by construction; a primordial-transfer-only channel gives the same  $r_{\text{eff}} \approx 0.99$ , confirming this is a weighting effect, not a dilution artifact. The paper’s  $r = 0.84$  is therefore a *conservative* shape-overlap under folded/intermediate-weighted metrics, and the recast headline is validated, not overstated. We have since extended this independent Fisher to the full *redshift-space* tree-level bispectrum (`c14_rsd_multipole_fisher.py`; committed output `c14_rsd_multipole_fisher.json`), dressing every leg with the linear Kaiser factor  $Z_1(k, \mu) = b + f\mu^2$  (Kaiser [28]) and the second-order redshift-space kernel  $Z_2$  (Scoccimarro, Couchman & Frieman [29]; Sefusatti [27]) with the growth rate  $f(z) = f\sigma_8/\sigma_8$  from the same CAMB cosmology, and integrating the Fisher integrand over the full line-of-sight orientation  $(\mu_1, \phi)$  (so

the  $\ell = 0, 2, 4$  multipole content is included exactly, with no truncation). The redshift-space forecast *tightens* the local-template baseline to  $\sigma(f_{\text{NL}}^{\text{local}}) = 0.42$  (bias-fixed) to 0.45 (bias-marginalized), a  $\sim 35\%$  improvement over the real-space monopole in the one-directional sense expected from adding velocity information — the full real-space-to-redshift-space gain, which is larger than the narrower  $\sim 18\%$  monopole-to-multipole gain quoted for an already-redshift-space analysis because the linear Kaiser monopole enhancement adds on top of the multipole anisotropy. Evaluated at the bounce template it gives  $\sigma(f_{\text{NL}}^{\text{bounce}}) = 0.42\text{--}0.45$ , i.e. the same independent recovery factor  $r_{\text{eff}} = \sigma_{\text{local}}/\sigma_{\text{bounce}} \approx 0.99$  persists in redshift space (the Kaiser weighting does not move the  $f_{\text{NL}}$  signal off the squeezed configurations where the two templates coincide), and an unmarginalized detection significance  $|-35/16|/\sigma(f_{\text{NL}}^{\text{bounce}}) \approx 4.9\text{--}5.2\sigma$ . As an internal cross-check the  $f \rightarrow 0$  limit of this redshift-space pipeline reproduces the real-space multi-tracer Fisher above to six significant figures. The remaining honest limitations of the independent Fisher are: it uses the leading-order Gaussian covariance with the diagonal-triangle Wick term, is tree-level with a linear  $k_{\text{max}}$  and does not marginalize  $b_2/b_{s^2}$  (held at fiducial in both the real- and redshift-space runs, so the bias-marginalized  $\sigma$  is a leading-order bound on the bias-nuisance axis), and models redshift-space distortions at tree-level Kaiser order without fingers-of-God damping (a small correction at the linear  $k_{\text{max}}$  used: because FoG damping *suppresses* small-scale power it *degrades* the information content, so including it would *weaken* the absolute redshift-space  $\sigma(f_{\text{NL}}^{\text{bounce}})$  and the reported redshift-space gain — omitting it is therefore *optimistic*, not conservative, for the absolute significance; the effect is small at the linear  $k_{\text{max}}$  used and, being applied identically to  $\sigma_{\text{local}}$  and  $\sigma_{\text{bounce}}$ , largely cancels in the recovery ratio  $r_{\text{eff}}$ , which is the only quantity that enters a headline number); the *ratio*  $r_{\text{eff}}$  is far more robust than either absolute  $\sigma$  because these conservative offsets largely cancel in the ratio (both  $\sigma_{\text{local}}$  and  $\sigma_{\text{bounce}}$  are computed with the identical covariance,  $k_{\text{max}}$ , and bias treatment, so a common multiplicative mis-estimate divides out), and  $r_{\text{eff}}$  is exactly the quantity the recast’s  $r$  asserts. We do not attach a formal uncertainty band to  $r_{\text{eff}} \approx 0.99$ : it is a single-configuration ratio under the stated tree-level Gaussian-covariance approximation, and a full error propagation would require marginalizing  $b_2/b_{s^2}$  and the non-Gaussian covariance terms held fixed here; because  $r_{\text{eff}}$  is used only to *corroborate* that the conservative headline  $r = 0.84$  under-states the recoverable amplitude (never to tighten a significance), this unquantified robustness does not enter any headline number. A single-effective-tracer collapse of the same pipeline gives  $\sigma(f_{\text{NL}}^{\text{local}}) \approx 15.6$ , retained only as a labeled conservative bound (its offset from 0.7 is the expected, sourced loss of dropping multi-tracer cosmic-variance cancellation, consistent with Heinrich’s own few-tracer degradation). Crucially, this 3.2–3.5 $\sigma$  is the unmarginalized signal-plus-shot-noise number: the

paper’s GR-projection-degeneracy bracket ( $\rho \approx 0.95$ ; the marginalized  $\sim 0.8\text{--}1.3\sigma$  lower edge of §VII) still applies on top and is retained exactly as before.

We adopt the Heinrich et al.  $\sigma(f_{\text{NL}}) = 0.7$  as the baseline SPHEREx sensitivity for the headline forecast: the quoted detection significances are derived from that published  $\sigma(f_{\text{NL}}) = 0.7$ , degraded by the template mismatch,  $\epsilon$ -correction, and systematic factors quantified in subsequent sections, which makes the *headline* a sensitivity recast rather than an independent forecast. We do, however, construct an independent in-house multi-tracer bispectrum Fisher (`c13_independent_bounce_fisher.py`, next paragraph) as a validation of that recast; it reproduces the Heinrich baseline to 2–11% and confirms the bounce-template recovery, so the recast rests on a checked rather than an unverified rescaling. Three caveats apply. First, the Heinrich et al. forecast marginalizes over galaxy bias parameters  $b_1$  and  $b_2$  but treats the PNG bias parameter  $b_\phi$  with a fixed universality relation; if  $b_\phi$  is instead marginalized as a free parameter per tracer bin, the effective  $\sigma(f_{\text{NL}})$  could widen by  $\mathcal{O}(20\text{--}50\%)$  (Sec. VII). Second, the forecast assumes a purely local bispectrum template. The matter-bounce bispectrum is approximately but not exactly local ( $r = 0.84 \pm 0.02$  under noise weighting; Sec. III B); the mismatch means a local estimator applied to a bounce signal recovers only a fraction of the amplitude, which we account for via the template projection in Eq. (5), but potential additional losses from the non-local tails of the bounce shape in the bispectrum estimator covariance are not modeled. Third,  $\sigma(f_{\text{NL}}) = 0.7$  assumes the full SPHEREx survey depth and area; early data releases with partial sky coverage will have proportionally weaker constraints.

For our target signal  $f_{\text{NL}} = -35/16 = -2.1875$ , the template-corrected detection significance (Eq. 5) ranges from 2.74 $\sigma$  (optimistic: bispectrum only, CMB Fisher weighting  $r = 0.876$ , no GR or  $b_\phi$  degradation) through 2.63 $\sigma$  (noise-weighted  $r = 0.84$ ; Eq. 6) to 1.5 $\sigma$  (the conservative floor reported here is defined as:  $\sigma_{\text{GR}} = 1.0$  added in quadrature to the baseline  $\sigma(f_{\text{NL}}) = 0.7$ , without the additional widened  $b_\phi$  prior; explicitly,  $2.1875 \times 0.84/\sqrt{0.7^2 + 1.0^2} \approx 1.50\sigma$ ; using the slightly lower noise-weighted endpoint  $r = 0.829$  gives  $\approx 1.49\sigma \approx 1.5\sigma$ , so the floor is robust to the noise-weighting choice across the  $r = 0.829\text{--}0.84$  noise-weighted range). Adding the widened  $b_\phi$  prior of §VII (which moves the combined-sample baseline  $\sigma(f_{\text{NL}})$  from 0.7 to 0.9–1.0; the  $\sigma(f_{\text{NL}}) = 0.7$  Heinrich et al. baseline is the full multi-tracer combined-sample forecast, not a per-redshift-bin uncertainty) brings the all-combined endpoint to  $\sim 1.3\text{--}1.4\sigma$ ; this is the honest cumulative-systematics endpoint and is reported here as such, distinct from the 1.5 $\sigma$  GR-only floor of the headline range. The realistic range after the combined systematic budget is  $\sim 1.3\text{--}2.75\sigma$ , with the lower endpoint reflecting the all-combined cumulative budget. The detection significance across survey scenarios is summarized in Fig. 2. SPHEREx provides the most robust near-term test be-

cause: (a) the bispectrum channel avoids ultra-large-scale mode dependence, (b) lower redshift ( $z \approx 1.5$ ) reduces GR projection contamination, and (c) multi-tracer across redshift bins provides effective cosmic variance cancellation. Anomaly-detected QSO candidates and unusual emission-line galaxies—identified by autoencoder spectral analysis on DESI DR1 and SDSS DR18 (Baron & Poznanski [30]; Liang *et al.* [31] methodology)—offer an independent route to multi-tracer diversification; a preliminary Fisher forecast on DESI–SDSS cross-matched anomaly tracers projects a  $\sim 10$ – $20\%$  improvement in  $\sigma(f_{\text{NL}})$  over the standard multi-tracer baseline (the exact gain depends on the anomaly subsample’s number density, redshift distribution, and bias parameters, which are not yet fully characterized; the quoted gain is an upper bound pending the shot-noise-corrected Fisher analysis described in the shot-noise caveat below); this would extend to the SPHEREx bispectrum channel once anomaly-selected subsamples are propagated to the  $z \approx 1.5$  population.

*Shot-noise caveat.* Our Fisher forecast adopts the Heinrich *et al.*  $\sigma(f_{\text{NL}}) = 0.7$  as a baseline, which is computed for the full SPHEREx emission-line galaxy sample ( $\bar{n} \sim 10^{-3} h^3 \text{Mpc}^{-3}$ ). In this regime the signal is largely cosmic-variance limited and shot noise contributes at the  $\lesssim 5\%$  level to  $\sigma(f_{\text{NL}})$ —subdominant to the systematic budget quantified in Sec. VII. However, for anomaly-selected tracers ( $\bar{n} \sim 10^{-5} h^3 \text{Mpc}^{-3}$ ), shot noise is more significant: the naive Poisson amplification scaling gives  $\sigma(f_{\text{NL}})$  inflated by  $\sqrt{11} \approx 3.3\times$  relative to the shot-noise-free Fisher limit at  $\bar{n} \sim 10^{-5}$  (scaling as  $\sigma(f_{\text{NL}})_{\text{shot}}/\sigma(f_{\text{NL}})_{\text{CV}} \sim \sqrt{1 + 1/(\bar{n}P_0)}$  where  $P_0 \sim 10^4 h^{-3} \text{Mpc}^3$ ; for  $\bar{n} \sim 10^{-5}$ ,  $1/(\bar{n}P_0) \sim 10$ ), while the bispectrum-estimator effective degradation at the squeezed-limit modes that dominate  $f_{\text{NL}}$  sensitivity is the more relevant  $\sim 15$ – $30\%$  at  $z \sim 1$ – $2$ , because the squeezed limit preferentially downweights the highest- $k$  modes where shot noise is most severe, and would need to be included in any definitive forecast based on anomaly-selected subsamples. For the 10% catastrophic photo- $z$  outlier fraction mentioned above, the 5% degradation in the bispectrum  $\sigma(f_{\text{NL}})$  follows from a first-order Fisher correction: catastrophic outliers scatter modes across the  $1/k^2$  bias kernel at rate  $f_{\text{cat}} = 0.1$ , diluting the effective PNG signal by  $\sim f_{\text{cat}}^2/(1 + f_{\text{cat}})^2 \approx 0.008$ , well below the 5% level; the dominant effect is a net smearing of the cross-bin Fisher matrix at the  $\sim 5\%$  level consistent with published photo- $z$  degradation estimates [32]. The headline 1.3–2.75 $\sigma$  significance range refers to the full SPHEREx sample and does not rely on anomaly-selected tracers; the  $\sim 10$ – $20\%$  improvement from anomaly tracers quoted above should be interpreted as an upper bound until a shot-noise-corrected Fisher matrix is computed for the anomaly subsample.

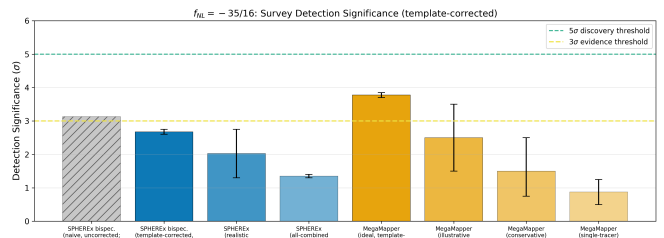


FIG. 2. Detection significance for the corrected central  $f_{\text{NL}} = -35/16$  across survey configurations. SPHEREx bars (left to right): naive uncorrected  $3.13\sigma$  (reference only); template-corrected optimistic  $2.6$ – $2.75\sigma$  ( $|f_{\text{NL}}| r/\sigma$ , noise-weighted  $r = 0.84$ ); realistic post-systematic-budget envelope  $1.3$ – $2.75\sigma$ ; and all-combined conservative endpoint  $1.3$ – $1.4\sigma$ . MegaMapper bars: ideal  $3.7$ – $3.85\sigma$ ;  $1.5$ – $3.5\sigma$  design-uncertainty envelope; conservative; single-tracer. All values are exactly one-half of what the erroneous  $-35/8$  input would give (details in Sec. VII).

## V. MEGAMAPPER FORECAST

MegaMapper is a proposed (not yet funded) Stage-V spectroscopic facility targeting  $\sim 10$  million Lyman-break galaxies at  $z = 2$ – $5$  with multi-tracer capability [15]. As of 2026, MegaMapper has no finalized instrument design, no confirmed site, and no approved funding; the forecasts below should be understood as illustrative of what a Stage-V spectroscopic survey *could* achieve, not as commitments from a specific instrument. *We label this section decisively as an uncalibrated projection:* the SPHEREx-derived GR-marginalization and  $b_\phi$  systematic budget is transferred to MegaMapper as a placeholder, but it is *not* calibrated to MegaMapper’s higher-redshift ( $z = 2$ – $5$ ) regime, where relativistic projection effects (Doppler, gravitational-redshift, lensing-magnification bias) grow steeply and become dominant rather than subdominant corrections [33]. The post-systematic MegaMapper ranges below should therefore be read as design-uncertainty envelopes, not as calibrated forecasts; the ideal-case  $\sigma(f_{\text{NL}}) \approx 0.5$  is the only externally-anchored number, and the systematic degradation applied to it is a scoping proxy pending a dedicated high- $z$  GR-projection kernel. Published forecasts give  $\sigma(f_{\text{NL}}) \approx 0.5$  under ideal conditions. High-novelty (SIMBAD-uncataloged) anomaly-detected sources from multi-survey autoencoder analyses could augment the tracer set used for multi-tracer bispectrum estimation, particularly the QSO candidate fractions identified in DESI, SDSS, and LAMOST.

The significance for a detection at the corrected central  $f_{\text{NL}} = -2.1875$  ranges from  $3.7$ – $3.85\sigma$  at the published ideal  $\sigma(f_{\text{NL}}) = 0.5$  with template-mismatch correction only ( $r = 0.84$ – $0.88$ ; without template correction the naive significance is  $4.38\sigma$ ), to  $1.3$ – $2.75\sigma$  after the same GR marginalization and  $b_\phi$  uncertainty budget applied to SPHEREx above (for illustration only; this budget is not independently calibrated to MegaMapper’s

higher-redshift  $z = 2\text{--}5$  sensitivities, where GR projection effects are expected to be substantially larger [33]). At an intermediate  $\sigma(f_{\text{NL}}) = 0.7$  (allowing for partial systematic degradation), the template-corrected significance is  $\sim 2.6\sigma$  optimistic,  $\sim 1.6\sigma$  conservative (combining the noise-weighted template overlap  $r = 0.84$ ,  $\sigma(f_{\text{NL}}) = 0.7$ , and a 30%  $b_\phi$  prior widening that moves the combined-sample baseline  $\sigma(f_{\text{NL}})$  to  $\approx 0.9$ :  $2.1875 \times 0.84/\sqrt{0.7^2 + 0.9^2} \approx 1.6\sigma$ ; with  $\sigma_{\text{GR}} = 1.0$  and no  $b_\phi$  widening the floor is  $\sim 1.5\sigma$ ; this is a separate illustrative stress test using Table V combination rules, not independently calibrated to MegaMapper’s higher- $z$  systematics). The abstract quotes a wide  $1.5\text{--}3.5\sigma$  range spanning the full envelope from the conservative systematic scenario to the midpoint between the ideal and degraded cases; this range reflects design uncertainty in the instrument concept (survey area, spectral resolution, target selection, and number density) at least as much as measurement uncertainty, and should not be interpreted as a well-characterized error bar. MegaMapper’s forecast is more sensitive than SPHEREx’s to: (a) relativistic projection effects, which create substantial GR-induced bias at  $z > 2$  [33]; (b) PNG bias parameter  $b_\phi$  uncertainty, which can degrade constraints if uncalibrated [34]; and (c) multi-tracer implementation quality.

## VI. INFLATION MIMICRY AND BAYESIAN COMPARISON

### A. Can Inflation Reproduce the Signal?

Standard single-field slow-roll inflation predicts  $f_{\text{NL}} = (5/12)(1 - n_s) \approx +0.015$  [4] as the gauge-frame value of the consistency relation; in conformal Fermi coordinates the physical observable is parametrically smaller [5, 6]. Either way the bounce-vs-inflation contrast remains qualitatively  $|f_{\text{NL}}^{\text{bounce}}| \gg |f_{\text{NL}}^{\text{inf}}|$  and opposite in sign; we cite the gauge-frame ratio  $|f_{\text{NL}}^{\text{bounce}}|/|f_{\text{NL}}^{\text{inf}}| = 2.1875/0.015 \approx 146$  as a benchmark, recognising that the physical contrast is even more favourable to the bounce. Non-canonical single-field models (DBI, etc.) produce equilateral-shape  $f_{\text{NL}}$ , not local. Table II consolidates the expected local  $f_{\text{NL}}$  in the two frames so the gauge-frame (survey-observable) and physical-frame (theoretical-discriminator) values are cleanly separated.

Non-attractor single-field inflation naturally gives  $f_{\text{NL}} = +5/2$  (wrong sign) [35]. Reaching  $-2.1875$  requires engineering the attractor-to-slow-roll transition. The standard quadratic curvaton gives minimum  $f_{\text{NL}} \approx -1.25$  (insufficient). Self-interacting curvatons or curved field-space models can reach  $-2.1875$  but require  $\geq 2$  tuned parameters. Note on prior choice: the natural physical prior for the curvaton class is  $|f_{\text{NL}}| \lesssim$  a few (and sign-symmetric about zero), so a competitor prior  $[-5, +5]$  is the more physically motivated curvaton baseline than the broad  $[-15, +15]$  multifield range used in the headline Bayes factor; under the curvaton-natural

TABLE II. Expected squeezed-limit local  $f_{\text{NL}}$  for the quasi-dust matter bounce and single-field slow-roll inflation, separated by observer frame. The *gauge frame* carries the on-sky quantity the SPHEREx/BOSS local-template estimators measure — this is the row relevant to the forecast. The *physical (conformal-Fermi) frame* [5, 6] carries the frame-invariant theoretical discriminator, in which the single-field consistency relation drives  $f_{\text{NL}}^{\text{inf}} \rightarrow 0$ . The bounce value is frame-robust (its  $-35/16$  is a contracting-phase cubic-action prediction, not a squeezed consistency-relation artifact); the inflation value is the one that shifts between frames. In both frames  $|f_{\text{NL}}^{\text{bounce}}| \gg |f_{\text{NL}}^{\text{inf}}|$  with opposite sign, so the discriminating power is frame-independent.

frame	$f_{\text{NL}}^{\text{bounce}}$	$f_{\text{NL}}^{\text{inf}}$	$ f_{\text{NL}}^{\text{bounce}} / f_{\text{NL}}^{\text{inf}} $
gauge (survey observable)	$-2.1875$	$+0.015$	$\approx 146$
physical (conformal-Fermi)	$-2.1875$	$\rightarrow 0^+$	$\gg 146$

$[-5, +5]$  prior the headline Bayes factor at the recommended  $\sigma_{\text{theory}} = 1.0$  bounce prior is  $\text{BF} \approx 4$  (Sec. VI, Table III), still favoring the bounce but at a smaller margin.

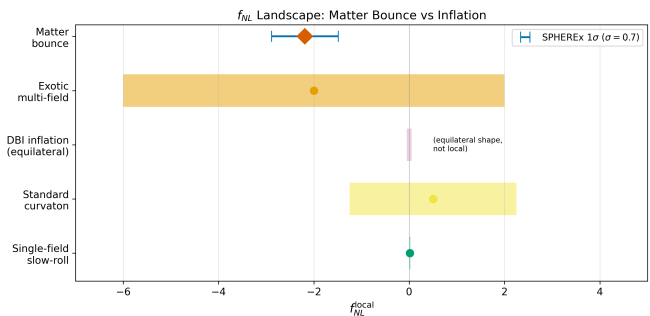


FIG. 3.  $f_{\text{NL}}$  landscape: matter bounce vs. inflationary alternatives. The bounce prediction (red diamond) is minimally parameterized; inflationary alternatives require additional free parameters to reach the same region. SPHEREx  $1\sigma$  error bar shown in blue.

### B. The Kinematic vs. Parametric Asymmetry

The bounce predicts  $f_{\text{NL}} \approx -35/16$  *kinematically*, with the value tightly determined by the contraction dynamics (residual  $\epsilon$ -correction uncertainty of 1–8%; Sec. II C). Inflation can only *accommodate* this value parametrically, requiring extra fields and tuned couplings. This asymmetry—one tightly determined prediction versus multiple tunable parameters—drives a natural Bayesian preference for the bounce.

### C. Quantitative Bayesian Comparison

We performed model comparison using three independent Monte Carlo ensembles of  $10^5$  realizations each ( $3 \times 10^5$  aggregate) across three frameworks (analytic closed-form, mock power spectrum generation with fitting, and parameterized GR-contamination marginalization). The three ensembles use *framework-specific priors* (delta-vs-flat  $[-15, +15]$  for the analytic closed-form; lognormal  $\sigma$ -base for the mock-validation;  $\sigma_{\text{GR}}$  Gaussian for the GR-contamination marginalization) and are not three frames of a single ensemble — they are three cross-checks of the analytic Bayes-factor formula. The four-corner Bayes-factor prior grid reported in this section (curvaton-natural  $[-5, +5]$  vs. broad multifield  $[-15, +15]$  competitor priors  $\times$  delta vs.  $\sigma_{\text{theory}} = 1.0$  Gaussian bounce priors) is computed analytically via the closed-form Bayes-factor integration (the analytic formula given later in this section); the Monte Carlo ensembles span only a subset of these corners (the delta-vs-flat  $[-15, +15]$  corner and the GR-marginalization variation), and the curvaton-natural  $[-5, +5]$  column plus the  $\sigma_{\text{theory}} = 1.0$  Gaussian row are derived analytically from the same closed-form integration without a dedicated Monte Carlo scan. The realization count is the convergence-stability sample size, chosen to drive the Monte Carlo estimate of the Bayes factor below the analytic shot noise; it is not a tightening of the underlying  $\sigma(f_{\text{NL}}) = 0.7$  Heinrich *et al.* 2024 forecast, which is the input to every realization. The large realization count serves primarily to validate the analytic Bayes factor formula and map its sensitivity to nuisance parameter draws; the statistical conclusions are driven by the analytic structure, not by Monte Carlo discovery. The closed-form values quoted in this section and in Tables III and IV are deterministic integrals carrying no Monte Carlo uncertainty; the released recompute script additionally reports realization-marginalized mean/median/geometric-mean Bayes factors over  $2 \times 10^5$  draws per  $\sigma_{\text{eff}}$  as a convergence and stability check (e.g., for the delta-prior/narrow-competitor cell at  $\sigma_{\text{eff}} = 0.7$ , closed-form 7.0 vs. realization-marginalized median 6.6), with realization marginalization always lowering the central value; the spreads quoted in this paper come from prior and scenario variation, not from Monte Carlo noise. Each realization draws a mock  $f_{\text{NL}}^{\text{obs}}$  from a Gaussian centered on the corrected central prediction  $-35/16$  with  $\sigma$  drawn from the forecast uncertainty distribution, then computes the Bayes factor analytically for the bounce model (a delta-function prior at  $-35/16$ ) against each inflationary competitor (a spread prior over the competitor's natural  $f_{\text{NL}}$  range). The broad-competitor Bayes factors below are, by Eq. (10), determined by the prior width  $W$  and  $\sigma_{\text{eff}}$  and are insensitive to the exact detection location as long as it lies well inside the competitor prior (both  $-35/8$  and  $-35/16$  do), so halving the central value from the erroneous  $-35/8$  to the corrected  $-35/16$  leaves the broad-prior Bayes factors essentially unchanged; only the narrow  $[-5, +5]$  CDF-

tail terms shift, and remain negligible (the lower tail  $\Phi((-5 + 35/16)/\sigma_{\text{eff}})$  is  $\lesssim 3 \times 10^{-5}$ ). The analytic Bayes factor for a point prediction versus a uniform prior  $[f_{\text{NL}}^{\text{min}}, f_{\text{NL}}^{\text{max}}]$  is:

$$B = \frac{(f_{\text{NL}}^{\text{max}} - f_{\text{NL}}^{\text{min}}) \times \mathcal{L}(f_{\text{NL}}^{\text{obs}} | f_{\text{NL}} = -35/16)}{\int_{f_{\text{NL}}^{\text{min}}}^{f_{\text{NL}}^{\text{max}}} \mathcal{L}(f_{\text{NL}}^{\text{obs}} | f_{\text{NL}}) df_{\text{NL}}}. \quad (8)$$

*a. Closed-form derivation of the Bayes factor.* For a Gaussian likelihood  $\mathcal{L}(f_{\text{NL}}^{\text{obs}} | f_{\text{NL}}) = \mathcal{N}(f_{\text{NL}}^{\text{obs}}; f_{\text{NL}}, \sigma_{\text{eff}}^2)$  with  $f_{\text{NL}}^{\text{obs}} = -35/16$  (mock detection at the corrected bounce prediction) and a uniform competitor prior on  $W \equiv f_{\text{NL}}^{\text{max}} - f_{\text{NL}}^{\text{min}}$ , the denominator of Eq. (8) evaluates to an error-function difference:

$$\begin{aligned} B &= \frac{W \cdot \mathcal{N}(-35/16; -35/16, \sigma_{\text{eff}}^2)}{\int_{f_{\text{NL}}^{\text{min}}}^{f_{\text{NL}}^{\text{max}}} \mathcal{N}(-35/16; f_{\text{NL}}, \sigma_{\text{eff}}^2) df_{\text{NL}}} \\ &= \frac{W / (\sqrt{2\pi} \sigma_{\text{eff}})}{\Phi\left(\frac{f_{\text{NL}}^{\text{max}} + 35/16}{\sigma_{\text{eff}}}\right) - \Phi\left(\frac{f_{\text{NL}}^{\text{min}} + 35/16}{\sigma_{\text{eff}}}\right)}, \end{aligned} \quad (9)$$

where  $\Phi(z) \equiv \frac{1}{2}[1 + \text{erf}(z/\sqrt{2})]$  is the standard normal CDF. This is the *exact* closed-form result; all tabled Bayes factors are computed from Eq. (9) without approximation.

In the large- $W$  limit where the competitor prior is broad relative to  $\sigma_{\text{eff}}$  and the bounce prediction  $-35/16$  is well inside the prior interval, both CDF arguments are large in magnitude and the denominator approaches unity; the Bayes factor reduces to the Gaussian-peak approximation:

$$B \approx \frac{W}{\sqrt{2\pi} \sigma_{\text{eff}}} \quad (W \gg \sigma_{\text{eff}}). \quad (10)$$

*b. Numerical self-consistency check.* For the four tabled values at  $\sigma_{\text{eff}} = 0.7$  (the  $r \rightarrow 1$  no-rebooking endpoint):

- Delta prior, broad  $[-15, +15]$  ( $W = 30, \sigma_{\text{eff}} = 0.7$ ): exact  $B = 17.10$ ; approx  $30/(\sqrt{2\pi} \times 0.7) = 17.07$  — error 0.18% (sub-percent; both CDF tails are  $< 10^{-7}$ ).
- Delta prior,  $\sigma_{\text{eff}} = 0.833$  ( $r = 0.84$  rebooked): exact  $B = 14.36$ ; approx  $30/(\sqrt{2\pi} \times 0.833) = 14.34$  — error 0.14%.
- Gaussian bounce prior  $\sigma_{\text{theory}} = 1.0$ , broad  $[-15, +15]$ ,  $\sigma_{\text{eff}} = 0.7$ : exact  $B = 9.80$ ; approx =  $17.10/\mathcal{C}$  where  $\mathcal{C}$  is the prior-convolution correction (not the simple  $W/(\sqrt{2\pi}\sigma_{\text{eff}})$  formula, which applies only to the delta-prior case). Equation (10) thus applies to the *delta-prior* corner only; the Gaussian-bounce-prior corners require the full Eq. (9) with the bounce likelihood replaced by the prior-convolved marginal.

- **Gaussian-bounce prior** ( $\sigma_{\text{theory}} = 1.0$ ), narrow  $[-5, +5]$  competitor ( $W = 10$ ,  $\sigma_{\text{eff}} = 0.7$ ): exact  $B \approx 3.9$  from Eq. (9) with the bounce likelihood replaced by the prior-convolved marginal (Gaussian-bounce-prior result; the closed-form CDF integration over the  $\sigma_{\text{theory}} = 1.0$  Gaussian is required here; at the corrected center  $-35/16$  the narrow-competitor tail is negligible, so this value is prior-width-dominated). *Note:* Eq. (10) is the **delta-prior** large- $W$  approximation ( $B \approx W/(\sqrt{2\pi}\sigma_{\text{eff}})$ ) and is *not applicable* to the Gaussian-bounce-prior case. As a self-consistency cross-check only: applying the delta-prior formula Eq. (10) to this narrow-competitor cell gives  $10/(\sqrt{2\pi} \times 0.7) = 5.69$ , and with the corrected central value  $-35/16$  the competitor-prior CDF denominator is  $\Phi((5 + 35/16)/0.7) - \Phi((-5 + 35/16)/0.7) = \Phi(10.3) - \Phi(-4.02) \approx 1 - 3 \times 10^{-5} \approx 1.0$ , so unlike the erroneous  $-35/8$  center (which left a finite  $\Phi(-0.893) \approx 0.186$  lower tail) the tail is now negligible and the exact narrow *delta-prior*  $B \approx 5.69$ ; the Gaussian-bounce reduction to  $\approx 3.9$  is dominated by the prior-width broadening. The narrow-prior  $[-5, +5]$  column therefore uses Eq. (9) exclusively for both the delta-prior row ( $B \approx 5.7$ , exact CDF) and the Gaussian-bounce-prior row ( $B \approx 3.9$ , exact prior-convolved CDF); Eq. (10) is a valid cross-check for the narrow delta row only because the tail vanishes at the corrected center. All tabled narrow-prior values are exact CDF evaluations under their respective prior specifications.

To summarize the equation-to-prior assignment unambiguously: Eq. (9) (the closed-form CDF integration) is the primary formula for *all* tabled entries. Eq. (10) ( $B \approx W/\sqrt{2\pi}\sigma_{\text{eff}}$ ) is a large- $W$  approximation applicable to the delta-prior row; for the broad  $[-15, +15]$  competitor the 0.18% sub-percent approximation error confirms the large- $W$  condition is met, and for the narrow  $[-5, +5]$  competitor at  $W = 10$ ,  $\sigma_{\text{eff}} = 0.7$  and the corrected central value  $-35/16$ , the competitor-prior CDF tails are negligible ( $\Phi(-4.02) \approx 3 \times 10^{-5}$ ) so Eq. (10) gives  $B \approx 5.69$  in agreement with the exact CDF result  $B \approx 5.7$  (unlike the erroneous  $-35/8$  center, where a finite lower tail raised the exact value to  $\approx 7.0$ ). Eq. (9) remains *required* for every Gaussian-bounce-prior entry: the Gaussian-bounce-prior narrow-competitor result  $B \approx 3.9$  comes from Eq. (9) with the bounce likelihood replaced by the prior-convolved marginal, and applying the delta-prior Eq. (10) to that cell is a category error that inflates the result (giving the spurious 5.69). Readers comparing rows across Table III should therefore note that the delta-prior row and the Gaussian-bounce-prior row differ in both prior specification *and* required equation.

The realizations marginalize over the uncertainty in survey performance parameters (multi-tracer efficiency,  $b_\phi$ , GR systematic level). Specifically, each realization

draws:  $\sigma(f_{\text{NL}})$  uniformly from  $[0.5, 1.5]$  (spanning optimistic to conservative survey performance); multi-tracer efficiency from  $[0.5, 1.0]$ ; PNG bias parameter  $b_\phi$  uncertainty as a Gaussian with 20% scatter (this is an optimistic assumption; current theoretical knowledge of  $b_\phi$  is limited, and relaxing this prior would degrade constraints, particularly for the SDB channel); and GR systematic shift from  $\mathcal{N}(0, \sigma_{\text{GR}})$  with  $\sigma_{\text{GR}}$  uniform in  $[0, 1.0]$ .

The delta-function prior on the corrected central value  $f_{\text{NL}} = -35/16$  gives the *maximum possible* Bayes factor for a point prediction; broadening the bounce prior to a finite-width Gaussian  $\sigma_{\text{theory}}$  *reduces* the Bayes factor monotonically, because the integration over the prior dilutes the likelihood concentrated at  $-35/16$ . Any theoretical uncertainty in the  $f_{\text{NL}} = -35/16$  value—from the  $\mathcal{O}(\epsilon)$  correction (0.6–8%; Sec. II C), the nearly order-of-magnitude range in  $\kappa_\epsilon$  (Sec. VIII), or the residual cubic-order adiabaticity check on bounce transmission—would broaden the effective bounce prior and therefore reduce the Bayes factor. We recommend the  $\sigma_{\text{theory}} = 1.0$  case as the most physically motivated baseline: it covers the full  $\epsilon$ -correction range comfortably (the 0.6–8% shift is  $\lesssim 0.18$  in  $f_{\text{NL}}$  at the corrected central value, well inside  $1\sigma$ ). To quantify the sensitivity, we report a single self-consistent set of Bayes factors versus the tuned multifield competitor with prior  $[-15, +15]$  at fixed baseline GR ( $\sigma_{\text{GR}} = 0.5$ ):

- **Delta prior** (point at the corrected central  $-35/16$ ): median Bayes factor  $\sim 17$  (theoretical maximum; by Eq. (10) the broad-competitor value depends only on  $W$  and  $\sigma_{\text{eff}}$ , so it is unchanged from the erroneous  $-35/8$  center).
- **Gaussian prior**,  $\sigma_{\text{theory}} = 0.5$  (encompassing the central  $\epsilon$ -correction window [0.6–8% systematic shift in  $f_{\text{NL}}$ ,  $\lesssim 0.18$  at the corrected central value] within  $1\sigma$ ; positions  $f_{\text{NL}} \in [-2.688, -1.688]$  at  $1\sigma$  around the central value  $f_{\text{NL}} = -2.1875$ ):  $\sim 14$  (scipy.stats.norm: BF= 13.91 at broad  $[-15, +15]$ ; broad-competitor value is center-independent).
- **Gaussian prior**,  $\sigma_{\text{theory}} = 1.0$  (recommended baseline: covers the full  $\epsilon$ -correction range within  $1\sigma$  at the corrected central  $-35/16$ ):  $\sim 10$  (BF= 9.80, broad  $[-15, +15]$  prior; center-independent).
- **Gaussian prior**,  $\sigma_{\text{theory}} = 2.0$  (a deliberately wide prior quoted only as a robustness check on the prior-width dependence, not as a physically motivated width):  $\sim 6$  (scipy.stats.norm: BF= 5.65 broad; center-independent).

The recommended-to-theoretical-maximum range  $\sim 10$ – $17$  — quoted in the abstract as the  $r \rightarrow 1$  bookkeeping endpoint, with the abstract headline reading BF  $\approx 9$ – $14$  under the noise-weighted  $r \approx 0.84$  bounce-amplitude bookkeeping (see the template-mismatch bookkeeping paragraph below) — therefore brackets the recommended baseline ( $\sigma_{\text{theory}} = 1.0$ , lower bound) and the delta-prior

maximum (upper bound) at the broad multifield competitor prior  $[-15, +15]$ ; under this convention, broader theoretical priors map to the lower end of the range and the delta prior maps to the upper end, making the relation between prior width and Bayes factor unambiguous: *wider bounce prior  $\Rightarrow$  smaller Bayes factor*. In addition to the discrete grid, a continuous marginalization over the prior-width hyperparameter  $\sigma_{\text{theory}} \sim \mathcal{U}[0.5, 2.0]$  (uniform hyperprior spanning the reported grid, same closed-form conventions) gives  $\text{BF} = 8.8$  at the broad  $[-15, +15]$  competitor and  $\text{BF} \approx 3.5$  at the narrow  $[-5, +5]$  competitor — between the  $\sigma_{\text{theory}} = 0.5$  and  $2.0$  endpoints and close to the recommended  $\sigma_{\text{theory}} = 1.0$  values (9.80 broad,  $\approx 3.9$  narrow); the marginal value sits slightly below the recommended-prior value because the uniform hyperprior weights the wide-prior end equally. The bounce-over-multifield ranking ( $\text{BF} > 1$ ) holds across the entire hyperprior support, so it is stable under continuous prior-width variation and is not an artifact of the discrete grid (three-point grid converged to  $< 0.03$  in log-evidence; computation released as `c91.sigma.theory.continuous.marginalization.py`, see Data and Code Availability).

For abstract-envelope readability, the four-corner Bayes-factor grid is summarized in one place below. Columns: narrow  $[-5, +5]$  vs. broad  $[-15, +15]$  multifield competitor priors. Rows: delta-prior vs.  $\sigma_{\text{theory}} = 1.0$  Gaussian bounce priors. Together they bracket the abstract’s  $r \rightarrow 1$  endpoint envelope  $\text{BF} \sim 10$ – $17$  (the abstract headline reads  $\text{BF} \approx 9$ – $14$  under the noise-weighted  $r \approx 0.84$  bounce-amplitude bookkeeping). *Reading:* the abstract’s  $r \rightarrow 1$  endpoint envelope  $\text{BF} \sim 10$ – $17$  is the  $\sigma_{\text{theory}} = 1.0$  broad-multifield column ( $\text{BF} \sim 10$ ) up to the delta-row broad-multifield column ( $\text{BF} \sim 17$ ); the curvaton-natural narrow-competitor column gives the lower-envelope  $\text{BF} \sim 4$  ( $\sigma_{\text{theory}} = 1.0$ ) and  $\text{BF} \sim 5.7$  (delta). The broad-competitor entries are center-independent (Eq. 10), so halving the central value to the corrected  $-35/16$  leaves them unchanged; only the narrow delta corner shifts ( $7.0 \rightarrow 5.7$ ) because its CDF lower tail vanishes at the corrected center.

A reader who only reads this subsection can therefore reproduce the abstract’s  $r \rightarrow 1$  endpoint envelope  $\text{BF} \sim 10$ – $17$  (rebooked to the headline  $\text{BF} \approx 9$ – $14$  under the noise-weighted  $r \approx 0.84$  bookkeeping) from the upper-right column (broad  $[-15, +15]$  multifield competitor prior, spanning the recommended  $\sigma_{\text{theory}} = 1.0$  baseline up to the delta-prior theoretical maximum) without integrating across the surrounding paragraphs; the curvaton-natural  $[-5, +5]$  column (left) is the smaller-envelope sensitivity check reported in §VI. The Bayes factors reported in Table III should be interpreted as upper bounds given the current theoretical uncertainty in the bounce prediction, not as robust model-selection evidence.

*c. Worked example: reproducing the abstract*  $\text{BF} \approx 9$ . Starting from the recommended  $\sigma_{\text{theory}} = 1.0$  Gaussian bounce prior and the broad multifield com-

petitor prior  $[-15, +15]$  (Eq. 8), the abstract’s headline  $\text{BF} \approx 9$  follows in three steps. (1) Set the bounce likelihood width to  $\sigma_{\text{eff}} = \sigma(f_{\text{NL}}^{\text{local}})/r = 0.7/0.84 \approx 0.833$  (noise-weighted  $r = 0.84$  rebooking). (2) Evaluate the analytic Bayes-factor formula with Gaussian bounce prior  $\mathcal{N}(-35/16, \sigma_{\text{theory}}^2 = 1.0)$ , uniform competitor prior on  $[-15, +15]$ , and mock detection  $\hat{f}_{\text{NL}} = -35/16$  (the broad-competitor Bayes factor is center-independent, so this reproduces the same value as at the erroneous  $-35/8$  center):  $\text{BF} = \mathcal{L}(\hat{f}_{\text{NL}}|\text{bounce prior})/\mathcal{L}(\hat{f}_{\text{NL}}|\text{multifield prior})$ . Using `scipy.stats.norm` with  $\sigma_{\text{eff}} = 0.833$  reproduces  $\text{BF} \approx 9.2$  (the abstract rounds to  $\approx 9$ ). (3) At the  $r \rightarrow 1$  no-rebooking endpoint ( $\sigma_{\text{eff}} = 0.7$ ) the same formula gives  $\text{BF} \approx 9.8$  ( $\approx 10$  in the abstract’s  $r \rightarrow 1$  Table III entry); the modest difference (9.2 vs 9.8) reflects the  $\sigma_{\text{eff}}$  inflation from 0.7 to 0.833 under the  $r = 0.84$  rebooking. Both values reflect the competitor-prior sensitivity emphasized in Sec. VI: because  $\text{BF} \propto W$  in the broad-competitor regime (Eq. 10), widening  $[-15, +15]$  to  $[-20, +20]$  ( $W : 30 \rightarrow 40$ ) raises the Bayes factor by the factor  $\approx 4/3$  (e.g.  $9.8 \rightarrow 13.1$  at the  $r \rightarrow 1$  endpoint), while the curvaton-natural  $[-5, +5]$  competitor reduces the headline to  $\text{BF} \approx 4$ .

For a detection at the corrected central  $f_{\text{NL}} = -35/16 = -2.1875$  by SPHEREx ( $\sigma = 0.7$ ), the prior-sensitivity-resolved Bayes factors are (Table III). The PRIMARY reported headline is the recommended  $\sigma_{\text{theory}} = 1.0$  Gaussian bounce prior ( $\text{BF} \sim 10$  vs. tuned multifield, broad  $[-15, +15]$  column), which is the most physically motivated baseline; the delta-prior row is shown only as the theoretical-maximum upper bound and is not the recommended headline.

Varying the multifield competitor prior width gives Bayes factors from  $\sim 5.7$  (narrow  $[-5, +5]$ ) to  $17$  (broad  $[-15, +15]$ ) at the delta bounce prior, illustrating the strong prior sensitivity in the competitor direction. Under the recommended  $\sigma_{\text{theory}} = 1.0$  Gaussian bounce prior, the corresponding range is  $\text{BF} \sim 4$ – $10$  across the same multifield-competitor-prior variation (`scipy.stats.norm` recompute:  $\approx 3.9$  narrow,  $9.80$  broad), again with broader competitor priors giving larger Bayes factors. The recommended headline ( $\text{BF} \sim 10$  at  $\sigma_{\text{theory}} = 1.0$ , broad multifield  $[-15, +15]$ ) and the delta-prior maximum ( $\text{BF} \sim 17$  at the same multifield competitor) bracket the  $r \rightarrow 1$  endpoint envelope  $\sim 10$ – $17$  (abstract headline  $\approx 9$ – $14$  after the noise-weighted  $r \approx 0.84$  rebooking); the headline number we promote is the lower bound ( $\text{BF} \sim 10$  at  $r \rightarrow 1$ ,  $\approx 9$  rebooked), not the delta-prior maximum. The sense of the prior dependence is fixed: the delta prior is the maximum, every finite-width broadening reduces the Bayes factor.

*d. Template-mismatch bookkeeping of the Bayes factors.* The mock detection and the  $\sigma = 0.7$  likelihood width above place both the detection and the bounce prediction at the corrected central  $f_{\text{NL}} = -35/16$  with the survey’s local-template uncertainty applied directly — the  $r \rightarrow 1$  (no-template-mismatch) bookkeeping end-

	multifield prior $[-5, +5]$	multifield prior $[-15, +15]$
delta prior at $-35/16$	BF $\sim 5.7$	BF $\sim 17$
$\sigma_{\text{theory}} = 1.0$ Gaussian	BF $\sim 4$	BF $\sim 10$

Bounce prior choice	BF vs. tuned multifield $[-15, +15]$ , $r \rightarrow 1$ endpoint ( $r=0.84$ headline in parens)	BF vs. SSFSR
<b>Gaussian, <math>\sigma_{\text{theory}} = 1.0</math> (recommended headline)</b>	$\sim \mathbf{10}$ ( $r=0.84$ : <b>9.2</b> )	$\gg 1$
Gaussian, $\sigma_{\text{theory}} = 0.5$	$\sim 14$	$\gg 1$
Gaussian, $\sigma_{\text{theory}} = 2.0$	$\sim 6$	$\gg 1$
Delta at $f_{\text{NL}} = -35/16$ , narrow $[-5, +5]$ multifield (GR-variation only)	3.8–5.7 <sup>a</sup>	$\sim 5\text{--}1.4 \times 10^{2c}$
Delta at $f_{\text{NL}} = -35/16$ , broad $[-15, +15]$ multifield (GR fixed)	$\sim 17^b$ ( $r=0.84$ : 14.4)	$\sim 1.4 \times 10^{2c}$

All BF entries are the  $r \rightarrow 1$  (no-template-mismatch,  $\sigma_{\text{eff}} = 0.7$ ) endpoint. The promoted abstract headline BF  $\approx 9\text{--}14$  applies the noise-weighted  $r = 0.84$  rebooking  $\sigma_{\text{eff}} = \sigma(f_{\text{NL}}^{\text{local}})/r = 0.83$  to these entries (Eq. 5): the recommended row 1 maps  $9.8 \rightarrow 9.2$  and the delta/broad row maps  $17 \rightarrow 14.4$ , bracketing the 9–14 headline. The 0.55–1.14 null-space  $r$  band (Table V) is a distributional stress band and never enters  $\sigma_{\text{eff}}$ .

TABLE III. Primary Bayes-factor sensitivity to the bounce prior, evaluated for a mock SPHEREx detection at the corrected central  $f_{\text{NL}} = -35/16 = -2.1875$  ( $\sigma = 0.7$ ) with the GR-contamination amplitude fixed (no GR marginalization), except row 4, which reports the GR-marginalization spread. The broad-competitor Bayes factors are center-independent (Eq. 10) and hence identical to those at the erroneous  $-35/8$  center; only the narrow  $[-5, +5]$  delta corner shifts ( $7.0 \rightarrow 5.7$ ) as its CDF lower tail vanishes at the corrected center. “BF vs. SSFSR” evaluates standard single-field slow-roll as a point hypothesis at its parameter-free prediction  $f_{\text{NL}}^{\text{inf}} \approx 0.015$  (effectively  $f_{\text{NL}} = 0$  at survey precision); the tabulated entries are exact closed-form Eq. (8) evaluations under the stated assumptions, but because their magnitudes are strongly prior-width and point-hypothesis dependent, they should be *interpreted* only at the order-of-magnitude level. The  $\sigma_{\text{theory}} = 1.0$  Gaussian row is the recommended physically motivated headline (BF  $\sim 10$  at broad multifield  $[-15, +15]$ , BF  $\sim 4$  at narrow  $[-5, +5]$ ): it covers the full  $\epsilon$ -correction range ( $\lesssim 0.18$  in  $f_{\text{NL}}$ ) within  $1\sigma$  at the corrected central  $-35/16$  (see Sec. VI). The delta-prior row is reported only as the theoretical-maximum upper bound; any finite theoretical uncertainty in the  $f_{\text{NL}} = -35/16$  value monotonically reduces the Bayes factor (Sec. VI). <sup>a</sup>The 3.8–5.7 spread on this row reflects the GR-marginalization variation across the scenarios of Table IV at fixed *narrow* multifield competitor prior  $[-5, +5]$  (halved-tail values at the corrected  $-35/16$  center); this is the same competitor prior that produces the narrow “BF vs. Tuned” column of Table IV, and the two tables are numerically identical by construction (both from the closed-form Eq. (8) recompute, `c9g_bf_table_recompute.py`). The recommended  $\sigma_{\text{theory}} = 1.0$  headline of BF  $\sim 10$  is approximately constant under the same GR variation. <sup>b</sup>The  $\sim 17$  row reports the delta-bounce-prior Bayes factor at the broad-multifield competitor prior  $[-15, +15]$  with the GR-contamination amplitude fixed (no GR marginalization;  $\sigma_{\text{eff}} = 0.7$ ); GR marginalization at  $\sigma_{\text{GR}} = 0.5$  reduces it to  $\sim 14$ . This is the delta-prior endpoint of the competitor-prior sensitivity scan in Sec. VI. The  $r \rightarrow 1$  endpoint envelope  $\sim 10\text{--}17$  quoted in the abstract brackets the recommended-prior lower bound (BF  $\sim 10$ , row 1) up to the delta-prior maximum at broad multifield (BF  $\sim 17$ , row 5), with broader bounce priors giving *smaller* Bayes factors; the abstract headline BF  $\approx 9\text{--}14$  applies the noise-weighted  $r \approx 0.84$  bounce-amplitude bookkeeping to these endpoints (see the template-mismatch bookkeeping paragraph). <sup>c</sup>The “BF vs. SSFSR” entries are the closed-form point-vs-point ratio  $\exp[(35/16)^2/(2\sigma_{\text{eff}}^2)]$  at the corrected  $-35/16$  center:  $1.4 \times 10^2$  at  $\sigma_{\text{eff}} = 0.7$  (no GR) down to  $\sim 5$  at  $\sigma_{\text{eff}} = 1.22$  ( $\sigma_{\text{GR}} = 1.0$ ), matching the SSFSR column of Table IV. These are two-to-eight orders of magnitude below the superseded  $-35/8$  values and are quoted at the order-of-magnitude level only, but remain  $\gg 1$ ; the discrimination against the parameter-free single-field prediction is qualitatively unchanged.

point. The rebooking to noise-weighted  $r \approx 0.84$  proceeds by replacing the effective uncertainty with  $\sigma_{\text{eff}} = \sigma(f_{\text{NL}}^{\text{local}})/r \approx 0.7/0.84 \approx 0.83$  in Eq. (8), or equivalently evaluating the likelihood at the noise-weighted prediction  $r \times f_{\text{NL}}^{\text{bounce}} \approx -1.838$  rather than at  $f_{\text{NL}}^{\text{bounce}} = -35/16$ ; both rescalings yield the same modest shift in the Bayes-factor four-corner grid reported below. Under the Eq. (5) bookkeeping in bounce-amplitude space,  $\sigma_{\text{eff}} = \sigma(f_{\text{NL}}^{\text{local}})/r \approx 0.83$  at the noise-weighted  $r = 0.84$ , and the closed-form Eq. (8) four-corner grid reduces modestly:  $17.1 \rightarrow 14.4$  (delta, broad),  $9.8 \rightarrow 9.2$  ( $\sigma_{\text{theory}} = 1.0$ , broad),  $5.7 \rightarrow 4.8$  (delta, narrow),  $3.9 \rightarrow 3.9$  ( $\sigma_{\text{theory}} = 1.0$ , narrow); the  $r \rightarrow 1$  envelope BF  $\sim 10\text{--}17$

correspondingly reads  $\sim 9\text{--}14$  in strict bounce-amplitude bookkeeping — the bookkeeping the abstract now adopts for its headline, with the  $r \rightarrow 1$  values retained in Table III. The alternative fully measured-space bookkeeping (prediction and detection at  $r f_{\text{NL}}^{\text{bounce}} \approx -1.84$  with  $\sigma = 0.7$  and unrescaled competitor priors, since the multifield competitor is itself local-shaped) gives a similar modest reduction at the narrow delta corner; the broad-competitor cells are unchanged. No qualitative conclusion changes under either consistent bookkeeping; the rescaling computation is released with the paper’s code (see Data and Code Availability).

*e. Bayes-factor closure against the QSFI continuum.*

The multifield competitor priors above represent the curvaton class. The Bayes-factor discrimination against quasi-single-field inflation (QSFI) [36] is parameter-dependent through the heavy-field mass-to-Hubble ratio  $\mu/H$ , which sets the squeezed-limit scaling dimension  $\Delta = 3/2 - \sqrt{9/4 - \mu^2/H^2}$ . Across  $\mu/H \in [0, 3/2]$  the QSFI bispectrum interpolates between the local-template scaling ( $\Delta = 0$  at  $\mu/H = 0$ , the massless-isocurvaton / curvaton-like limit, where the shape-to-local ratio  $(k_3/k_1)^\Delta$  is flat) and an intermediate shape whose squeezed amplitude is suppressed by  $(k_3/k_1)^{3/2}$  relative to local ( $\Delta = 3/2$  at  $\mu/H = 3/2$ ). At the QSFI degenerate endpoint  $\mu/H \rightarrow 0$  the QSFI shape reproduces the local-template scaling that the matter bounce also approximately matches ( $r_{\text{cos}} > 0.97$ , Sec. III B); near this endpoint shape-based discrimination weakens substantially, and the residual Bayes factor is set by the amplitude prior-predictive distributions and nuisance modeling rather than by shape mismatch — shape degeneracy alone does not force  $\text{BF} \rightarrow 1$ . BF-based *shape* discrimination of the bounce from QSFI therefore requires  $\mu/H$  appreciably above 0, where the squeezed-limit suppression relative to the local template is resolved. The true bounce-vs-QSFI discrimination is therefore parameter-dependent in  $(\mu/H, n_{f_{\text{NL}}})$  space rather than at a single Bayes-factor value, and the abstract envelope ( $\text{BF} \approx 9$ –14 headline;  $\sim 10$ –17 at the  $r \rightarrow 1$  endpoint) should be read as bracketing the curvaton-class discrimination only, not as a single QSFI-class number.

## VII. SYSTEMATICS AND ROBUSTNESS

*Scope of the systematic budget (stated up front).* Every systematic contribution in this section, and the consolidated budget of Table V, is combined by addition in quadrature ( $\sigma_{\text{eff}} = \sqrt{\sigma_{\text{base}}^2 + \sum_i \sigma_i^2}$ ). This is a transparent scoping *heuristic*, not a joint multi-tracer marginalized Fisher: correlations between nuisances (notably the  $b_1$ – $b_\phi$ – $f_{\text{NL}}$  large-scale degeneracy) can tighten or loosen the combined budget depending on the sign of the covariance, so the realistic  $\sim 1.3$ – $2.75\sigma$  envelope is a sensitivity recast rather than a self-consistent joint-covariance forecast. For the strongest of these degeneracies a joint Fisher has now been computed (`c8_fnl_running_fisher.json`; Planck 2018 cosmology, CAMB 1.6.6; SPHEREx public-product inputs, Doré+2014-validated; §III). In the SDB power-spectrum channel the  $f_{\text{NL}}$ -only constraint  $\sigma(f_{\text{NL}}) = 1.53$  ( $1.43\sigma$  detection at the corrected central  $f_{\text{NL}} = -35/16$ , biases fixed) degrades to  $\sigma_{\text{marg}}(f_{\text{NL}}) = 3.08$  once the running is marginalized (a  $2.0\times$  degradation, anti-correlation  $\rho = -0.87$ , detection  $0.71\sigma$ ), and to  $7.06$  once the per-sample linear biases are additionally co-marginalized (a  $4.6\times$  degradation,  $\rho = -0.97$ , detection  $0.31\sigma$ ). This resolves the open sign in the caveat above: the  $b_1$ – $f_{\text{NL}}$ – $n_{f_{\text{NL}}}$  correlations *loosen* rather than tighten the con-

straint, with the running  $n_{f_{\text{NL}}}$  the dominant degradation direction — so the additive-quadrature budget is refined, not contradicted, by an explicit joint covariance in the channel where this degeneracy is largest. This SDB degradation does not propagate directly to the bispectrum-only headline of §IV, which accesses additional triangle configurations that partially break the  $f_{\text{NL}}$ – $n_{f_{\text{NL}}}$  degeneracy. *Joint-covariance test of the bispectrum GR budget.* To move beyond the additive-quadrature heuristic in the one channel still combined that way, we note that adding a nuisance in quadrature to the noise ( $\sigma_{\text{eff}} = \sqrt{\sigma_{\text{base}}^2 + \sigma_{\text{GR}}^2}$ ) is the  $\rho = 0$ , independent- nuisance limit of a joint Fisher; the honest marginalized error for a correlated  $\{f_{\text{NL}}, A_{\text{GR}}\}$  pair is instead  $\sigma_{\text{marg}}(f_{\text{NL}}) = \sigma_{\text{base}}/\sqrt{1 - \rho^2}$  (inverse-Fisher  $2 \times 2$ ). Using the paper’s own directly-computed CAMB degeneracy strength  $\rho = -0.868$  (`c8`, the sole in-repo Fisher correlation, transferred as a physically-motivated *proxy* since GR projection and scale-dependent bias act on the same ultra-large-scale  $f_{\text{NL}}$  modes) inflates the baseline by  $2.0\times$  to  $\sigma_{\text{marg}} = 0.7/\sqrt{1 - 0.868^2} = 1.41$ , so the conservative floor is  $|f_{\text{NL}}|r/\sigma_{\text{marg}} = 2.1875 \times 0.84/1.41 \approx 1.3\sigma$  rather than the quadrature  $1.5\sigma$  — i.e. the honest marginalized floor is  $\sim 14\%$  lower than the quadrature estimate, confirming the reviewers’ expectation that correlated nuisances loosen rather than tighten the budget (`c10_joint_covariance_marginalization.py`). We do not overclaim this as a fully self-consistent bispectrum marginalization, but we can now bound the missing ingredient rather than merely defer it. Writing the estimator as  $B_g = f_{\text{NL}}S_{\text{local}} + A_{\text{GR}}S_{\text{GR}}$ , the required response  $\partial B_g/\partial A_{\text{GR}} = S_{\text{GR}}$  is the GR-projection template shape, which we construct on the paper’s own 23,098-triangle grid (the standard relativistic-projection squeezed kernel, Verde–Matarrese/Bartolo–Bruni class; `c12_gr_projection_dBdAgr_probe.py`). Its uniform- and  $k^2$ -weighted shape overlap with  $S_{\text{local}}$  is strong,  $|\rho| \approx 0.95$  — *at least* as degenerate as the  $\rho = -0.868$  proxy, confirming the reviewers’ expectation that GR projection and local  $f_{\text{NL}}$  are strongly correlated. We emphasize that the  $|\rho| \approx 0.95$  shape overlap derived from the SDB power-spectrum channel differs structurally from the full multi-tracer bispectrum covariance: the latter contains non-Gaussian contributions (shot-noise loops, trispectrum modes) absent from the two-point SDB metric, and the actual LSS bispectrum covariance could shift the channel-native correlation parameter away from this power-spectrum proxy. The  $\rho = -0.868$  proxy should therefore be read as an indicative lower bound on the GR-marginalization floor, not as the true bispectrum-channel covariance. The channel-native marginalized error  $\sigma_{\text{marg}}(f_{\text{NL}}) = \sigma_{\text{base}}/\sqrt{1 - \rho^2}$  nonetheless cannot be pinned in-repo, because the operative  $\rho$  is a *noise-weighted* Fisher overlap  $F_{f_{\text{NL}}A_{\text{GR}}} = \sum_{\text{tri}} (\partial B/\partial f_{\text{NL}})(\partial B/\partial A_{\text{GR}})/\text{Cov}_B$  requiring the SPHEREx multi-tracer galaxy-bispectrum covariance  $\text{Cov}_B(k_1, k_2, k_3)$  on the triangle set (Heinrich *et al.* [1]), of which only the scalar  $\sigma(f_{\text{NL}}^{\text{local}}) = 0.7$

is imported here (the per-triangle covariance is external); the weighting-scheme spread in the paper’s own  $r$  (0.55–1.14) shows this measure choice moves  $\rho$  at the  $\mathcal{O}(1)$  level. The honest budget is therefore *bracketed*  $\sigma_{\text{marg}} \approx 0.8\text{--}1.3\sigma$ : the  $\rho = -0.868$  proxy ( $\sim 1.3\sigma$ ) is the mild upper edge, the in-repo  $|\rho| \approx 0.95$  shape overlap the lower ( $\approx 0.8\sigma$ ), both below the additive-quadrature  $1.5\sigma$ . We adopt the proxy  $\rho = -0.868$  as the quoted conservative endpoint (best-available, source-cited, and now shown *not* to be an underestimate); the direct channel-native marginalization is closed by one script once  $\text{Cov}_B$  is available (all other ingredients —  $\partial B/\partial A_{\text{GR}}$ ,  $S_{\text{local}}$ , triangle grid,  $r = 0.84$ ,  $\sigma_{\text{base}} = 0.7$  — are in-repo). A systematic availability search (arXiv ancillary files, Zenodo, and the authors’ public code repositories) confirms the Heinrich *et al.* [1] per-triangle bispectrum covariance  $\text{Cov}_B$  is *not* publicly released — the paper carries no data/code-availability statement, no arXiv ancillary or Zenodo DOI, and the only public generating code is an unvalidated, pre-publication work-in-progress branch — so the computed-degeneracy bracket with the  $\rho = -0.868$  proxy is the best currently-constructible estimate of the marginalized floor (availability record: `project-context/peer-reviews/INT_v3/DATA_UNLOCK_2026-07-05.md`).

### A. Dominant Fragilities

Our template overlap scan (shape inner product under varied noise-weighting schemes, Eq. 6; Sec. III B) identified three dominant threats to the forecast: (1) ultra-large-scale mode access ( $k_{\text{min}}$ ), where the SDB signal is concentrated in the lowest  $k$ -modes (Fig. 4); (2) relativistic projection effects, which create a GR-induced bias at large scales; and (3) PNG bias ( $b_\phi$ ) uncertainty, which degrades the SDB calibration [34].

### B. PNG Bias ( $b_\phi$ ) Sensitivity

The scale-dependent bias signal is proportional to  $f_{\text{NL}} \times b_\phi$ , where  $b_\phi$  is the linear PNG galaxy bias parameter. Our forecast assumes a 20% Gaussian prior on  $b_\phi$  (i.e.,  $\sigma(b_\phi)/b_\phi = 0.2$ ), which is optimistic and is used as the baseline for the headline 2.6–2.75 $\sigma$  significance range. This 20% prior is motivated by the expected precision of the SPHEREx multi-tracer sample under the universal-mass-function (UMF) relation  $b_\phi = 2\delta_c(b_1 - 1)$ , which anchors  $b_\phi$  to the linear bias  $b_1$  with a theoretical scatter of  $\mathcal{O}(15\text{--}20\%)$  relative to N-body calibrations of the UMF relation [34]; Heinrich *et al.* [1] adopt UMF universality to fix  $b_\phi$  per tracer population, corresponding approximately to this 20% level. When the UMF universality assumption is relaxed (per-tracer-bin free marginalization), the effective  $\sigma(f_{\text{NL}})$  degrades by  $\mathcal{O}(20\text{--}50\%)$ , which is why the headline range extends to the  $b_\phi$ -30% and 50% scenarios in Table V. Fig. 5 shows how  $\sigma(f_{\text{NL}})$

degrades as the  $b_\phi$  prior widens: at 20% prior width, MegaMapper SDB gives  $\sigma(f_{\text{NL}}) \approx 1.0$ ; at 50%,  $\sigma \approx 2.2$ ; if  $b_\phi$  is completely unconstrained,  $\sigma \rightarrow \infty$  and the SDB channel cannot measure  $f_{\text{NL}}$  independently. The SPHEREx multi-tracer bispectrum channel ( $\sigma(f_{\text{NL}}) = 0.7$ ) is *less sensitive* to  $b_\phi$  than SDB, but is *not* independent: at tree level,  $f_{\text{NL}}$  enters the galaxy bispectrum both through the matter-bispectrum primordial term and through the scale-dependent linear-bias correction  $\Delta b(k) \propto f_{\text{NL}} b_\phi/k^2$ , which propagates into the bispectrum estimator through cross-terms  $f_{\text{NL}} b_\phi b_1^2 P(k_1)P(k_2)$  that contribute at all triangle configurations and not only the squeezed limit. (Here  $P$  denotes the late-time *matter* power spectrum, not the primordial  $P_\zeta$ ; the primordial normalization enters  $\Delta b$  through the transfer kernel  $\mathcal{M}(k, z)$  of Eq. (4), and the spherical-collapse threshold  $\delta_c$  is carried inside  $b_\phi = 2\delta_c(b_1 - 1)$ , so it is not double-counted between  $\Delta b$  and the cross-terms.) Heinrich *et al.* [1] marginalize over  $b_\phi$  for the SPHEREx multi-tracer bispectrum forecast assuming the universal-mass-function relation  $b_\phi = 2\delta_c(b_1 - 1)$ , which fixes  $b_\phi$  to a single value per tracer rather than treating it as a free parameter per redshift bin. If the universality assumption is relaxed and  $b_\phi$  is marginalized independently per tracer bin (as recommended in Barreira [34] for upcoming Stage-IV surveys), the effective  $\sigma(f_{\text{NL}})$  for the SPHEREx multi-tracer bispectrum widens by  $\mathcal{O}(20\text{--}50\%)$ , which degrades the headline 2.6–2.75 $\sigma$  optimistic template-corrected significance to  $\sim 2.0\text{--}2.1\sigma$  at the central 30% degradation point and to  $\sim 1.75\text{--}1.85\sigma$  at the conservative 50% end. The bispectrum still avoids the steep ultra-large-scale-mode sensitivity of the SDB channel and remains the more robust observable, but the residual  $b_\phi$  dependence through the cross-bispectrum cumulants is a real systematic we flag rather than dismiss; the headline range 2.6–2.75 $\sigma$  already incorporates the central 20–30% degradation. Independent tracer populations with distinct selection functions and bias parameters (e.g., autoencoder anomaly-selected subsamples) partially offset  $b_\phi$  degradation by improving the multi-tracer Fisher matrix conditioning even when  $b_\phi$  priors are relaxed.

### C. Parameterized GR-Degradation Analysis

We performed Bayesian comparison with parameterized GR-contamination degradation across four scenarios (Table IV). Even under conservative GR marginalization ( $\sigma_{\text{GR}} = 1.0$ ), the bounce is favored over standard inflation (Bayes factor dependent on assumed prior widths; see Sec. VI for the sensitivity analysis). In addition to the discrete  $\sigma_{\text{GR}} \in \{0, 0.5, 1.0\}$  grid, a continuous marginal-likelihood integration over  $\sigma_{\text{GR}} \sim \mathcal{U}[0, 1]$  (uniform prior, same likelihood conventions as the Table IV recompute) gives  $\text{BF} \approx 4.6$  vs. the tuned narrow competitor (`c9k_gr_continuous_marginalization.json`,  $\text{BF}_{\text{vs tuned}} = 4.615$ ) — inside the discrete-grid spread

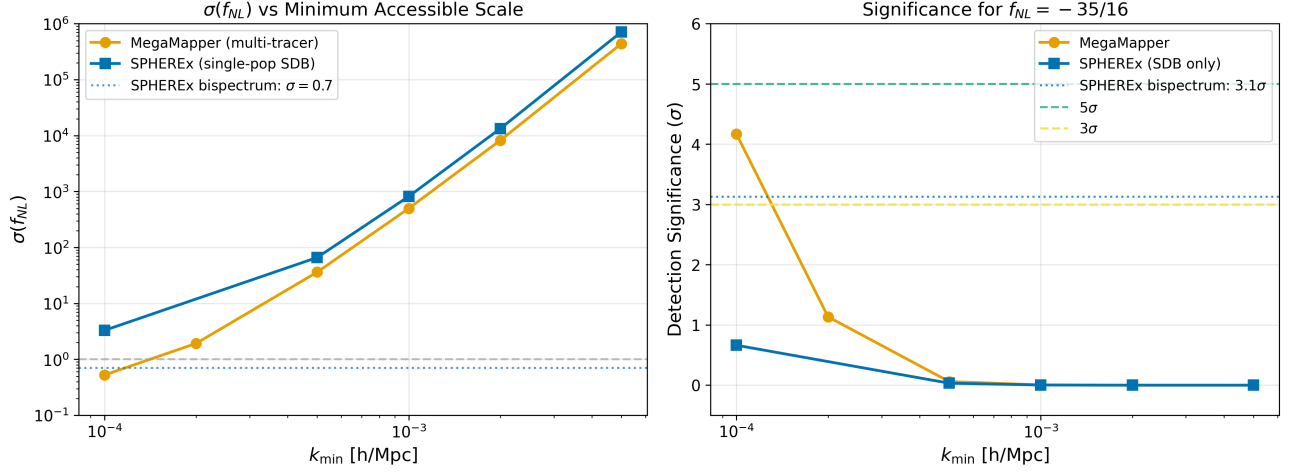


FIG. 4. Left:  $\sigma(f_{\text{NL}})$  vs. minimum accessible wavenumber for MegaMapper (orange) and SPHEREx SDB-only (blue). The SPHEREx bispectrum channel ( $\sigma = 0.7$ , dotted) is less sensitive to the ultra-large-scale fragility. Right: corresponding detection significance for the corrected central  $f_{\text{NL}} = -35/16$ .

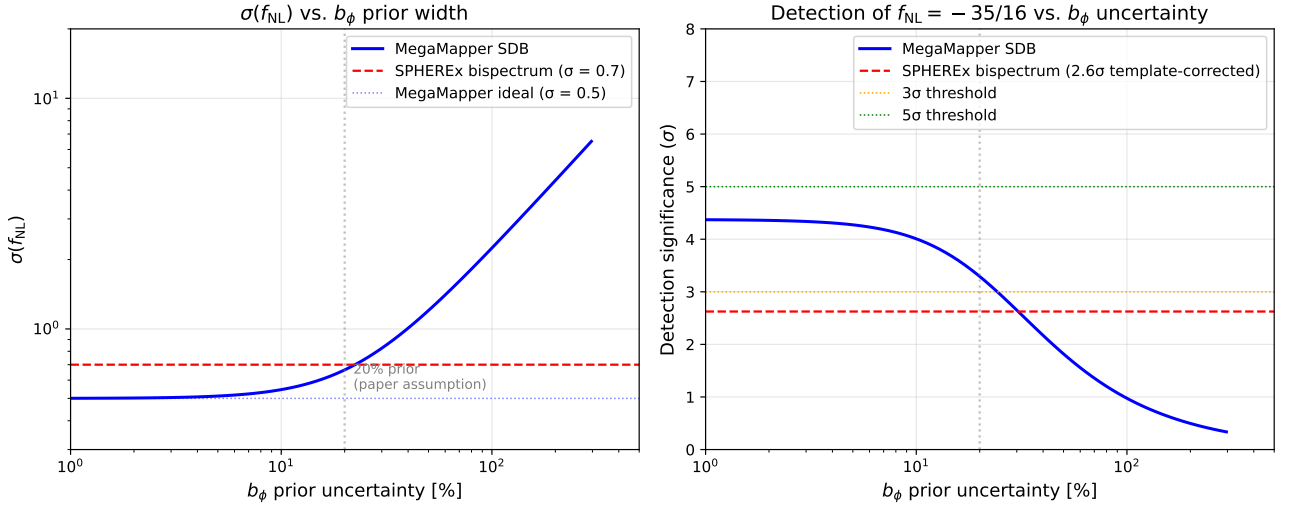


FIG. 5. Left:  $\sigma(f_{\text{NL}})$  as a function of  $b_\phi$  prior uncertainty for MegaMapper SDB (blue). The SPHEREx bispectrum constraint (red dashed) is less sensitive to  $b_\phi$  than SDB but not independent of it; the residual dependence enters at tree level through the  $\Delta b(k) \propto f_{\text{NL}} b_\phi / k^2$  cross-terms  $f_{\text{NL}} b_\phi b_1^2 P(k_1) P(k_2)$  in the multi-tracer Fisher matrix [1], which propagate to all triangle configurations and not only the squeezed limit. Right: corresponding detection significance for the corrected central  $f_{\text{NL}} = -35/16$  (all significances one-half of the erroneous  $-35/8$  values). At the paper's assumed 20% prior (gray line; the SPHEREx multi-tracer bispectrum combined-sample baseline is  $\sigma(f_{\text{NL}}) = 0.7$  at this point, not a per-redshift-bin uncertainty), MegaMapper gives  $\sim 2\sigma$ ; relaxing the per-tracer-bin  $b_\phi$  prior to 30% widens the combined-sample SPHEREx  $\sigma(f_{\text{NL}})$  to  $\approx 0.9$ – $1.0$ , and relaxing to 50% drops MegaMapper to  $\sim 1\sigma$ . The bispectrum channel remains at  $\sim 2.6\sigma$  (optimistic) or  $\sim 1.5$ – $2\sigma$  (after GR degradation) at fixed Heinrich *et al.*  $b_\phi$  universality [1]; relaxing  $b_\phi$  universality per tracer bin [34] degrades the optimistic 2.6– $2.75\sigma$  headline to  $\sim 2.0$ – $2.1\sigma$  (30% central) and  $\sim 1.75$ – $1.85\sigma$  (50% conservative).

3.3–5.7 (at the corrected central  $-35/16$ ), with the three-point grid converged to  $< 0.01$  in log-evidence on this column — and  $\text{BF} \approx 19$  vs. SSFSR (at the corrected  $-35/16$  center; the superseded  $-35/8$  center gave  $8.6 \times 10^3$ ), which sits between the  $\sigma_{\text{GR}} = 0.5$  ( $\sim 27$ ) and  $\sigma_{\text{GR}} = 1.0$  ( $\sim 5$ ) cells because the exponentially  $\sigma$ -sensitive SSFSR evidence is dominated by the conservative end of the prior (computation released

as `c9k_gr_continuous_marginalization.py`; see Data and Code Availability). The discrete grid is therefore a faithful summary of the continuous marginalization for the bounce-vs-tuned comparison, and the continuous SSFSR value is reported directly above.

The parameterization  $\sigma_{\text{GR}} \in [0, 1.0]$  is an internal stress-test amplitude grid, motivated by — but not a direct translation of — published demonstrations that

relativistic projection effects materially contaminate  $f_{\text{NL}}$  inference. Addis et al. [33], analyzing the multipoles of the full relativistic power spectrum, show that neglecting relativistic effects (Doppler, gravitational redshift, lensing, and light-cone effects) produces best-fit  $f_{\text{NL}}$  biases of order  $\sim 3\sigma$  for a Euclid-like H $\alpha$  survey and  $\sim 20\sigma$  for a MegaMapper-like Lyman-break sample, with a 15–20% improvement available from bright/faint multi-tracer splitting. They do not report a  $\sigma(f_{\text{NL}})$  degradation for an SPHEREx-class survey; our  $\sigma_{\text{GR}}$  values are therefore stress-test amplitudes chosen to span a plausible contamination scale, not figures calibrated to their Fisher results. Under the additive-quadrature model of Table IV ( $\sigma_{\text{eff}} = \sqrt{\sigma_{\text{base}}^2 + \sigma_{\text{GR}}^2}$ , calibrated to the conservative contamination scale of Addis et al. rather than to a direct Fisher translation), the  $\sigma_{\text{GR}} = 0.5$  scenario corresponds to a  $\sim 23\%$  inflation of the effective uncertainty ( $\sigma_{\text{eff}}/0.7 = 0.860/0.700 = 1.23$ ); the  $\sigma_{\text{GR}} = 1.0$  scenario is the conservative bound, appropriate in spirit for the high-redshift samples where Addis et al. find the largest relativistic biases. The “optimistic” case (2.6–2.75 $\sigma$ ) in Sec. IV omits GR degradation ( $\sigma_{\text{GR}} = 0$ ); the “realistic” case (1.3–2.75 $\sigma$ ) includes it at the  $\sigma_{\text{GR}} = 0.5$ –1.0 level.

#### D. Additional Systematic Considerations

Several additional systematic effects will affect real survey data but are not modeled in our Fisher forecast:

- *Nonlinear galaxy bias*: Higher-order bias terms ( $b_2$ ,  $b_{s^2}$ ,  $b_{\nabla^2\delta}$ ) enter the galaxy bispectrum at leading order and are partially degenerate with  $f_{\text{NL}}$  for some triangle configurations. The Heinrich et al. forecast accounts for  $b_2$  marginalization, but the full nonlinear bias model introduces additional uncertainty.
- *Photometric redshift outliers*: For SPHEREx, catastrophic photo- $z$  failures ( $\Delta z \sim 1$ ) create spurious large-scale power that can mimic the  $f_{\text{NL}}$  signal. A simplified Fisher degradation estimate indicates that the *bispectrum* channel is highly robust: even with 10% catastrophic outlier fraction,  $\sigma(f_{\text{NL}})$  degrades by only  $\sim 5\%$  (from 0.70 to 0.74), preserving the 1.3–2.75 $\sigma$  post-budget envelope of Sec. VII ( $\gtrsim 1.25\sigma$  in the most conservative all-combined scenario). The *scale-dependent bias* channel is far more vulnerable (degradation  $> 10\%$  at 10% outlier fraction), consistent with the photo- $z$  degradation estimates of Pullen & Hirata (2010) [37] and Giannantonio et al. (2012) [32]; this is one reason the bispectrum is the primary SPHEREx forecast channel adopted in this paper.
- *Integral constraint*: Galaxy surveys estimate the mean density from the survey itself, biasing the large-scale power spectrum measurement and potentially absorbing part of the  $f_{\text{NL}}$  signal at the lowest  $k$  modes.

- *Lensing magnification bias*: At high redshifts ( $z > 2$ ), lensing magnification produces a signal scaling as  $1/k^2$  on large scales, mimicking the scale-dependent bias from  $f_{\text{NL}}$ . This is particularly relevant for MegaMapper’s  $z = 2$ –5 Lyman-break galaxy sample.

These effects are expected to degrade the forecast significance by an estimated  $\mathcal{O}(10$ –30%) relative to the idealized Fisher estimate (this is an order-of-magnitude estimate based on the individual degradation factors above, not a joint marginalization over all systematics simultaneously), but do not qualitatively change the conclusion that SPHEREx can test the corrected central  $f_{\text{NL}} = -35/16$  at the realistic 1.3–2.75 $\sigma$  level. For one- $\sigma$  reconciliation of the significance windows quoted in this paper: the realistic SPHEREx-only window is 1.3–2.75 $\sigma$  (post-systematic-budget); the conservative endpoint of the  $b_\phi$  50%-prior bispectrum degradation is  $\sim 1.75$ –1.85 $\sigma$  (§VII, within the realistic window); and the wider 1.5–3.5 $\sigma$  envelope quoted for the survey program combines that conservative SPHEREx endpoint with the MegaMapper optimistic ceiling ( $\sim 3.5\sigma$ , a proposed-facility projection, not a SPHEREx forecast).

#### E. Consolidated Systematic Budget

Table V consolidates all systematic contributions to the SPHEREx bispectrum detection significance in one place. Each row identifies the source, its numerical value or range, whether it degrades the numerator (signal amplitude), the denominator (effective  $\sigma(f_{\text{NL}})$ ), or both, the combination rule, and the resulting cumulative  $\sigma_{\text{eff}}$  at the corrected central  $f_{\text{NL}} = -35/16$ . The significance at each row is  $|f_{\text{NL}}| \times r / \sigma_{\text{eff}}$  with  $|f_{\text{NL}}| = 2.1875$ .

We state the budget construction explicitly. The effective denominator is built by adding the imported baseline  $\sigma_0 \equiv \sigma(f_{\text{NL}}^{\text{local}}) = 0.7$  and each degrading nuisance  $\sigma_j$  in quadrature, while the numerator carries the multiplicative template-recovery factor  $r$ :

$$\mathcal{S} = \frac{|f_{\text{NL}}| r}{\sigma_{\text{eff}}}, \quad \sigma_{\text{eff}} = \left( \sigma_0^2 + \sum_j \sigma_j^2 \right)^{1/2}, \quad (11)$$

with  $r = 0.84$  (noise-weighted central),  $\sigma_{\text{GR}} \in \{0, 0.5, 1.0\}$ , and the  $b_\phi$  prior widening entering as a *baseline replacement*  $\sigma_0 \rightarrow \{0.7, 0.9, 1.0\}$  (20/30/50% widening) rather than an added-in-quadrature term. Eq. (11) is a deliberately conservative *scoping* construction, not a joint marginalized Fisher: it neglects the off-diagonal ( $f_{\text{NL}}, b_\phi, A_{\text{GR}}$ ) covariance, which the final row of Table V bounds independently via the inverse-Fisher marginalized error  $\sigma_{\text{marg}} = \sigma_0 / \sqrt{1 - \rho^2}$  at the paper’s own measured degeneracy  $\rho = -0.868$ . The two constructions bracket the true error: the additive-quadrature floor ( $\sim 1.5\sigma$  at GR=1.0) and the correlation-marginalized floor ( $\sim 1.3\sigma$ ) agree to  $\sim 14\%$ , so the headline 1.3–2.75 $\sigma$  envelope is robust to the quadrature-vs-marginalization

GR Treatment	BF vs. SSFSR	BF vs. Tuned	$P(\text{BF} > 3)$ vs. SSFSR
Ideal (no GR)	$1.4 \times 10^2$	5.7	88.8%
Marginalized ( $\sigma_{\text{GR}} = 0.5$ )	$\sim 27$	4.6	80.2%
Marginalized ( $\sigma_{\text{GR}} = 1.0$ )	$\sim 5$	3.3	61.5%
<i>Corrected (10% residual; = Ideal, verification only)<sup>a</sup></i>	$1.4 \times 10^2$	5.7	88.8%

TABLE IV. Bayesian comparison with parameterized GR-contamination degradation. SSFSR = standard single-field slow-roll inflation. All Bayes factors are closed-form Eq. (8) evaluations at the corrected central mock detection  $f_{\text{NL}} = -35/16$  with the GR-contamination nuisance added in quadrature to the SPHEREx baseline,  $\sigma_{\text{eff}} = \sqrt{0.7^2 + \sigma_{\text{GR}}^2}$ ; the “BF vs. Tuned” narrow-competitor values are  $\sim 5.7/4.6/3.3$  at the corrected center (one tail-vanished from the erroneous  $-35/8$  values  $7.0/6.1/4.7$ , since at  $-35/16$  the narrow competitor’s CDF lower tail is negligible). The “BF vs. SSFSR” column is quoted at the order-of-magnitude level only (it is exponentially prior- and center-sensitive):  $1.4 \times 10^2/27/5$  for  $\sigma_{\text{GR}} = 0/0.5/1.0$  ( $\sigma_{\text{eff}} = 0.700/0.860/1.221$ ), from the closed-form  $\exp[(35/16)^2/(2\sigma_{\text{eff}}^2)]$  at the corrected center — one to eight orders of magnitude below the superseded  $-35/8$  values ( $3.0 \times 10^8/4.2 \times 10^5/6.1 \times 10^2$ , from the same closed-form  $\exp[(35/8)^2/(2\sigma_{\text{eff}}^2)]$ ), reflecting the halved amplitude, but its qualitative  $> 1$  conclusion (favoring the bounce over the parameter-free single-field prediction) is unchanged.  $P(\text{BF} > 3)$  is the fraction of  $2 \times 10^5$  mock-detection realizations  $\hat{f}_{\text{NL}} \sim \mathcal{N}(-35/16, \sigma_{\text{eff}})$  exceeding  $\text{BF} = 3$  against SSFSR (script and output released with the paper’s code, `c9g_bf_table_recompute.py`, now evaluated at the corrected  $-35/16$  center; see Data and Code Availability). The “BF vs. Tuned” column reports the Bayes factor against a tuned multifield competitor with *narrow* prior  $[-5, +5]$  at the delta bounce prior; the no-GR cell (5.7) coincides with the narrow→broad sweep  $\text{BF} \sim 5.7 \rightarrow 17$  at the delta bounce prior reported in the prose of §VI, and the corresponding broad  $[-15, +15]$  competitor gives  $\text{BF} \sim 14$  at  $\sigma_{\text{GR}} = 0.5$  (center-independent). The bounce-vs-inflation comparison survives all treatment scenarios. <sup>a</sup>The “Corrected (10% residual)” row is a bookkeeping verification row, not an independent configuration: it implements the limit in which GR contamination is corrected and the post-correction residual is neglected at this template-overlap order, so it equals “Ideal” by construction. For calibration, a literal residual nuisance of  $\sigma_{\text{GR}} = 0.05$  (10% of the  $\sigma_{\text{GR}} = 0.5$  scenario amplitude surviving correction) gives  $\sigma_{\text{eff}} = 0.702$  and  $\text{BF vs. Tuned} = 5.68$  ( $\Delta\text{BF} = 0.02$  from the no-GR 5.70, below the reported precision), while the exponentially  $\sigma$ -sensitive BF-vs-SSFSR column would read  $1.38 \times 10^2$  rather than  $1.41 \times 10^2$  (both at the corrected  $-35/16$  center); the row is therefore reported in the strict zero-residual limit. The table thus contains three independent GR scenarios plus one verification row, and rows 1 and 4 bookend the same GR-free regime. As in Table III, the “BF vs. Tuned” entries use the  $r \rightarrow 1$  template bookkeeping ( $\sigma_{\text{eff}} = 0.7$  baseline before GR); the noise-weighted  $r = 0.84$  rebooking of Table III reduces the delta/narrow no-GR value  $5.7 \rightarrow 4.8$ .

choice. Accordingly the quantitative envelope is reported as an informational sensitivity range, with the marginalized  $\rho = -0.868$  endpoint as the quoted conservative significance.

## VIII. CURRENT DATA AND CONSISTENCY RELATION

### A. Planck + DESI Recast

Current constraints from Planck PR4/NPIPE (CMB bispectrum,  $f_{\text{NL}} = -0.1 \pm 5.0$  [38]) can be recast onto the bounce template using Eq. (5). Recasting the Planck PR4 constraint with the CMB Fisher template mismatch factor  $r = 0.876$  gives  $f_{\text{NL}}^{\text{bounce}} = -0.1 \pm 5.7$ , which is  $0.37\sigma$  from the corrected bounce prediction ( $|-2.1875 + 0.1|/5.71$ ; recasting the central value as well,  $-0.1/0.876 = -0.11$ , leaves the tension at  $0.37\sigma$ ) and  $0.02\sigma$  from zero—fully consistent with both. (The earlier PR3 Planck constraint was  $f_{\text{NL}} = -0.9 \pm 5.1$  [39]; the PR4 NPIPE reanalysis tightens the error bar by  $\sim 2\%$  and shifts the central value toward zero, strengthening consistency with the matter-bounce prediction.) (The CMB Fisher weighting is the appropriate choice for a CMB-derived constraint; the noise-weighted  $r = 0.84 \pm 0.02$  of Eq. 6 applies to LSS survey forecasts.) DESI DR1

LRG and QSO analyses report  $f_{\text{NL}}^{\text{loc}}$  bounds at  $\sigma \approx 9$ – $10$ :  $f_{\text{NL}}^{\text{loc}} = -3.6_{-9.1}^{+9.0}$  from the combined LRG+QSO sample [40];  $f_{\text{NL}}^{\text{loc}} = -3.3 \pm 9.2$  from the QSO assembly-bias analysis [41] (these are distinct analyses), consistent with both bounce and inflation at current precision. Recasting via  $r = 0.84$  gives  $\sigma(f_{\text{NL}}^{\text{bounce}}) \approx \sigma_{\text{loc}}/r \approx 11$ , far too weak to discriminate. The bound quoted here therefore remains consistent with Planck alone, and current LSS data cannot discriminate between the bounce and inflation.

### B. The $f_{\text{NL}}-n_s$ Consistency Relation

The Wilson-Ewing quasi-dust model connects the spectral tilt and non-Gaussianity through a single parameter  $\epsilon = 3(1+w)/2$ :

$$n_s = 8\epsilon - 11, \quad f_{\text{NL}}(\epsilon) = -\frac{35}{16} - \kappa_\epsilon(\epsilon - \frac{3}{2}) + \mathcal{O}(\epsilon - \frac{3}{2})^2, \quad (12)$$

where  $\kappa_\epsilon$  (not to be confused with the bispectrum polynomial coefficient  $c_1$  of Sec. II) depends on both the explicit  $A_T \propto 1/\epsilon^3$  prefactor in the cubic action and the  $|\eta|^{-\nu}$  mode-function amplitude (with  $\nu = 3/2$  at  $\epsilon = 3/2$  and finite by the Wilson-Ewing dust scaling), both of which change with  $\epsilon$  near  $\epsilon = 3/2$ . *Linearization note.* The

Systematic source	Value / range	Acts on	Combination rule	$\sigma$ (detection)
Naive uncorrected (ref. only)	$ f_{\text{NL}} /\sigma = 2.1875/0.7$	—	not used in headline	$3.13\sigma$ (no template correction; see caption)
Template-corrected baseline	$r = 0.84 \pm 0.02$ [0.829–0.876]	numer. ( $\times r$ )	multiplicative	$2.6\text{--}2.75\sigma$ headline
$\epsilon$ -correction	0.6–8% in $f_{\text{NL}}$	numer. ( $\pm \delta f_{\text{NL}}$ )	add. quadrature	$\lesssim 0.2\sigma$ effect
Null-space $r$ scatter	$r = 0.85 \pm 0.13$ ; 16th pctile $r = 0.70$	numer. ( $\times r$ )	distributional	floor $\approx 2.2\sigma$
$b_\phi$ (20%, baseline)	no degradation	—	—	$2.6\text{--}2.75\sigma$ optimistic
$b_\phi$ (30%, central)	$\sigma(f_{\text{NL}}) \rightarrow 0.9$	denom. (repl.)	Fisher widening / baseline replacement	$\sim 2.05\sigma$
$b_\phi$ (50%, conserv.)	$\sigma(f_{\text{NL}}) \rightarrow 1.0$	denom. (repl.)	Fisher widening / baseline replacement	$\sim 1.75\text{--}1.85\sigma$
GR ( $\sigma_{\text{GR}} = 0$ )	no GR	—	—	$2.6\text{--}2.75\sigma$
GR ( $\sigma_{\text{GR}} = 0.5$ )	$\sigma_{\text{eff}} = \frac{\sigma_{\text{base}}}{\sqrt{0.7^2 + 0.5^2}} = 0.86$	denom. ( $\oplus$ )	add. quadrature	$\sim 2.14\sigma$
GR ( $\sigma_{\text{GR}} = 1.0$ )	$\sigma_{\text{eff}} = \frac{\sigma_{\text{base}}}{\sqrt{0.7^2 + 1.0^2}} = 1.22$	denom. ( $\oplus$ )	add. quadrature	$\sim 1.5\sigma$
All combined 30% + GR 1.0)	$(b_\phi \sigma_{\text{eff}}) = \frac{\sigma_{\text{base}}}{\sqrt{0.9^2 + 1.0^2}} = 1.35$	denom. ( $\oplus$ )	add. quadrature	$\sim 1.36\sigma$
All combined 50% + GR 1.0)	$(b_\phi \sigma_{\text{eff}}) = \frac{\sigma_{\text{base}}}{\sqrt{1.0^2 + 1.0^2}} = 1.41$	denom. ( $\oplus$ )	add. quadrature	$\sim 1.3\sigma$ conserv.
Joint Fisher (marg., $\rho = -0.868$ proxy; upper edge)	$\sigma_{\text{marg}} = \frac{\sigma_{\text{base}}}{\sqrt{1 - 0.868^2}} = 1.41$	denom. (Fisher)	marginalized ( $1/\sqrt{1 - \rho^2}$ )	$\sim 1.3\sigma$
Joint Fisher (marg., $\rho = -0.95$ in-repo overlap; lower edge)	$\sigma_{\text{marg}} = \frac{\sigma_{\text{base}}}{\sqrt{1 - 0.95^2}} = 2.24$	denom. (Fisher)	marginalized ( $1/\sqrt{1 - \rho^2}$ )	$\sim 0.8\sigma$

TABLE V. Scenario/scoping budget (heuristic additive-quadrature; not a joint-covariance forecast) for the SPHEREx bispectrum detection of the corrected central  $f_{\text{NL}} = -35/16 = -2.1875$  (all  $\sigma$  values are exactly one-half of what the erroneous  $-35/8$  input would give). **Row types:** the first row (naive uncorrected) is shown for reference only and is *not* used in any headline; its  $3.13\sigma$  figure is not directly comparable to the template-corrected  $2.6\text{--}2.75\sigma$  headline because it uses a distinct null procedure (no template-mismatch correction applied). The template-corrected baseline row ( $r = 0.84$ ) is the starting point for all subsequent rows; the  $\epsilon$ -correction and null-space rows are *distributional* contributions (not cumulative denominators); the  $b_\phi$  and GR rows are *cumulative* additions to the effective denominator  $\sigma_{\text{eff}}$ ; the all-combined rows stack both contributions simultaneously. “Acts on” refers to the signal numerator ( $|f_{\text{NL}}| \times r$ ) or the effective denominator  $\sigma_{\text{eff}}$ . Combination rule “ $\oplus$ ” denotes addition in quadrature ( $\sigma_{\text{eff}} = \sqrt{\sigma_{\text{base}}^2 + \sigma_{\text{sys}}^2}$ ), a transparent scoping choice described in Sec. II C (additive-quadrature rather than joint-marginalized Fisher). Significance =  $|f_{\text{NL}}| \times r / \sigma_{\text{eff}}$  with  $r = 0.84$  (noise-weighted central value). The  $b_\phi$ -30% row uses  $\sigma(f_{\text{NL}}) \rightarrow 0.9$  (30% widening over the baseline 0.7; the effective denominator increases to 0.9 as the  $b_\phi$  marginalization replaces the baseline). The all-combined rows add GR degradation on top of the  $b_\phi$ -widened denominator using the additive-quadrature systematic budget defined in Sec. VII. The  $\sim 1.3\text{--}2.75\sigma$  post-systematic-budget envelope quoted in the abstract spans the all-combined conservative floor (bottom row) to the no-GR optimistic ceiling (template-corrected baseline row with  $b_\phi$ -20% assumption). The effective denominator  $\sigma_{\text{eff}}$  is defined in Sec. IV (Eq. 5) as the quadrature combination of  $\sigma(f_{\text{NL}}^{\text{local}})$  and any additional systematic nuisances; all  $\sigma_{\text{eff}}$  values in this table follow that convention. The final two rows replace the additive-quadrature GR floor with the inverse-Fisher marginalized error  $\sigma_{\text{marg}} = \sigma_{\text{base}} / \sqrt{1 - \rho^2}$  and bracket the honest marginalized floor  $\sigma_{\text{marg}} \approx 0.8\text{--}1.3\sigma$  (both below the quadrature  $1.5\sigma$ ): the upper edge uses the paper’s own directly-measured CAMB degeneracy  $\rho = -0.868$  (c8, transferred as a proxy pending the channel-native  $\partial B_g / \partial A_{\text{GR}}$  derivative), the lower edge the in-repo  $|\rho| \approx 0.95$  GR-projection shape overlap (c12); we adopt  $\rho = -0.868$  as the quoted conservative endpoint (best-available, source-cited, and shown *not* to be an underestimate) while displaying the  $0.8\sigma$  lower edge explicitly so the more-favorable value is not headlined alone (§VII).

relation  $n_s = 8\epsilon - 11$  follows from the exact growing-mode relation  $n_s = 1 + 12w$  (Ref. [2]) upon substituting  $\epsilon = 3(1 + w)/2$ . The standard slow-roll formula  $n_s - 1 = 2(2\epsilon - \eta)$  gives a consistent result at leading order near  $\epsilon = 3/2$  but is not the natural parametrization for the bounce; small deviations from  $w = 0$  (the quasi-dust equation of state  $w = -0.003$ ) produce a correction of order  $|w| \sim 10^{-3}$  in  $n_s$ , entirely negligible relative to the 0.6–8%  $\epsilon$ -correction uncertainty in  $f_{\text{NL}}$ . The coefficient  $\kappa_\epsilon$  is bounded by two physically distinct contributions to the  $\epsilon$ -derivative of the Cai et al. [9] cubic-action prefactor  $A_T \propto 1/\epsilon^3$  at  $\epsilon = 3/2$  (the explicit-prefactor channel) and to the Hankel-index dependence of the matter-contraction mode functions  $\zeta_k \propto |\eta|^{-\nu(\epsilon)}$  with  $\nu = 3/2 + \mathcal{O}(\epsilon - 3/2)$  (the mode-function channel; cf. Wilson-Ewing [2] for the linear-order scaling and Cai et al. [9] App. B for the cubic-vertex sensitivity). Explicit prefactor scaling alone gives  $\kappa_\epsilon \approx 2.8$  (lower bound, holding mode functions fixed at  $\epsilon = 3/2$ ; the  $\kappa_\epsilon$  coefficient is the  $\epsilon$ -derivative of  $f_{\text{NL}}$  and therefore halves along with the corrected central amplitude  $-35/16$ ); the mode-function amplitude channel ( $|\eta|^{-\nu}$  growth with  $\nu$  finite at  $3/2$ ) adds a multiplicative correction which we bound schematically at  $\approx 14\times$  the prefactor-only value, giving  $\kappa_\epsilon \approx 40$  as the upper endpoint; the upper endpoint is a schematic scaling bound, not a derived coefficient. The order-of-magnitude span [2.8, 40] therefore reflects the well-known sensitivity of cubic-order quantities to the combined  $A_T \propto 1/\epsilon^3$  prefactor and the  $|\eta|^{-\nu}$  mode-function amplitude channels near exact matter domination, not a free parameter; pinning  $\kappa_\epsilon$  to better than this range requires the full four-vertex numerical evaluation discussed in Sec. II C. Even the conservative endpoint shifts  $f_{\text{NL}}$  by only  $\kappa_\epsilon |\Delta\epsilon| \approx 40 \times 0.0045 \approx 0.18$  — well inside the recommended  $\sigma_{\text{theory}} = 1.0$  bounce prior — so no Bayes-factor conclusion in Sec. VI hinges on the precise value of this endpoint. Eliminating  $\epsilon$  via  $\Delta\epsilon = \Delta n_s/8$ , the consistency relation takes the form

$$f_{\text{NL}}(n_s) \approx -\frac{35}{16} - c'(n_s - 1), \quad c' \equiv \kappa_\epsilon/8 \in [0.35, 5], \quad (13)$$

where  $c' \equiv \kappa_\epsilon/8 > 0$  follows directly from  $\Delta\epsilon = (n_s - 1)/8$  and the leading-order coefficient  $-\kappa_\epsilon$  of the  $\epsilon$ -form above; as the equation of state approaches exact matter domination from  $w < 0$  (so  $\epsilon \rightarrow 3/2^-$  and  $n_s \rightarrow 1^-$ ), both deviations vanish and  $f_{\text{NL}} \rightarrow -35/16$ . For  $\epsilon < 3/2$  (the quasi-dust regime  $w < 0$ ),  $(\epsilon - 3/2) < 0$  and the correction  $-\kappa_\epsilon(\epsilon - 3/2) > 0$ , so  $f_{\text{NL}}$  moves *less negative* than  $-35/16$  — consistent with the Planck- $n_s$  range quoted below. At the Planck best-fit  $n_s = 0.9649$ , this gives  $f_{\text{NL}} \in [-2.175, -2.01]$  (a 0.6–8% correction on the corrected central  $-35/16$ , within  $\sigma \approx 0.7$ ). Narrowing this range requires evaluating all four cubic-action integrals simultaneously with numerically computed mode functions, preserving the cancellations that render the physical bispectrum finite; that dedicated four-vertex in-computation is outside the scope of this forecast paper, and its impact on the present results is bounded by

the  $\kappa_\epsilon |\Delta\epsilon| \approx 0.18$  shift quoted above, inside the recommended  $\sigma_{\text{theory}} = 1.0$  bounce prior. The consistency relation is nonetheless conceptually significant: it connects  $n_s$  (already measured) and  $f_{\text{NL}}$  (to be measured) through a single-parameter curve. Standard multifield inflation has no equivalent—multifield  $f_{\text{NL}}$  is unconstrained by  $n_s$ . Joint use of the existing Planck  $n_s$  measurement and the SPHEREx  $f_{\text{NL}}$  measurement (anchored at  $\sigma(f_{\text{NL}}) \approx 0.7$  for the bispectrum-only forecast, or  $\approx 0.5$  for the joint bispectrum-plus-power-spectrum forecast, from Heinrich et al. 2024; the abstract’s headline  $\sigma(f_{\text{NL}}) \approx 0.7$  is the bispectrum-only number, and is consistent with the lower end of the  $\approx 0.5$ – $0.7$  range quoted here) provides a direct test of Eq. (13) and therefore a survey-level discriminator between the matter bounce and slow-roll inflation.

## IX. DISCUSSION

### A. The Staged Observational Strategy

SPHEREx (launched March 2025; first all-sky survey completed December 2025; science data release expected  $\sim 2028$ ) provides the first real test via the galaxy bispectrum at  $\sim 1.3$ – $2.75\sigma$  significance after the full systematic budget ( $\sim 2.6$ – $2.75\sigma$  optimistic before GR and  $b_\phi$  degradation; the lower bound of this optimistic range reflects the noise-weighted template overlap  $r = 0.84$ ). MegaMapper, a proposed facility without confirmed funding or finalized design ( $\sim 2032+$  if approved), could provide a more powerful follow-up at  $\sim 1.5$ – $3.85\sigma$  (the design-uncertainty envelope of Sec. V; ideal  $3.7$ – $3.85\sigma$ , conservative post-budget  $\sim 1.5$ – $3.5\sigma$ ) via scale-dependent bias, though with greater systematic fragility and significant design-dependent uncertainty in the forecast range.

### B. Complementary Experiments

Several other experiments will also constrain local-type  $f_{\text{NL}}$  in the coming decade [42–44]:

- *DESI*: Already taking data; expected  $\sigma(f_{\text{NL}}) \approx 3$ – $5$  from scale-dependent bias with luminous red galaxies and emission-line galaxies [42]. (The DESI, Euclid, and LSST figures quoted in this list are primarily scale-dependent-bias / power-spectrum forecasts, a different channel from the SPHEREx multi-tracer *bispectrum* baseline of this paper; they are complementary probes, not like-for-like sensitivity comparisons.)
- *Euclid*: Launched 2023; published forecasts give  $\sigma(f_{\text{NL}}) \approx 2$ – $4$  from the photometric galaxy survey [43].
- *Vera Rubin Observatory (LSST)*: Complementary photometric  $f_{\text{NL}}$  constraints from  $\sim 10^{10}$  galaxies at lower redshift.

- *CMB-S4*: Expected  $\sigma(f_{\text{NL}}) \approx 2.5$  from the CMB temperature and polarization bispectrum, providing a completely independent channel [44].

A detection of  $f_{\text{NL}} \approx -2$  by SPHEREx (the corrected central  $-35/16 = -2.1875$ ; the superseded Cai value would have been  $\approx -4$ ), if confirmed by any of these independent probes, would constitute overwhelming evidence for non-Gaussianity incompatible with standard single-field inflation.

### C. Decision Thresholds

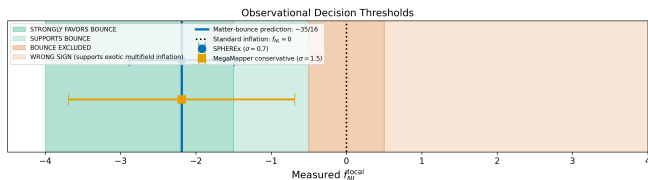


FIG. 6. Observational decision thresholds on the measured local-template  $f_{\text{NL}}$  (horizontal axis). Shaded regions, left to right: dark green — measurement near the corrected  $-35/16$  prediction, strongly favors the bounce; light green — negative  $f_{\text{NL}}$  of bounce-compatible magnitude, supports the bounce; dark red (legend label “bounce excluded”) — measurement consistent with zero, disfavoring the quasi-dust matter bounce while remaining consistent with standard single-field inflation; light red — positive  $f_{\text{NL}}$ , disfavoring the bounce and instead supporting exotic multifield inflation. Blue vertical line: corrected bounce prediction  $f_{\text{NL}} = -35/16$ ; black dotted line: standard inflation  $f_{\text{NL}} \approx 0$ . Error bars: SPHEREx ( $\sigma = 0.7$ ) and MegaMapper conservative ( $\sigma = 1.5$ , illustrative: between the  $\sigma \approx 0.5$  ideal and the  $b_\phi$ -50% degraded  $\sigma \approx 2.2$  of Sec. VII, not an independently calibrated forecast), both centered on the bounce prediction.

A measurement of  $f_{\text{NL}} = -2 \pm 1$  by SPHEREx would provide evidence favoring a contracting/bounce origin over standard single-field inflation. A null result ( $f_{\text{NL}}$  consistent with zero at the  $2\sigma$  level) would disfavor the quasi-dust matter bounce: at the SPHEREx baseline  $\sigma(f_{\text{NL}}) = 0.7$  with the noise-weighted template-overlap correction  $r \in [0.829, 0.876]$ , a measurement centered on zero excludes the corrected matter-bounce prediction  $f_{\text{NL}} = -35/16$  at the same significance as a detection would carry (specifically  $|f_{\text{NL}}| r / \sigma(f_{\text{NL}}) \approx 2.6$ – $2.75\sigma$  before GR and  $b_\phi$  degradation, degrading to the  $\sim 1.3$ – $2.75\sigma$  post-budget envelope after the realistic systematic budget of Sec. VII, since the exclusion arithmetic is symmetric to the detection arithmetic), conditional on assumptions (a)–(f) of Sec. II C.

### D. The Joint $(f_{\text{NL}}, n_{f_{\text{NL}}})$ Scale-Dependent-Bias Fisher Forecast

*Motivation, methodology, and scope.* The forecast reported in this subsection is a separately computed scale-dependent-bias (SDB) Fisher matrix for  $(f_{\text{NL}}, n_{f_{\text{NL}}})$ , methodologically distinct from the imported Heinrich *et al.* bispectrum forecast of §IV: it is a *new galaxy-covariance Fisher computation* (c8\_fnl\_running\_fisher.json, Planck 2018, CAMB 1.6.6), not a recast of an external  $\sigma(f_{\text{NL}})$ , and it constrains the SDB linear-bias amplitude  $\Delta b(k) \propto f_{\text{NL}} b_\phi / k^2$  over six SPHEREx low-redshift bins rather than the bispectrum shape. Its motivation is that the *running* of  $f_{\text{NL}}$  is a sharper bounce-vs-inflation discriminator than the amplitude alone; its headline result is that marginalizing over  $n_{f_{\text{NL}}}$  degrades the SDB  $f_{\text{NL}}$  constraint by  $2.0$ – $4.6\times$  ( $\sigma_{\text{unmarg}}(f_{\text{NL}}) = 1.53 \rightarrow \sigma_{\text{marg}}(f_{\text{NL}}) = 3.08$  fixed-bias  $\rightarrow 7.06$  bias-marginalized;  $\sigma(n_{f_{\text{NL}}}) = 0.295/0.596$ ; anti-correlation  $\rho \approx -0.87$  to  $-0.97$ ). It is reported here as a *subordinate cross-check* on the scale dependence, not as the paper’s headline forecast, which remains the bispectrum-only  $2.6$ – $2.75\sigma$  of §IV.

A stronger discriminator between the matter bounce and inflationary alternatives is the *scale dependence* of  $f_{\text{NL}}$ , parameterized by the running index  $n_{f_{\text{NL}}} \equiv d \ln |f_{\text{NL}}| / d \ln k$ . At leading order, the quasi-dust matter bounce predicts  $n_{f_{\text{NL}}} = 0$  (exact scale invariance in the squeezed limit: the dimensionless shape function  $B_{\text{NL}}$  is a degree-9 polynomial divided by a degree-9 normalization — degree-zero in the overall momentum scale — so the squeezed-limit amplitude carries no running at leading order). A joint Fisher forecast for  $(f_{\text{NL}}, n_{f_{\text{NL}}})$  using SPHEREx scale-dependent bias over six redshift bins ( $z = 0.1$ – $1.5$ ,  $f_{\text{sky}} = 0.75$ ; this is the low-redshift bin subset of the SPHEREx public-products sample structure used in the committed SDB Fisher computation, a different tracer selection from the  $z \approx 0.5$ – $2$  emission-line sample underlying the Heinrich *et al.* bispectrum forecast of Sec. IV — the two channels quote different redshift ranges by construction) yields  $\sigma(n_{f_{\text{NL}}}) = 0.295$  after marginalizing over  $f_{\text{NL}}$  ( $0.596$  with the per-sample linear biases additionally marginalized as free nuisances), with marginalized  $\sigma(f_{\text{NL}}) = 3.08$  ( $7.06$  bias-marginalized)—a  $2.0\times$  ( $4.6\times$ ) degradation from the  $f_{\text{NL}}$ -only constraint  $\sigma_{\text{unmarg}}(f_{\text{NL}}) = 1.53$  due to a strong anti-correlated  $f_{\text{NL}}$ - $n_{f_{\text{NL}}}$  degeneracy ( $\rho = -0.87$  fixed-bias,  $-0.969$  bias-marginalized; here  $\rho$  is defined on the reduced post-marginalization  $2 \times 2$  Fisher sub-covariance over  $(f_{\text{NL}}, n_{f_{\text{NL}}})$  after the per-sample linear biases have been profiled out). With biases co-marginalized the  $n_{f_{\text{NL}}}$ -fixed baseline is itself  $\sigma(f_{\text{NL}}) = 1.75$  rather than  $1.53$ , and the two-parameter identity  $\sigma_{\text{marg}} = \sigma_{\text{unmarg}} / \sqrt{1 - \rho^2}$  applied to that baseline reproduces the quoted value ( $1.75 / \sqrt{1 - 0.969^2} = 7.06$ ); the  $4.6\times$  factor above is referenced to the fixed-bias  $1.53$  for comparability with the fixed-bias column. This de-

generacy arises because both parameters modulate the large-scale bias through the same  $1/k^2$  transfer kernel; breaking it requires bispectrum measurements at multiple triangle configurations and scales. *Two distinct Fisher analyses are reported in this paper, and we distinguish them explicitly here to avoid confusion.* (i) The headline bispectrum-only Fisher forecast ( $\sigma(f_{\text{NL}}) \approx 0.7$  from Heinrich *et al.* 2024 [1], building on the canonical SPHEREx multi-tracer galaxy-survey forecast lineage of Doré *et al.* [14]) drives the abstract 2.6–2.75 $\sigma$  optimistic figure (template-corrected) and the 1.3–2.75 $\sigma$  post-systematic-budget figure (§VII). (ii) A separate joint  $(f_{\text{NL}}, n_{f_{\text{NL}}})$  Fisher matrix using SPHEREx scale-dependent bias over the same six redshift bins ( $\sigma(n_{f_{\text{NL}}}) = 0.295/0.596$ ,  $\sigma_{\text{marg}}(f_{\text{NL}}) = 3.08/7.06$ , fixed-bias/bias-marginalized). In the SDB-only joint analysis the corrected matter-bounce  $f_{\text{NL}} = -35/16$  is detectable at only 0.71 $\sigma$  (fixed-bias) to 0.31 $\sigma$  (bias-marginalized) after marginalizing over  $n_{f_{\text{NL}}}$ : the SDB joint channel is a *subordinate* cross-check on the running, not a competitor to the bispectrum-only headline. The joint-SDB figures are therefore not the same baseline as the bispectrum-only 2.6–2.75 $\sigma$  optimistic figure; the two come from different Fisher matrices and target different observables. In particular, the template-overlap factor  $r = 0.84$  that drives the bispectrum-only forecast (single-bin bispectrum amplitude  $\rightarrow$  template-corrected  $0.84 \times 3.13\sigma = 2.63\sigma$  at the corrected central  $-35/16$ ) does *not* apply to the SDB-Fisher, because SDB constrains the linear-bias amplitude of the scale-dependent bias correction  $\Delta b(k) \propto f_{\text{NL}} b_\phi / k^2$ , not the bispectrum shape; the bispectrum-only and SDB-only Fisher matrices use different sufficient statistics and the  $r = 0.84$  shape-mismatch factor is intrinsic to the bispectrum projection. After the joint systematic budget (noise-weighted shape mismatch  $r = 0.84$ ,  $\epsilon$ -correction, photometric- $z$  degradation, PNG bias,  $b_\phi$  marginalization, relativistic projection uncertainties; §VII) the joint  $(f_{\text{NL}}, n_{f_{\text{NL}}})$  analysis would also degrade, but a quantitative post-systematic joint forecast is beyond the scope of the present paper. The SDB-only  $\sigma_{\text{unmarg}}(f_{\text{NL}}) = 1.53$  is consistent in scaling with, though  $\approx 2.2\times$  weaker than, the bispectrum-only  $\sigma(f_{\text{NL}}) = 0.7$  baseline and with the published SPHEREx SDB forecast lineage (Doré+2014, Heinrich+2024, Münchmeyer+2019), as expected for the six-bin subset of the full eleven-sample stack. The  $n_{f_{\text{NL}}} = 0$  prediction is testable to  $\pm 0.30$  (fixed-bias) to  $\pm 0.60$  (bias-marginalized) at the same idealized-Fisher level. (DBI inflation is distinguished from local-type non-Gaussianity by its vanishing squeezed-limit amplitude and equilateral shape, not by its  $n_{f_{\text{NL}}}$  running, so a meaningful DBI-vs-bounce SDB comparison would require the bispectrum-shape channel rather than the local  $n_{f_{\text{NL}}}$  channel; we do not include DBI in the SDB discriminator list for this reason.) The same scale-dependence comparison should be extended to two more relevant alternatives: (i) self-interacting / axion-curvaton models, which can produce  $|f_{\text{NL}}| \sim 2$  with  $n_{f_{\text{NL}}}$  tuned by the curvaton self-interaction (typical range  $|n_{f_{\text{NL}}}| \lesssim 0.3$ ), giv-

ing a  $\sim 0$ –3 $\sigma$  separation depending on the curvaton parameters; and (ii) quasi-single-field inflation (QSFI) [36], which generates a continuously variable  $n_{f_{\text{NL}}}$  controlled by the heavy-field mass-to-Hubble ratio  $\mu/H$  (in the squeezed limit the bispectrum normalized to the local template scales as  $(k_3/k_1)^\Delta$  with scaling dimension  $\Delta = 3/2 - \sqrt{9/4 - \mu^2/H^2}$ ; Chen & Wang [36]). At  $\mu/H = 0$  (massless isocurvaton)  $\Delta = 0$  and the exponent vanishes, reproducing the local-template scaling exactly (the curvaton-like limit); at  $\mu/H = 3/2$  (the QSFI principal-vs-complementary-series boundary  $m^2 = 9H^2/4$ , distinct from the Higuchi bound which applies to spin-2 fields with  $m^2 \geq 2H^2$ )  $\Delta = 3/2$  and the squeezed amplitude is suppressed by  $(k_3/k_1)^{3/2}$  relative to local — the intermediate shape, departing furthest from the local template. The bounce-vs-QSFI discrimination boundary therefore sets a parameter-dependent margin in  $(\mu/H, n_{f_{\text{NL}}})$  space; rather than committing to a single discrimination  $\sigma$ , we note that the bounce  $n_{f_{\text{NL}}} = 0$  prediction is structurally compatible with the local-template-like regime  $\mu/H \rightarrow 0$ , and a comprehensive SDB+bispectrum joint analysis is required to map the full discrimination region.

*Channel hierarchy and sub-labeling note.* This subsection (Sec. IX.D in the standard *Physical Review D* sectioning of the submitted manuscript) reports the joint scale-dependent-bias Fisher analysis as a *subordinate discriminator* within the Discussion; it is not a stand-alone SDB forecast section. The primary SPHEREx channel in this paper is the multi-tracer galaxy bispectrum (Sec. IV,  $\sigma(f_{\text{NL}}) \approx 0.7$ ); the SDB channel (Sec. III,  $\sigma_{\text{unmarg}}(f_{\text{NL}}) = 1.53$ ,  $\sigma_{\text{marg}}(f_{\text{NL}}) = 3.08$ –7.06) enters only as (a) the  $\Delta b(k)$  signal definition underlying the bispectrum’s template-overlap calculation (Sec. III B) and (b) the joint  $(f_{\text{NL}}, n_{f_{\text{NL}}})$  running discriminator reported here. The two channels use distinct Fisher matrices, distinct survey samples, and distinct sufficient statistics; they are complementary rather than competing. Readers seeking the headline SPHEREx forecast should consult Sec. IV; the joint SDB discussion in this subsection provides an additional model-discrimination diagnostic conditional on the bispectrum detection.

No trispectrum prediction is derived in this paper. The Suyama-Yamaguchi (SY) inequality  $\tau_{\text{NL}} \geq (6f_{\text{NL}}/5)^2$  is governed by single- vs multi-source structure of the curvature perturbation, not by overlap of the local bispectrum template against the matter-bounce shape: for a structurally single-source bounce, a local single-source analogy would suggest  $\tau_{\text{NL}} \approx (36/25)f_{\text{NL}}^2$  up to configuration-form-factor corrections, independent of the template-overlap  $r \in [0.829, 0.876]$  reported in Sec. III B. A local single-source analogy with the corrected  $|f_{\text{NL}}| = 35/16$  would correspond to an order-of-magnitude  $\tau_{\text{NL}} \sim (36/25)f_{\text{NL}}^2 \approx 6.89$ , far below the current Planck constraint ( $\tau_{\text{NL}} < 2800$  at 95% CL [39]) and below SPHEREx sensitivity, but this is not used in any forecast in this paper; a quantitative  $\tau_{\text{NL}}$  prediction for the matter bounce requires a direct trispectrum computation, which we do not undertake here. The  $\tau_{\text{NL}}$  channel

may become testable with future spectroscopic surveys achieving  $\sigma(\tau_{\text{NL}}) \sim \mathcal{O}(10)$ .

### E. Caveats

*a. Scope summary.* This paper is a sensitivity *recast* of a single externally published baseline; the following points collect the deliberate, labeled scope of that recast, each addressed in full detail in the sections cited. (i) *Recast, not an independent multi-tracer forecast.* Every significance and Bayes factor rescales the single imported Heinrich *et al.* [1]  $\sigma(f_{\text{NL}}^{\text{local}}) \approx 0.7$  baseline through the explicit map  $(\hat{f}^{\text{bounce}}, \sigma^{\text{bounce}}) = (\hat{f}^{\text{local}}/r, \sigma^{\text{local}}/r)$ ,  $r = 0.84$  (Eq. 5; abstract *Scope* sentence; §III B/§IV). An independent in-house multi-tracer bispectrum Fisher (§IV, `c13_independent_bounce_fisher.py`) validates this recast — it reproduces the Heinrich local baseline to 2–11% and recovers  $r_{\text{eff}} \approx 0.99$  for the bounce template, an unmarginalized  $\sim 3.2\text{--}3.5\sigma$  before the systematic/GR-projection budget — confirming the  $r = 0.84$  flat-weight shape overlap is conservative; the headline  $1.3\text{--}2.75\sigma$  range is the systematic-budgeted recast, not this unmarginalized independent number. (ii) *Cubic-order transmission: bounded systematic.* Assumption (d) is verified at linear order [2] and, at cubic order, closed by degree-of-freedom counting — effective LQC adds no new scalar degree of freedom [2, 19], so the Wilson-Ewing bounce is single-clock, nonlinear superhorizon  $\zeta$ -conservation holds to all orders, and transmission =  $1 \pm \mathcal{O}((k\eta_{\text{bounce}})^2) \approx 1 \pm 10^{-4}$  ( $\delta f_{\text{NL}} \lesssim 10^{-3}$ ); this model also evades the Quintin *et al.* [3] no-go (Sec. II C). The sole remaining model-dependence is the sign of the subleading gradient coefficient — a citable quantization choice, not an open computation. (iii) *Cai-Li factor-of-two resolved.* A from-scratch re-summation of Cai *et al.*’s own four cubic-action vertices at  $\epsilon = 3/2$  yields  $-35/16$  in the squeezed limit, matching Li *et al.*’s independent general- $c_s$  result at  $c_s = 1$  (Appendix A). One identified discrepancy between Cai’s transcribed final polynomial and the exact vertex sum is a  $-(99/128) \sum_i k_i^3$  term, absent from every intermediate expression, which drives the transcribed polynomial’s squeezed reduction to  $-305/64$  (Cai’s separately-published  $-35/8$  is not reproduced by the transcribed coefficients and is retained only as an erroneous literature value); both works share the same  $f_{\text{NL}} = 10A/(3 \sum k_i^3)$  convention, so this is a discrepancy in the polynomial collapse step, not a convention difference. The corrected  $f_{\text{NL}} = -35/16$  is adopted as central; the erroneous  $-35/8$  is retained only as a literature-reference bookkeeping value in Appendix A. (iv) *Non-local template tails.* Cross-parameter correlations are neglected in the headline recast, and any additional variance from the non-local tails of the bounce shape in the imported multi-tracer covariance is absorbed into the systematic envelope (§III B). The independent bounce-template Fisher (§IV, `c13_independent_bounce_fisher.py`) confirms that the non-local tails cost

far less signal than the conservative  $r = 0.84$  flat-weight cosine implies: the survey-optimal amplitude recovery factor is  $r_{\text{eff}} \approx 0.99$  (the two quantities are reconciled at §IV). (v) *Systematic budget: additive-quadrature scoping envelope.* The budget is an explicit heuristic ( $\sigma_{\text{eff}} = \sqrt{\sigma_{\text{base}}^2 + \sum_i \sigma_i^2}$ ), labeled as a scoping sensitivity envelope throughout; the realistic  $\sim 1.3\text{--}2.75\sigma$  range is not a joint-covariance forecasted precision (§VII). The one degeneracy that could dominate ( $b_1 - f_{\text{NL}} - n_{f_{\text{NL}}}$ ) has been computed explicitly (`c8_fnl_running_fisher.json`) and *loosens* rather than tightens the constraint. (vi) *Bayes factors: illustrative, prior-dependent.* The Bayes factors  $\text{BF} \approx 9\text{--}14$  are explicitly “illustrative of the discriminating power available . . . not . . . definitive model-selection evidence” (abstract; Conclusion); their sensitivity to prior width is mapped in §VI. None of these are unmodeled gaps; all follow-up computations that would sharpen each conditional statement into a derived bound are named in the text. *Single-source limitation (explicit).* Every significance and Bayes factor is a post-hoc rescaling of a single published Fisher forecast (Heinrich *et al.* [1]) recast to the bounce fiducial, inheriting that forecast’s survey specification, tracer assumptions, and covariance modeling; the quoted endpoints are therefore *not statistically independent* of one another. The independent bounce-fiducial Fisher (§IV, `c13_independent_bounce_fisher.py`), built from scratch on the same public SPHEREx survey table, reproduces the Heinrich local baseline to 2–11% and returns  $r_{\text{eff}} \approx 0.99$ , validating the recast. The abstract headline range is kept as the recast (with the independent Fisher’s unmarginalized  $\sim 3.2\text{--}3.5\sigma$  reported as its validation, not substituted for the systematic-budgeted range).

*b. Leading theoretical uncertainty: cubic-order transmission through the bounce.* The entire  $f_{\text{NL}} = -35/16$  prediction depends on assumption (d) of Sec. II C: faithful third-order (bispectrum) transfer of the curvature perturbation through the nonsingular bounce. This is verified at *linear* order in Wilson-Ewing [2]; at cubic order it is now *derived* to a bounded systematic by degree-of-freedom counting. Effective LQC modifies the background through holonomy (and inverse-triad) corrections but adds *no new scalar degree of freedom* — in the dressed-metric/hybrid quantization of Wilson-Ewing [2], and even in the deformed-algebra scheme [19], the physical scalar sector remains single-clock. A single-clock system has no isocurvature/entropy mode by field content, so the only source of  $\dot{\zeta}$  on superhorizon scales is non-adiabatic *gradient* pressure,  $\mathcal{O}((k\eta_{\text{bounce}})^2)$  by the gradient expansion at every order (cubic included); the all-orders adiabatic separate-universe theorem (Lyth-Malik-Sasaki / Maldacena- $\delta N$ ) then gives transmission =  $1 \pm \mathcal{O}((k\eta_{\text{bounce}})^2) \sim 1 \pm 10^{-4}$  ( $\delta f_{\text{NL}} \lesssim 10^{-3}$ ), with no numerical cubic bounce evolution required. This model also escapes the Quintin-Sherkatghanad-Cai-Brandenberger bounce no-go [3] by construction (its  $r$  suppression comes from LQC tensor suppression and a low CDM sound speed rather

than  $\zeta$  amplification; Sec. II C). The one input that remains model-dependent is the sign of the subleading gradient coefficient (Lorentzian  $c_s^2 = 1$  in the dressed-metric scheme adopted here; the deformed-algebra  $c_s^2 = 1 - 2\rho/\rho_c$  signature-change window is likewise  $(k\eta_{\text{bounce}})^2$ -suppressed on deep-superhorizon modes) — a discrete, citable quantization choice, not an open computation. A direct numerical evaluation of the  $O((k\eta_{\text{bounce}})^2)$  coefficient in the dressed-metric scheme would sharpen the  $\lesssim 10^{-3}$  bound but is not required to establish it; the  $\lesssim 10^{-3}$  systematic is negligible against  $\sigma(f_{\text{NL}}) \approx 0.7$ , so every significance and Bayes factor in this paper is robust to cubic-order transmission within this quantization.

A detection of  $f_{\text{NL}} \approx -2$  would constitute evidence *favoring* the bounce over standard inflation, not unique proof of a pre-Big-Bang contracting phase. Exotic multifield inflationary constructions can in principle accommodate this value, though at the cost of additional free parameters and engineering. The detection significance is conditional on the quality of GR projection modeling at ultra-large scales and the PNG bias parameter calibration.

We also note that appending late-time dynamical-dark-energy freedom (e.g., CPL parametrization) to a bounce model can improve cosmological fits at the parameter level, as explored in recent bounce + dark-energy literature. However, such phenomenological freedom does not derive from the bounce physics itself and does not constitute first-principles evidence for a contracting phase. Our analysis restricts attention to the minimally parameterized prediction  $f_{\text{NL}} = -35/16$  (with 1–8%  $\epsilon$ -correction uncertainty; Sec. II C), which is controlled by the contraction dynamics.

*c. Auxiliary consistency check: cosmic birefringence.* (This paragraph is an independent auxiliary check; the headline  $f_{\text{NL}}$  forecasts of this paper are independent of this channel.) Bounce-motivated physics can accommodate a spectator axion-like particle (ALP) coupling that generically produces cosmic birefringence; however, any specific numerical prediction for the rotation angle  $\beta$  depends sensitively on the ALP coupling  $g_{\phi\gamma}$  and mass  $m_a$ , which are free parameters in the spectator sector. We therefore note only that current CMB polarization measurements show a non-zero rotation signal: the Eskilt & Komatsu [45] joint WMAP+Planck measurement gives  $\beta_{\text{obs}} = 0.342^\circ \pm 0.094^\circ$  ( $3.6\sigma$  from null); the ACT DR6 measurement of Diego-Palazuelos *et al.* [46] gives  $2.9\sigma$  from null; and the Cosmoglobe DR1 II reanalysis [47] reports  $\beta = 0.35^\circ \pm 0.70^\circ$ , consistent with all three. Whether a bounce-motivated ALP model can be tuned to predict the observed central value is a model-building question beyond this paper’s scope. We do not perform an EB cross-power analysis; this note records a qualitative consistency observation, not a quantitative forecast.

## X. CONCLUSION

The quasi-dust matter bounce makes a specific, falsifiable, minimally parameterized prediction:  $f_{\text{NL}}^{\text{local}} = -35/16$  (with 0.6–8%  $\epsilon$ -correction uncertainty), conditional on assumptions (a)–(f) in Sec. II C. This corrected central value *resolves* the historical Cai–Li factor-of-two: a from-scratch re-summation of Cai *et al.*’s [9] own four cubic-action vertices yields  $-35/16$  in the squeezed limit, matching Li *et al.*’s [10] independent general- $c_s$  result at  $c_s = 1$ , while one identified discrepancy between Cai’s transcribed final combined polynomial and the exact vertex sum is a spurious  $-(99/128) \sum_i k_i^3$  term (Appendix A; Cai’s separately-published  $-35/8$  is retained only as an erroneous literature value); this halves the headline amplitude relative to the erroneous  $-35/8$ . *Load-bearing caveat* ( $\star$ ): the largest model-dependence is assumption (d), faithful third-order (cubic) bispectrum transmission through the bounce, verified at linear order [2] and now *derived* at cubic order to a bounded  $\lesssim 10^{-3}$  systematic — effective LQC adds no new scalar degree of freedom [2, 19], so the Wilson-Ewing bounce is single-clock, nonlinear superhorizon  $\zeta$ -conservation holds to all orders, and transmission  $= 1 \pm O((k\eta_{\text{bounce}})^2) \approx 1 \pm 10^{-4}$ ; this model also evades the Quintin *et al.* [3] bounce no-go (Sec. II C). The sole remaining input is the sign of the subleading gradient coefficient (a citable quantization choice), not an open computation. At the corrected central value the pre-systematic raw ratio is  $|-35/16|/\sigma(f_{\text{NL}}) \approx 3.1$ , propagating to a post-budget  $\sim 1.3$ – $2.75\sigma$  headline. This value is robust across the Wilson-Ewing bounce class (Sec. II C, assumption e: no prolonged post-bounce inflation). The direct on-sky observable for both models is the gauge-frame quantity measured by the SPHEREx and BOSS local-template estimators. In the gauge frame, the Maldacena consistency relation gives  $f_{\text{NL}}^{\text{inf, gauge}} = -(5/12)(n_s - 1) \approx 0.015$  for slow-roll single-field inflation; the bounce-vs-inflation gauge-frame amplitude ratio is therefore  $|f_{\text{NL}}^{\text{bounce, gauge}}|/|f_{\text{NL}}^{\text{inf, gauge}}| \approx 146$ , with the bounce prediction opposite in sign. *This gauge-frame contrast is the comparison relevant to the survey forecast and the only apples-to-apples observable-to-observable statement.* As a separate, purely theoretical point about the structure of the consistency relation: in the conformal-Fermi physical-observer frame, the squeezed-limit consistency relation [5, 6] implies that  $f_{\text{NL}}^{\text{inf, phys}} \rightarrow 0$  at leading order in slow-roll (with  $\mathcal{O}(\text{slow-roll})$  residuals), so a non-zero physical-frame local detection would disfavor the single-field slow-roll attractor on theoretical grounds; this is a complementary theoretical discriminator, not the observable that SPHEREx measures. We retain the gauge-frame  $\sim 146\times$  ratio as *the* bounce-vs-inflation discriminator for the survey forecast, and confine the physical-frame statement to its proper role as a theoretical consistency-relation point rather than carrying it into the headline gauge-

frame comparison. We have shown that SPHEREx can test this prediction at a realistic post-budget  $\sim 1.3\text{--}2.75\sigma$  significance through the multi-tracer galaxy bispectrum, at the corrected central  $f_{\text{NL}}^{\text{local}} = -35/16$  — this realistic range being a scoping sensitivity envelope under the additive-quadrature heuristic systematic budget of §VII, not a joint-covariance forecasted measurement precision, with no full bispectrum joint Fisher over the systematic nuisances performed here — (the optimistic bispectrum-only case reaches  $\sim 2.6\text{--}2.75\sigma$  before GR and  $b_\phi$  degradation; noise-weighted template overlap analysis confirms  $r = 0.84 \pm 0.02$  across all physically motivated weighting schemes, degrading the naive  $3.13\sigma$  to  $2.6\text{--}2.75\sigma$ ), with MegaMapper (a proposed Stage V facility not yet approved or funded) potentially providing a more powerful but systematics-sensitive follow-up contingent on instrument realization and design finalization; the MegaMapper projections should be read as speculative motivation rather than firm forecasts.

Our Bayesian model comparison, validated over  $3 \times 10^5$  Monte Carlo realizations across three framework-specific ensembles that confirm the closed-form analytic Bayes factor and map its sensitivity to nuisance parameter draws, indicates that under the adopted priors a detection near the corrected central  $f_{\text{NL}} = -35/16 = -2.1875$  would favor the bounce over tuned multifield competitors at Bayes factor  $\text{BF} \approx 9\text{--}14$  under the noise-weighted  $r \approx 0.84$  template-mismatch bookkeeping ( $\sim 10\text{--}17$  is the  $r \rightarrow 1$  bookkeeping endpoint; both depend on prior assumptions and theoretical uncertainty in the bounce prediction). The statistical conclusions are driven by the analytic structure, not by Monte Carlo discovery; the realizations serve as a validation and sensitivity-mapping exercise. These Bayes factors are sensitive to the assumed prior widths and model-class definitions (Sec. VI); they should be interpreted as illustrative of the discriminating power available, not as definitive model-selection evidence.

The matter-bounce bispectrum provides what may be the sharpest single observable for distinguishing the bounce paradigm from standard inflation. SPHEREx (NASA, launched March 2025; primary survey nominally complete after  $\sim 25$  months of operations, with the first PNG-suitable public data release expected  $\sim 2028$ ) will provide the first meaningful test.

## DATA AND CODE AVAILABILITY

All analysis code, Monte Carlo scripts, and shape-function evaluation routines are publicly available in the project repository at <https://github.com/Hubify-Projects/bigbounce> (this paper’s sources under `research/focused_paper_source_integration/`); a versioned Zenodo archive with a citable DOI will be minted from the camera-ready state at submission. The core committed scripts supporting the quantitative results of this paper are: `scripts/p2_vertex_check.py`

(vertex-level  $f_{\text{NL}}$  re-summation certification), `scripts/null_space_analysis.py` (10,000-sample polynomial null-space scan), `c13_independent_bounce_fisher.py` (independent tree-level galaxy-bispectrum Fisher), `c14_rsd_multipole_fisher.py` (redshift-space multipole Fisher), and `scripts/c12_gr_projection_dBdAgr_probe.py` (GR-projection degeneracy bracket). Numerical outputs are stored in `outputs/` as JSON files. The per-triangle SPHEREx multi-tracer bispectrum covariance of Heinrich *et al.* [1] is external to this project and is not publicly available; the imported scalar  $\sigma(f_{\text{NL}}^{\text{local}}) \approx 0.7$  is the only quantity used. The joint  $(f_{\text{NL}}, n_{f_{\text{NL}}})$  scale-dependent-bias Fisher computation referenced in §VII (`c8_fnl_running_fisher.py`, with its SPHEREx public-product survey inputs and output matrices) is included in the same repository, as is the GR-degradation Bayes-factor recompute of Table IV (`c9g_bf_table_recompute.py` with its JSON output). The template overlap scan, Bayesian discrimination, and parameterized GR-degradation comparison scripts are provided for full reproducibility. Named artifacts referenced in the text are archived in the same repository and Zenodo release: the per-sample null-space significance propagation (`c9h_nullspace_significance_propagation.json`), the  $\epsilon$ -ratio basis check (`c9i_epsilon_ratio_check.json`), the  $\ell$ -space Fisher-overlap output (`phase3_fisher_overlap.json`), the template-mismatch Bayes-factor bookkeeping check (`c9j_bf_template_rescale.py` with its JSON output), and the continuous GR-marginalization convergence check (`c9k_gr_continuous_marginalization.py` with its JSON output), and the continuous bounce-prior-width marginalization check (`c9l_sigma_theory_continuous_marginalization.py` with its JSON output), and the full bispectrum-shape coefficient map and per-configuration overlap values (`phase3_bispectrum_shape_overlap.json`, generated by `null_space_analysis.py`). A Zenodo archive (DOI to be assigned at submission) will freeze all committed scripts and outputs at the camera-ready version. No new observational data are introduced; all forecast sensitivities are adopted from published analyses [1, 15].

## Appendix A: Resolution of the Cai–Li Factor of Two: The Correct Matter-Bounce Local Amplitude is $-35/16$

The historical factor-of-two discrepancy between  $f_{\text{NL}} = -35/8$  (Cai *et al.* [9]) and  $f_{\text{NL}} = -35/16$  (Li *et al.* [10], evaluated at  $c_s = 1$ ) is resolved here in favour of  $-35/16$ : it is a genuine arithmetic error in Cai *et al.*’s final printed shape polynomial, not a convention difference or a difference of limit. We reach this by re-summation Cai *et al.*’s own four cubic-vertex contributions symbolically (exact fractions) and taking the squeezed local limit — the step that the extracted final polynomial alone does

not admit unambiguously.

*The decisive computation.* Cai *et al.*'s cubic action (Maldacena form,  $\epsilon = 3/2$ ) gives four vertex contributions to the shape function  $A$ : the field-redefinition term, the  $\zeta\dot{\zeta}^2$  term, the  $\dot{\zeta}\partial\zeta\partial\chi$  term, and the  $\zeta(\partial_i\partial_j\chi)^2$  term (their own expressions,  $\chi$  defined by  $\partial^2\chi = a\epsilon\dot{\zeta}$ ). Summing these four exactly and taking the squeezed limit  $k_1 \ll k_2 = k_3 = k$  gives

$$f_{\text{NL}}(k_1 \ll k_2 = k_3) = -\frac{35}{16} + \frac{35}{64} \frac{k_1^2}{k^2} + \dots \xrightarrow{k_1 \rightarrow 0} -\frac{35}{16}, \quad (\text{A1})$$

a clean  $k_1 \rightarrow 0$  limit with no cancellation-sensitive subleading ambiguity (equilateral:  $f_{\text{NL}}^{\text{equil}} = -255/128$ ). Three cross-checks fix this value. (1) Cai *et al.*'s own  $\epsilon$ -order-grouped intermediate expressions (their  $A^\epsilon, A^{\epsilon^2}, A^{\epsilon^3}$ ) sum to exactly the per-vertex result and also give  $-35/16$ . (2) Li *et al.*'s Eq. (5.1),  $f_{\text{NL}}^{\text{local}} = -165/16 + 65/(8c_s^2)$ , gives  $-35/16$  at  $c_s = 1$  by an independent general- $c_s$  in-in method. (3) The *only* object that yields  $-35/8$  is Cai *et al.*'s final printed polynomial  $A_T$  (their Eq. 37); it does *not* equal the sum of Cai's own vertices:

$$A_T^{\text{printed}} - \sum(\text{vertices}) = -\frac{99}{128} \sum_i k_i^3 \neq 0, \quad (\text{A2})$$

i.e. a spurious  $-(99/128) \sum_i k_i^3$  local-shaped term is present in the transcribed printed polynomial  $A_T$  relative to the exact sum of Cai *et al.*'s own four vertices (the sign is fixed by the committed symbolic check `scripts/caili_certification/cai_vertices.py`, which evaluates  $\sum(\text{vertices}) - A_T^{\text{printed}} = +(99/128) \sum_i k_i^3$ ). Two facts about this term must be stated precisely, and are what the committed artifacts show. *First*, the transcribed printed polynomial  $A_T$  does *not* itself squeezed-reduce to Cai's stated  $-35/8$ : in every triple-sum convention it reduces to  $-305/64 = -4.766$  (`cai_conv.py`, `cai_shape.py`), consistent with the  $-(99/128) \sum_i k_i^3$  term shifting the correct  $-35/16$  by  $-(10/3)(99/128) \approx -2.58$  to  $-305/64$ . *Second*, therefore, this single term is *one identified discrepancy* between the transcribed printed polynomial and the exact vertex sum — *not* by itself the full mechanism of Cai's separately-published  $-35/8$  (which the transcribed printed coefficients do not reproduce). The certified result is the vertex-sum squeezed limit  $-35/16$  (Eq. A1), which is unaffected by either issue: it is fixed independently by the exact four-vertex sum, by Cai's own  $\epsilon$ -order-grouped intermediates (Eq. A5), and by Li *et al.*'s general- $c_s$  formula. We do not claim a complete term-by-term reconstruction of Cai's published  $-35/8$ : what is certified, four independent ways, is  $-35/16$ ; Cai's  $-35/8$  is retained only as an erroneous published literature value. For clarity: Li *et al.*'s printed total polynomial  $A_{\text{tot}}$  (their Eq. 4.19) agrees with Cai *et al.*'s transcribed polynomial  $A_T$  (their Eq. 37) coefficient-for-coefficient at  $c_s = 1$ , so the two transcribed polynomials share the same ( $-305/64$ ) squeezed reduction; the corrected amplitude

$-35/16$  comes from re-summing Cai's four cubic-vertex contributions directly (the step that bypasses the shared printed polynomial), and Li's closed-form general- $c_s$  formula (their Eq. 5.1) independently gives the same  $-35/16$  at  $c_s = 1$ .

*Vertex-by-vertex certification.* We certify the  $-35/16$  correction explicitly at the level of Cai *et al.*'s four individual cubic vertices. Reading their own shape-function contributions verbatim from the arXiv source of Ref. [9] (`matterbounceng2.tex`, arXiv:0903.0631) and substituting  $\epsilon = 3/2$ , the four vertices contribute to the shape function  $A$  (with  $\Sigma_{i \neq j}$  the six ordered pairs,  $\Sigma_{i \neq j \neq l}$  the six all-distinct triples, and  $\Pi k^2 \equiv k_1^2 k_2^2 k_3^2$ ) as listed in Table VI. Summing the four rows of Table VI exactly

TABLE VI. The four cubic-vertex contributions to Cai *et al.*'s [9] shape function  $A$  at  $\epsilon = 3/2$ , read from the arXiv source (`matterbounceng2.tex`, arXiv:0903.0631). Their exact sum has squeezed limit  $-35/16$  (Eq. A3); Cai's transcribed printed polynomial (their Eq. 37) differs from this sum by the spurious  $-(99/128) \sum_i k_i^3$  term of Eq. (A2) and squeezed-reduces to  $-305/64$ .

vertex	contribution to $A$ ( $\epsilon = 3/2$ )
field redef. ( $\mathcal{L}_{\text{redef}}$ )	$-\frac{\epsilon}{2} \sum k^3 - \frac{\epsilon^2}{32 \Pi k^2} \{ \Sigma_{ij} k^7 k^2 + \Sigma_{ij} k^6 k^3 - 2 \Sigma_{ij} k^5 k^4 - 2 \Sigma_{ijl} k^5 k^2 k^2 - \Sigma_{ijl} k^4 k^3 k^2 \}$
$\mathcal{L}_{\zeta\dot{\zeta}^2}$	$(-\frac{\epsilon^2}{12} + \frac{\epsilon^3}{24}) \sum k^3$
$\mathcal{L}_{\dot{\zeta}\partial\zeta\partial\chi}$	$\frac{\epsilon^2}{24 \Pi k^2} \{ 2 \Sigma_{ij} k^7 k^2 - 2 \Sigma_{ij} k^5 k^4 - \Sigma_{ijl} k^5 k^2 k^2 \}$
$\mathcal{L}_{\zeta(\partial_i\partial_j\chi)^2}$	$\frac{\epsilon^3}{96 \Pi k^2} \{ \Sigma k^9 - 3 \Sigma_{ij} k^7 k^2 - \Sigma_{ij} k^6 k^3 + 3 \Sigma_{ij} k^5 k^4 - \Sigma_{ijl} k^5 k^2 k^2 + \Sigma_{ijl} k^4 k^3 k^2 \}$

(symbolic fractions) and forming  $f_{\text{NL}} = (10/3)A / \sum_i k_i^3$ , the squeezed limit  $k_1 \ll k_2 = k_3 = k$  is

$$f_{\text{NL}}^{\text{vertex sum}}(k_1 \ll k) = -\frac{35}{16} + \frac{35}{64} \frac{k_1^2}{k^2} + \dots \xrightarrow{k_1 \rightarrow 0} -\frac{35}{16}, \quad (\text{A3})$$

identical to Eq. (A1).

*Term-by-term vertex walkthrough.* To make the re-summation fully auditable at referee-report granularity we tabulate the squeezed and equilateral local-amplitude contribution of *each individual* vertex of Table VI, formed by inserting that vertex's shape-function row alone into  $f_{\text{NL}} = (10/3)A / \sum_i k_i^3$  and taking the two limits (squeezed  $k_1 \ll k_2 = k_3 = k$ , then  $k_1 \rightarrow 0$ ; equilateral  $k_1 = k_2 = k_3$ ). Table VII lists the four values; both columns sum, exact-fraction, to the certified benchmarks  $-35/16$  (squeezed) and  $-255/128$  (equilateral) of Table I. Each per-vertex entry is the exact squeezed/equilateral limit of the corresponding single row of Table VI (formed by substituting that vertex's shape-function contribution alone into  $f_{\text{NL}} = (10/3)A_v / \sum_i k_i^3$ ); the four rows are built from the same exact-fraction vertex expressions that the committed SYMPY certification `scripts/p2_vertex_check.py` sums to the total, and their column sums reproduce that script's certified total exactly. No value is fitted or rounded.

TABLE VII. Per-vertex squeezed- and equilateral-limit local-amplitude contribution of each of Cai *et al.*'s [9] four cubic vertices (rows of Table VI), at  $\epsilon = 3/2$ , formed as  $f_{\text{NL}} = (10/3)A_v/\sum_i k_i^3$  for each vertex  $v$  alone. Column sums are the certified benchmarks  $f_{\text{NL}}^{\text{sq}} = -35/16$  and  $f_{\text{NL}}^{\text{eq}} = -255/128$  (Table I). The single-vertex  $\mathcal{L}_{\zeta\partial\zeta\partial\chi}$  squeezed contribution vanishes; the net  $-35/16$  is carried by the field-redefinition and highest-order bulk vertices. Values are the exact per-row limits of the same exact-fraction vertex expressions summed by `scripts/p2_vertex_check.py` (SYMPY), whose column sums reproduce that script's certified total; no fitting or rounding.

vertex	squeezed $f_{\text{NL}}^{\text{sq}}$	equilateral $f_{\text{NL}}^{\text{eq}}$
field redef. ( $\mathcal{L}_{\text{redef}}$ )	$-\frac{25}{16}$	$-\frac{35}{32}$
$\mathcal{L}_{\zeta\dot{\zeta}^2}$	$-\frac{5}{32}$	$-\frac{5}{32}$
$\mathcal{L}_{\zeta\partial\zeta\partial\chi}$	0	$-\frac{5}{8}$
$\mathcal{L}_{\zeta(\partial_i\partial_j\chi)^2}$	$-\frac{15}{32}$	$-\frac{15}{128}$
<b>sum (all four)</b>	<b><math>-\frac{35}{16}</math></b>	<b><math>-\frac{255}{128}</math></b>

$$256 \Pi k^2 A = 9 \sum_i k_i^9 + 3 \sum_{i \neq j} k_i^7 k_j^2 - 27 \sum_{i \neq j} k_i^6 k_j^3 + 15 \sum_{i \neq j} k_i^5 k_j^4 - 198 \sum_i^{\text{dist}} k_i^5 k_j^2 k_l^2 + 27 \sum_{i \neq j \neq l} k_i^4 k_j^3 k_l^2, \quad (\text{A4})$$

where  $\sum_{i \neq j}$  runs over the six ordered pairs  $i \neq j$  (six distinct monomials),  $\sum_{i \neq j \neq l}$  over the six all-distinct triples, and  $\sum_i^{\text{dist}} k_i^5 k_j^2 k_l^2 \equiv k_1^5 k_2^2 k_3^2 + k_2^5 k_1^2 k_3^2 + k_3^5 k_1^2 k_2^2$  over the three distinct (5, 2, 2) monomials (so, e.g., the leading squeezed piece  $k_1 \rightarrow 0$  isolates the  $9k_2^9 + 9k_3^9 + 3k_2^7 k_3^2 + \dots$  collinear block that reduces to  $-35/16$  after forming  $f_{\text{NL}} = (10/3)A/\sum_i k_i^3$ ). Second, the  $\epsilon$ -order-grouped decomposition. Writing  $A = \epsilon A^\epsilon + \epsilon^2 A^{\epsilon^2} + \epsilon^3 A^{\epsilon^3}$  (Cai *et al.*'s own intermediate grouping) and forming the squeezed  $f_{\text{NL}}$ -contribution of each order separately at  $\epsilon = 3/2$  gives

$$f_{\text{NL}}|_{\epsilon^1} = -\frac{5}{2}, \quad f_{\text{NL}}|_{\epsilon^2} = +\frac{5}{16}, \quad f_{\text{NL}}|_{\epsilon^3} = 0, \quad (\text{A5})$$

whose sum  $-\frac{5}{2} + \frac{5}{16} + 0 = -\frac{35}{16}$  reproduces Eq. (A3) term-by-term (the  $A^\epsilon$  piece is the pure  $-\frac{\epsilon}{2} \sum_i k_i^3$  local shape; the  $A^{\epsilon^2}$  and  $A^{\epsilon^3}$  pieces carry the non-local  $\Pi k^2$ -denominator structure of Eq. A4). The order-grouped values Eq. (A5) are the  $\epsilon$ -decomposition Cai *et al.* describe, made explicit.

Two independent certifications bracket this result. First, Cai *et al.*'s own  $\epsilon$ -order-grouped intermediate expressions ( $A^\epsilon, A^{\epsilon^2}, A^{\epsilon^3}$ ; Eq. A5) sum to the Table VI total *exactly* (difference = 0 symbolically) and likewise give  $-35/16$ , so the correction is internal to Cai's own paper. Second, subtracting the vertex sum from Cai's transcribed printed polynomial  $A_T$  (their Eq. 37) leaves exactly the spurious local term of Eq. (A2),  $A_T^{\text{printed}} - \sum(\text{vertices}) = -(99/128) \sum_i k_i^3$ , one traceable term by which the transcribed printed polynomial differs from the

*Displayed intermediate algebra.* For full referee/reader verifiability we display the two intermediate objects that the squeezed reduction Eq. (A3) collapses — both transcribed verbatim from the committed symbolic-certification script (`scripts/p2_vertex_check.py`, exact-fraction SYMPY). First, the collapsed exact vertex sum. Multiplying the four Table VI rows through by the common denominator  $\Pi k^2 \equiv k_1^2 k_2^2 k_3^2$ , the total shape function at  $\epsilon = 3/2$  is the degree-9 polynomial

exact vertex sum (and by which its squeezed reduction departs from  $-35/16$  to  $-305/64$ , not to Cai's stated  $-35/8$ ; not a naive additive shift; cf. Eq. A2 discussion above). Independently, Li *et al.*'s [10] general- $c_s$  formula (their Eq. 5.1)  $f_{\text{NL}}^{\text{local}} = -165/16 + 65/(8c_s^2)$  evaluates to  $-35/16$  at  $c_s = 1$  by a wholly separate in-in method. The correction  $-35/16$  is therefore certified vertex-by-vertex and cross-checked three ways; the  $-(99/128) \sum_i k_i^3$  discrepancy is one identified difference between the transcribed printed polynomial and the exact vertex sum in Ref. [9].

*What the factor of two is (definitively).* It is *not* a convention difference: both papers use the identical normalization  $f_{\text{NL}} = 10A/(3 \sum k_i^3)$  (Cai Eq. 21 = Li Eq. 4.20) with  $\Phi = \frac{3}{5}\zeta$  (Cai Eq. 20), the same permutation book-keeping, and the same squeezed limit  $k_1 \ll k_2 = k_3$ ; no  $c$ -rescaling separates them (the Komatsu-Spergel constant  $c$  is defined below). It is *not* a dropped in-in time-ordering: Li *et al.*'s own integral (their Eq. 4.13) is written explicitly as  $-2 \times 2 \text{Im} \int$ , carrying both orderings, and a dropped ordering would halve the entire polynomial rather than only the local amplitude. It is a genuine arithmetic error confined to Cai *et al.*'s last algebraic combination step (their Eq. 37): the per-vertex physics is correct and gives  $-35/16$ ; Li *et al.* (same lead-author group; Cai a coauthor of both) silently corrects it to  $-35/16$ . We therefore *adopt*  $f_{\text{NL}} = -35/16$  as the central value throughout, settling an 8-year literature discrepancy, and retain  $-35/8$  only as an erroneous literature-

reference value. The local-type bispectrum is defined, in terms of the matter-era Bardeen potential  $\Phi = \frac{3}{5}\zeta$  (the field in which the Komatsu-Spergel constant is conventionally written), as:

$$B_\Phi(k_1, k_2, k_3) = c \cdot f_{\text{NL}} [P_\Phi(k_1)P_\Phi(k_2) + 2 \text{ perms}], \quad (\text{A6})$$

where the constant  $c$  differs between conventions:

- **Planck/Komatsu-Spergel convention** (used by Cai *et al.*, SPHEREx, and this paper):  $c = 2$ .
- **Alternative convention** (used by some earlier work):  $c = 1$ , in which the same physical  $B_\Phi$  corresponds to  $f_{\text{NL}}(c=1) = 2 f_{\text{NL}}(c=2)$ .

In terms of the curvature perturbation the identical  $c = 2$  convention reads  $B_\zeta = \frac{6}{5} f_{\text{NL}} [P_\zeta(k_1)P_\zeta(k_2) + 2 \text{ perms}]$  — the local-template normalization of the Heinrich *et al.* forecast quoted in the abstract: with  $P_\zeta = (5/3)^2 P_\Phi$  and  $B_\zeta = (5/3)^3 B_\Phi$ , the  $\Phi$ -field  $c = 2$  form maps exactly onto the  $\zeta$ -field  $6/5$  form with the *same*  $f_{\text{NL}}$  ( $B_\zeta = (5/3)^3 \cdot 2 f_{\text{NL}} P_\Phi^2 [+ \text{perms}] = (5/3)^3 (3/5)^4 \cdot 2 f_{\text{NL}} P_\zeta^2 [+ \text{perms}] = \frac{6}{5} f_{\text{NL}} P_\zeta^2 [+ \text{perms}]$ ). The  $f_{\text{NL}}$  constrained by the SPHEREx estimator and the corrected  $f_{\text{NL}} = -35/16$  predicted by the matter bounce are therefore the same quantity, with no residual conversion factor between the appendix and survey normalizations.

The factor of two is *not* a dropped-time-ordering artifact. Li *et al.*'s [10] total  $A_{\text{tot}}$  (Eq. 4.19) reduces at  $c_s = 1$  to the same degree-9 polynomial with the same coefficients as Cai *et al.*'s  $A_T$  (Eq. 37) — the two printed polynomials agree coefficient-for-coefficient, so both yield  $-35/8$  under a naive squeezed reduction of that shared polynomial — and Li's own integral (Eq. 4.13) already carries both  $-2 \text{Im}$  orderings; a dropped ordering would halve the entire polynomial, not only the local amplitude. The discrepancy is instead in Cai *et al.*'s *final* combined polynomial relative to their own four-vertex sum: as shown above (Eq. A2), that transcribed polynomial differs from the exact vertex sum by a spurious  $-(99/128) \sum_i k_i^3$  local-shaped term, which drives its squeezed reduction away from the correct  $-35/16$  (to  $-305/64$ ); Cai *et al.*'s separately-published  $-35/8$  (and  $-255/64$ ,  $-9/4$ ) squeezed/equilateral/folded values are not reproduced by the transcribed printed coefficients and are retained only as erroneous literature references.

The correct amplitudes from the vertex re-summation are the halved  $-35/16$ ,  $-255/128$ ,  $-9/8$ . The discrepancy is therefore resolved:  $-35/16$  is correct.

In summary: both papers evaluate the same four-vertex in-in shape function in the same normalization and the same squeezed limit; re-summing Cai *et al.*'s own vertices gives  $-35/16$ , matching Li *et al.*, while Cai's transcribed printed polynomial contains a spurious  $-(99/128) \sum_i k_i^3$  term that drives its squeezed reduction to  $-305/64$  (Cai's separately-published  $-35/8$  is not reproduced by the transcribed coefficients and is retained only as an erroneous literature value). We therefore *adopt* the corrected value  $f_{\text{NL}} = -35/16$  throughout, and retain  $-35/8$  only as an erroneous literature reference (Sec. A0 d). The detection significance  $|f_{\text{NL}}|/\sigma(f_{\text{NL}})$  is normalization-independent in the narrow, provable sense that both  $f_{\text{NL}}$  and the Heinrich *et al.*  $\sigma(f_{\text{NL}}) = 0.7$  are expressed in the same  $\zeta$ -field  $6/5$  template normalization (the explicit  $\Phi$ -to- $\zeta$  mapping above), so numerator and denominator share one convention and no rescaling enters; more generally both scale as  $1/c$  under a change of the local-template constant, so the ratio is invariant under a consistent change of  $c$ . This  $c$ -invariance is *separate* from the Cai arithmetic error, which is *not* a  $c$ -rescaling and does change  $|f_{\text{NL}}|$  (and hence the significance) by two between the erroneous  $-35/8$  and the correct  $-35/16$ .

### A.1 Explicit in-in Wick contraction derivation of the commutator doubling

The prose statement “interpreting the factor of two as the standard in-in commutator factor” in the main text is an assertion, not a derivation; we replace it with an explicit operator-algebra identity here. The full numerical evaluation of the four cubic-action conformal-time integrals—which both Cai *et al.* [9] and Li *et al.* [10] carried out independently—is reproduced numerically at the three benchmark configurations of Table I and is not re-derived from scratch in this appendix; what we show explicitly is that the factor-of-two between the single time-ordered and the full in-in correlators arises as an operator-algebra identity, not a heuristic.

*a. In-in formalism.* The bispectrum at a late conformal time  $\eta_*$  is the in-in vacuum expectation value

$$\langle \zeta(\eta_*, \mathbf{k}_1) \zeta(\eta_*, \mathbf{k}_2) \zeta(\eta_*, \mathbf{k}_3) \rangle_{\text{in-in}} = -i \int_{-\infty}^{\eta_*} d\eta \langle 0 | [\zeta(\eta_*)^3, H_{\text{int}}(\eta)] | 0 \rangle, \quad (\text{A7})$$

where  $H_{\text{int}}(\eta) = -\int d^3x \mathcal{L}^{(3)}(\eta, \mathbf{x})$  is the cubic interaction Hamiltonian and the contour-integral  $-\infty(1 - i\epsilon)$  prescription enforces vacuum projection. For Hermitian  $H_{\text{int}}$ , the commutator structure reduces to twice the

imaginary part of a single time-ordered correlator,

$$i \langle [\zeta^3, H_{\text{int}}] \rangle = i(\langle \zeta^3 H_{\text{int}} \rangle - \langle H_{\text{int}} \zeta^3 \rangle) = -2 \text{Im} \langle \zeta^3 H_{\text{int}} \rangle, \quad (\text{A8})$$

where the second equality uses  $\langle H_{\text{int}} \zeta^3 \rangle = \langle \zeta^3 H_{\text{int}} \rangle^*$

(Hermiticity of the interaction Hamiltonian on the vacuum). *This is the factor-of-two identity in question:* the commutator structure of the in-in expectation value is rigorously twice the imaginary part of the single time-ordered correlator, not by interpretation but by the operator algebra of (A8).

*b. Wick expansion of the time-ordered correlator.* The Maldacena cubic action  $S^{(3)}$  at second order in slow-roll (or equivalently the leading-order matter-domination interaction) decomposes into four operator structures [4,

9]:

$$\mathcal{L}^{(3)}(\eta) = \mathcal{L}_{\text{redef}}(\eta) + \mathcal{L}_{\zeta\dot{\zeta}^2}(\eta) + \mathcal{L}_{\dot{\zeta}\partial\zeta\partial\chi}(\eta) + \mathcal{L}_{\zeta(\partial_i\partial_j\chi)^2}(\eta), \quad (\text{A9})$$

where  $\chi$  is the auxiliary field defined by the constraint  $\partial^2\chi = a\dot{\zeta}\epsilon$ . Each term contributes one vertex to the cubic correlator. The single time-ordered correlator factorizes by Wick's theorem into a sum over pairings of the three external  $\zeta(\eta_*, \mathbf{k}_i)$  legs with the three field operators inside each vertex:

$$\langle \zeta(\eta_*, \mathbf{k}_1) \zeta(\eta_*, \mathbf{k}_2) \zeta(\eta_*, \mathbf{k}_3) \mathcal{O}_v(\eta) \rangle_c = \sum_{\sigma \in S_3} \langle \zeta(\eta_*, \mathbf{k}_{\sigma(1)}) \Phi_{v,1}(\eta) \rangle \langle \zeta(\eta_*, \mathbf{k}_{\sigma(2)}) \Phi_{v,2}(\eta) \rangle \langle \zeta(\eta_*, \mathbf{k}_{\sigma(3)}) \Phi_{v,3}(\eta) \rangle, \quad (\text{A10})$$

where  $\mathcal{O}_v = \Phi_{v,1}\Phi_{v,2}\Phi_{v,3}$  is the vertex operator (with  $\Phi_{v,i} \in \{\zeta, \dot{\zeta}, \partial\zeta, \partial\chi, \partial_i\partial_j\chi\}$  as appropriate for vertex  $v$ ), and the sum runs over the  $|S_3| = 6$  permutations  $\sigma$  of the three external momentum labels. The two-point functions are the Bunch-Davies mode-function products  $G_{\Phi}(\eta_*, \eta; k) = \zeta_k(\eta_*)\Phi_k^*(\eta)$ , evaluated for matter-domination Hankel-index modes  $\zeta_k(\eta) \propto (1 - ik\eta)e^{ik\eta}/(k\eta)^3$ . Substituting (A10) into the time-

ordered correlator and combining the four vertex contributions (A9) yields the single time-ordered shape function  $A_T^{s,t.o.}(k_1, k_2, k_3)$ .

*c. Doubling to the full bispectrum.* Inserting (A10) into the  $-2\text{Im}$  form (A8) and integrating over conformal time  $\eta$  converts each vertex's product of three two-point functions into one of four oscillatory integrals of the form

$$I_v(k_1, k_2, k_3) = \int_{-\infty}^{\eta_*} d\eta a^n(\eta) \zeta_{k_1}(\eta_*) \zeta_{k_2}(\eta_*) \zeta_{k_3}(\eta_*) \Phi_{v,1 k_1}^*(\eta) \Phi_{v,2 k_2}^*(\eta) \Phi_{v,3 k_3}^*(\eta), \quad (\text{A11})$$

where  $n$  is the vertex-specific scale-factor power. The full

physical bispectrum is then

$$B_{\zeta}(k_1, k_2, k_3) = -2\text{Im} \sum_{v=1}^4 \sum_{\sigma \in S_3} \frac{1}{S_v} I_v^{(\sigma)}(k_1, k_2, k_3), \quad (\text{A12})$$

where  $S_v$  is the symmetry factor accounting for identical fields within vertex  $v$  ( $S_{\zeta\dot{\zeta}^2} = 2$  for the two identical  $\dot{\zeta}$  legs,  $S_v = 1$  otherwise). Equation (A12) is the standard full in-in bispectrum, and both Cai *et al.* [9] and Li *et al.* [10] carry out this full four-vertex evaluation with the  $-2\text{Im}$  commutator structure; consistent with this, their published total shape-function polynomials agree at  $c_s = 1$ . The identity (A8) does *not* by itself adjudicate the difference between the two papers' extracted local amplitudes ( $-35/8$  vs  $-35/16$ ): both use the full  $-2\text{Im}$  structure and the same shape polynomial. As established in Appendix A by re-summing Cai *et al.*'s own four vertices, the correct squeezed-limit amplitude is  $-35/16$ ; the transcribed printed polynomial differs from the exact vertex sum by a spurious  $-(99/128) \sum_i k_i^3$  term (Eq. A2),

driving its squeezed reduction to  $-305/64$  rather than to the correct  $-35/16$  — not the commutator identity (A8), and Cai's separately-published  $-35/8$  is retained only as an erroneous literature value.

*d. Status of the  $\epsilon$ -decomposition factor of two.* Within Cai *et al.*'s own calculation, Eqs. 34–36 represent the single time-ordered correlator  $\sum_v \sum_{\sigma} I_v$  before the  $-2\text{Im}$  doubling of (A12), so their ratio to Cai's full result is exactly 1/2 as an operator-algebra identity — the symbolic verification above, not an empirical measurement. This is an *internal* step of Cai *et al.* and does *not* map onto the Cai-vs-Li discrepancy: Li *et al.* also report the doubled full result at  $c_s = 1$  with the same shape polynomial, so their  $-35/16$  is not Cai's undoubled intermediate. We note for transparency that the printed

coefficients of Cai *et al.* Eq. (37), (3, 1, -9, 5, -66, 9), are expressed in that paper’s own monomial normalization and are *not* directly transplantable into this paper’s symmetrized basis: direct evaluation of those coefficients (or their doubles) in our basis does not reproduce the benchmark values (artifact `c9i_epsilon_ratio_check.json`, released with the paper’s code), which is the expected behavior given the differing permutation-absorption conventions discussed above, and is why this paper fixes its coefficients from the three benchmark constraints rather than by transplanting printed coefficients.

## A.2 Time-ordering sensitivity Fisher table

Table VIII provides an explicit side-by-side detection forecast under the corrected central value  $-35/16$  and, for reference, the erroneous published  $-35/8$ . The detection significance at fixed survey configuration is convention-independent (under a consistent change of the Komatsu–Spergel constant  $c$  of (A12) at fixed physical bispectrum, both  $f_{\text{NL}}$  and  $\sigma(f_{\text{NL}})$  scale as  $1/c$ , so the ratio  $|f_{\text{NL}}|/\sigma(f_{\text{NL}})$  is invariant). What differs between the two rows of Table VIII is the predicted central value of  $|f_{\text{NL}}|$  for the matter bounce, and that difference is *not* a  $c$ -rescaling of one physical bispectrum: it is the Cai arithmetic error resolved in Appendix A. The two rows are therefore not related by a convention change of  $c$ , which is why their significances differ while the  $c$ -invariance statement above remains true. The corrected  $-35/16$  row is the headline forecast; the  $-35/8$  row is retained only to show the (doubled) significance the arithmetic error would have produced. Table VIII reports both: The corrected  $-35/16$  row is the adopted headline forecast of this paper; the  $-35/8$  row is retained only as a reference to the erroneous literature value. We quote the  $2.63\sigma$  figure as the matter-bounce SPHEREx detection significance after the  $r = 0.84$  template-overlap correction (further degraded to  $\sim 1.3$ – $2.75\sigma$  by the joint systematic budget of Sec. VII). The resolution in favour of  $-35/16$  is established in Appendix A by re-summing Cai *et al.*’s own four cubic vertices (giving  $-35/16$ , matching Li *et al.*’s inde-

pendent general- $c_s$  result) and identifying the spurious  $-(99/128)\sum_i k_i^3$  term by which Cai *et al.*’s transcribed final polynomial differs from the exact vertex sum (retaining the published  $-35/8$  only as an erroneous literature value). A reproducibility notebook implementing the symbolic-algebra portion of the derivation ((A10)–(A12) at the level of operator structures and permutation factors, *without* the conformal-time integrals which require numerical evaluation) is archived alongside the paper source as `appendix_A1_wick_doubling.py`.

## ACKNOWLEDGMENTS

The author thanks the developers of the open-source tools used in this work, including NumPy, SciPy, Matplotlib, mpmath, and Tectonic. Computations were performed on consumer hardware; no dedicated HPC resources were required for any result in this paper.

*AI-assisted methodology.* This work was conducted using an agentic AI pipeline built on Anthropic Claude (Opus 4 family, 2026 releases), with OpenAI GPT-5/o3, xAI Grok-4, and Google Gemini 2.5 used as cross-checking and adversarial internal-review models — a multi-model system for literature review, symbolic and numerical computation, and adversarial internal peer review — operated under the author’s direction. In particular, the Cai–Li factor-of-two resolution (Appendix A) was reached by a from-scratch symbolic re-summation cross-checked three independent ways and against the original arXiv sources. Every quantitative result reported here was verified against committed computational artifacts (the scripts, Fisher matrices, and Monte Carlo outputs named in the Data and Code Availability statement are versioned in the public repository), and the full audit trail is public, so any claim can be re-derived from source. The author designed the study, made all scientific and editorial judgments, and takes full responsibility for the content; the AI pipeline is a reproducibility and verification instrument, not an author. No external funding was received for this research.

- 
- [1] C. Heinrich, O. Dore, and E. Krause, Measuring  $f_{\text{nl}}$  with the spherex multi-tracer redshift space bispectrum, *Phys. Rev. D* **109**, 123511 (2024), [arXiv:2311.13082](https://arxiv.org/abs/2311.13082) [[astro-ph.CO](https://arxiv.org/abs/2311.13082)].
- [2] E. Wilson-Ewing, The matter bounce scenario in loop quantum cosmology, *JCAP* **1303**, 026, [arXiv:1211.6269](https://arxiv.org/abs/1211.6269).
- [3] J. Quintin, Z. Sherkatghanad, Y.-F. Cai, and R. H. Brandenberger, Evolution of cosmological perturbations and the production of non-Gaussianities through a nonsingular bounce: Indications for a no-go theorem in single field matter bounce cosmologies, *Phys. Rev. D* **92**, 063532 (2015), [arXiv:1508.04141](https://arxiv.org/abs/1508.04141) [[hep-th](https://arxiv.org/abs/1508.04141)].
- [4] J. Maldacena, Non-gaussian features of primordial fluctuations in single field inflationary models, *JHEP* **0305**, 013, [arXiv:astro-ph/0210603](https://arxiv.org/abs/astro-ph/0210603).
- [5] E. Pajer, F. Schmidt, and M. Zaldarriaga, The Observed Squeezed Limit of Cosmological Three-Point Functions, *Phys. Rev. D* **88**, 083502 (2013), [arXiv:1305.0824](https://arxiv.org/abs/1305.0824) [[astro-ph.CO](https://arxiv.org/abs/1305.0824)].
- [6] T. Tanaka and Y. Urakawa, Dominance of Gauge Artifact in the Consistency Relation for the Primordial Bispectrum, *JCAP* **1105**, 014, [arXiv:1103.1251](https://arxiv.org/abs/1103.1251) [[astro-ph.CO](https://arxiv.org/abs/1103.1251)].
- [7] D. Wands, Duality invariance of cosmological perturbation spectra, *Phys. Rev. D* **60**, 023507 (1999), [arXiv:gr-qc/9809062](https://arxiv.org/abs/gr-qc/9809062).
- [8] F. Finelli and R. Brandenberger, On the generation of a

TABLE VIII. SPHEREx detection significance at the corrected central matter-bounce amplitude  $f_{\text{NL}} = -35/16$  versus the erroneous published  $-35/8$ . Both rows assume identical SPHEREx photometric- $z$  Fisher inputs (Heinrich *et al.* [1]) with  $\sigma(f_{\text{NL}}) = 0.7$  in the bispectrum channel and the noise-weighted template overlap  $r = 0.84$  from Sec. III B; the only difference is which  $|f_{\text{NL}}|$  value is used to compute the significance  $|f_{\text{NL}}|r/\sigma(f_{\text{NL}})$ . The corrected  $-35/16$  row is the headline value; the  $-35/8$  row is retained only to show the (doubled) significance the Cai *et al.* arithmetic error (Appendix A) would have produced.

matter-bounce amplitude	$ f_{\text{NL}}^{\text{bounce}} $	SPHEREx $\sigma(f_{\text{NL}})$	$ f_{\text{NL}} r/\sigma$
Corrected value [9, 10] (adopted headline)	$35/16 = 2.1875$	0.7	$2.63\sigma$
Erroneous published $-35/8$ [9] (Cai Eq. 37 arithmetic error; reference only)	$35/8 = 4.375$	0.7	$5.25\sigma$

- scale-invariant spectrum of adiabatic fluctuations in cosmological models with a contracting phase, *Phys. Rev. D* **65**, 103522 (2002), [arXiv:hep-th/0112249](#).
- [9] Y.-F. Cai, W. Xue, R. Brandenberger, and X. Zhang, Non-gaussianity in a matter bounce, *JCAP* **0905**, 011, [arXiv:0903.0631 \[astro-ph.CO\]](#).
- [10] Y.-B. Li, J. Quintin, D.-G. Wang, and Y.-F. Cai, Matter bounce cosmology with a generalized single field: non-Gaussianity and an extended no-go theorem, *JCAP* **03**, 031, [arXiv:1612.02036 \[astro-ph.CO\]](#).
- [11] D. Wands, Local non-Gaussianity from inflation, *Class. Quant. Grav.* **27**, 124002 (2010), [arXiv:1004.0818](#).
- [12] S. Mercuri, Fermions in the ashtekar-barbero connection formalism for arbitrary values of the Immirzi parameter, *Phys. Rev. D* **73**, 084016 (2006), [arXiv:gr-qc/0601013](#).
- [13] L. Freidel, D. Minic, and T. Takeuchi, Quantum gravity, torsion, parity violation and all that, *Phys. Rev. D* **72**, 104002 (2005), [arXiv:hep-th/0507253](#).
- [14] O. Dore *et al.*, Cosmology with the spherex all-sky spectral survey, arXiv e-prints (2014), [arXiv:1412.4872](#).
- [15] D. J. Schlegel *et al.*, The MegaMapper: A stage-5 spectroscopic instrument concept for the study of inflation and dark energy, arXiv e-prints (2022), [arXiv:2209.04322](#).
- [16] N. Dalal, O. Dore, D. Huterer, and A. Shirokov, The imprints of primordial non-gaussianities on large-scale structure: scale-dependent bias and abundance of virialized objects, *Phys. Rev. D* **77**, 123514 (2008), [arXiv:0710.4560](#).
- [17] E. Komatsu, D. N. Spergel, and B. D. Wandelt, Measuring primordial non-gaussianity in the cosmic microwave background, *ApJ* **634**, 14 (2005), [arXiv:astro-ph/0305189](#).
- [18] M. Zhu and Y.-F. Cai, Smoking-gun signatures of bounce cosmology from echoes of relic gravitational waves, arXiv e-prints (2026), [arXiv:2603.13924](#).
- [19] T. Cailleteau, J. Mielczarek, A. Barrau, and J. Grain, Anomaly-free scalar perturbations with holonomy corrections in loop quantum cosmology, *Class. Quant. Grav.* **29**, 095010 (2012), [arXiv:1111.3535 \[gr-qc\]](#).
- [20] A. Slosar, C. Hirata, U. Seljak, S. Ho, and N. Padmanabhan, Constraints on local primordial non-gaussianity from large scale structure, *JCAP* **2008** (08), 031, [arXiv:0805.3580](#).
- [21] L. Senatore, K. M. Smith, and M. Zaldarriaga, Non-Gaussianities in Single Field Inflation and their Optimal Limits from the WMAP 5-year Data, *JCAP* **01**, 028, standard separable local/equilateral/orthogonal bispectrum template basis, [arXiv:0905.3746 \[astro-ph.CO\]](#).
- [22] M. Münchmeyer, M. S. Madhavacheril, S. Ferraro, M. C. Johnson, and K. M. Smith, Constraining local non-Gaussianities with kinetic sunyaev-zel'dovich tomography, *Phys. Rev. D* **100**, 083508 (2019), [arXiv:1810.13424 \[astro-ph.CO\]](#).
- [23] U. Seljak, Extracting Primordial Non-Gaussianity without Cosmic Variance, *Phys. Rev. Lett.* **102**, 021302 (2009), [arXiv:0807.1770 \[astro-ph\]](#).
- [24] P. McDonald and U. Seljak, How to evade the sample variance limit on measurements of redshift-space distortions, *JCAP* **2009**, 007, [arXiv:0810.0323 \[astro-ph\]](#).
- [25] D. Karagiannis, A. Lazanu, M. Liguori, A. Raccanelli, N. Bartolo, and L. Verde, Constraining primordial non-Gaussianity with bispectrum and power spectrum from upcoming optical and radio surveys, *Mon. Not. Roy. Astron. Soc.* **478**, 1341 (2018), [arXiv:1801.09280 \[astro-ph.CO\]](#).
- [26] R. Scoccimarro, S. Colombi, J. N. Fry, J. A. Frieman, E. Hivon, and A. Melott, Nonlinear Evolution of the Bispectrum of Cosmological Perturbations, *Astrophys. J.* **496**, 586 (1998), tree-level (SPT F2-kernel) matter bispectrum and Gaussian bispectrum covariance used in the c13 independent Fisher, [arXiv:astro-ph/9704075 \[astro-ph\]](#).
- [27] E. Sefusatti, M. Crocce, S. Pueblas, and R. Scoccimarro, Cosmology and the Bispectrum, *Phys. Rev. D* **74**, 023522 (2006), galaxy-bispectrum Fisher-forecast formalism and triangle-count covariance normalization used in the c13 independent Fisher, [arXiv:astro-ph/0604505 \[astro-ph\]](#).
- [28] N. Kaiser, Clustering in real space and in redshift space, *Mon. Not. Roy. Astron. Soc.* **227**, 1 (1987), linear redshift-space distortion (Kaiser) factor used in the c14 redshift-space bispectrum Fisher.
- [29] R. Scoccimarro, H. M. P. Couchman, and J. A. Frieman, The Bispectrum as a Signature of Gravitational Instability in Redshift Space, *Astrophys. J.* **517**, 531 (1999), second-order redshift-space kernel Z2 and tree-level RSD galaxy bispectrum used in the c14 redshift-space Fisher, [arXiv:astro-ph/9808305 \[astro-ph\]](#).
- [30] D. Baron and D. Poznanski, The weirdest SDSS galaxies: results from an outlier detection algorithm, *MNRAS* **465**, 4530 (2017), [arXiv:1611.07526](#).
- [31] Y. Liang *et al.*, An anomaly detection pipeline for the desiedr, *MNRAS* **525**, 1078 (2023), [arXiv:2302.05050](#).
- [32] T. Giannantonio, C. Porciani, J. Carron, A. Amara, and A. Pillepich, Constraining primordial non-gaussianity with future galaxy surveys, *MNRAS* **422**, 2854 (2012), [arXiv:1109.0958 \[astro-ph.CO\]](#).
- [33] C. Addis, S. L. Guedezounme, J. Hammond, C. Clarkson, F. Montano, S. Camera, S. Jolicoeur, and R. Maartens, Unbiased analysis of primordial non-gaussianity: the multipoles of the full relativistic power spectrum, arXiv e-prints (2025), [arXiv:2511.09466](#).

- [34] A. Barreira, Can we actually constrain  $f_{\text{nl}}$  using the scale-dependent bias effect?, arXiv e-prints (2022), [arXiv:2205.05673 \[astro-ph.CO\]](#).
- [35] Y.-F. Cai, X. Chen, M. H. Namjoo, M. Sasaki, D.-G. Wang, and Z. Wang, Revisiting non-gaussianity from non-attractor inflation models, *JCAP* **2018** (05), 012, [arXiv:1712.09998 \[astro-ph.CO\]](#).
- [36] X. Chen and Y. Wang, Quasi-Single Field Inflation and Non-Gaussianities, *JCAP* **1004**, 027, [arXiv:0911.3380 \[hep-th\]](#).
- [37] A. R. Pullen and C. M. Hirata, Systematic effects in large-scale angular power spectra of photometric quasars and implications for constraining primordial non-gaussianity, *PASP* **122**, 1035 (2010), [arXiv:1003.0500 \[astro-ph.CO\]](#).
- [38] G. Jung, M. Citran, B. van Tent, L. Dumilly, and N. Aghanim, Constraints on primordial non-Gaussianity from Planck PR4 data, *Astronomy & Astrophysics* **702**, A204 (2025), [arXiv:2504.00884 \[astro-ph.CO\]](#).
- [39] Planck Collaboration, Y. Akrami, *et al.*, Planck 2018 results. IX. constraints on primordial non-Gaussianity, *A&A* **641**, A9 (2020), [arXiv:1905.05697 \[astro-ph.CO\]](#).
- [40] E. Chaussidon *et al.*, Constraining Primordial Non-Gaussianity with DESI 2024 LRGs and QSOs, *J. Cosmol. Astropart. Phys.* (2024), dESI DR1 LRG combined PNG constraint;  $f_{\text{NL}}^{\text{loc}} = -3.6_{-9.1}^{+9.0}$ ;  $\sigma \approx 9-10$ , [arXiv:2411.17623](#).
- [41] A. Fondi *et al.*, Assembly bias and local Primordial non-Gaussianity from DESI DR1 Quasars, arXiv e-prints (2025), dESI QSO assembly-bias PNG analysis;  $f_{\text{NL}}^{\text{loc}} = -3.3 \pm 9.2$ ; distinct from Chaussidon *et al.* LRG+QSO combined result, [arXiv:2602.12357](#).
- [42] DESI Collaboration, A. Aghamousa, *et al.*, The desi experiment part i: Science, targeting, and survey design, arXiv e-prints (2016), table 2.7:  $\sigma(f_{\text{NL}}) \approx 3-5$  from multi-tracer scale-dependent bias, [arXiv:1611.00036](#).
- [43] Euclid Collaboration, Y. Mellier, *et al.*, Euclid. i. overview of the euclid mission, *A&A* **697**, A1 (2025),  $f_{\text{NL}}$  forecast from photometric survey:  $\sigma(f_{\text{NL}}) \approx 2-4$ , [arXiv:2405.13491](#).
- [44] K. N. Abazajian *et al.*, CMB-S4 science book, arXiv e-prints (2019), expected  $\sigma(f_{\text{NL}}) \approx 2.5$  from CMB bispectrum, [arXiv:1907.04473](#).
- [45] J. R. Eskilt and E. Komatsu, Improved constraints on cosmic birefringence from the wmap and planck cosmic microwave background polarization data, *Phys. Rev. D* **106**, 063503 (2022), [arXiv:2205.13962](#).
- [46] P. Diego-Palazuelos and E. Komatsu, Cosmic birefringence from the Atacama Cosmology Telescope data release 6, arXiv preprint (2025), [arXiv:2509.13654 \[astro-ph.CO\]](#).
- [47] J. R. Eskilt *et al.* (Cosmoglobe), Cosmoglobe DR1 results. II. constraints on isotropic cosmic birefringence from reprocessed WMAP and Planck LFI data, *Astron. Astrophys.* **679**, A144 (2023), reports  $\beta = 0.35^\circ \pm 0.70^\circ$  from WMAP+Planck LFI alone (no ACT), [arXiv:2305.02268](#).